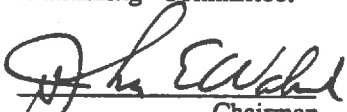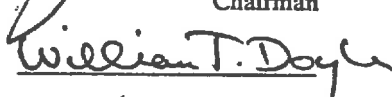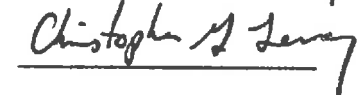DIELECTRIC PROPERTIES OF MOIST SOILS AT RF AND MICROWAVE
FREQUENCIES

A Thesis
Submitted to the Faculty
in partial fulfillment of the requirements for the
degree of
Doctor of Philosophy

by
Jeffrey Erle Campbell

Dartmouth College
Hanover, New Hampshire
September, 1988

Examining Committee:

_____
Chairman

_____

_____

_____

_____
Dean of Graduate Studies

ABSTRACT

The dielectric properties of soils in a wide textural and moisture content range were investigated with coaxial dielectric probe and resonant cavity techniques. The frequencies employed were varied from 1 MHz to approximately 1.5 GHz. The dielectric properties are in general agreement with earlier measurements. There is a marked dispersion in the dielectric constant over the frequency range 1 to 50 MHz with both the real and imaginary parts of the dielectric constant decreasing with increasing frequency. The dielectric response also displays a significant temperature dependence. Over the frequency range from 1 to 50 MHz, the imaginary component increases rapidly with increasing temperature while at microwave frequencies it decreases rapidly with increasing temperature.

A number of different loss mechanisms in moist soils were tested against the data base. At RF frequencies, the evidence supports the claim that an ionic conductivity loss mechanism is predominant and at microwave frequencies, the dielectric loss is caused by the relaxation of free water. Exceptions are noted.

Mixing models of the dielectric response of moist soils are reviewed and it is shown that a Looyenga type mixing best explains the observed RF dispersion. An elementary fractal model of the dielectric behavior of the soils is developed and compared with the general features of the data.

ii

ACKNOWLEDGEMENTS

To my family, thanks for putting up with me through these long years of schooling. Your support, both financial and moral, has largely made this work possible. I would especially like to thank my grandmother, Doris, in whose memory this thesis is dedicated.

TABLE OF CONTENTS

LIST OF FIGURES

INTRODUCTION

The research presented in this thesis is divided into two main categories: 1) An extensive data base of soil dielectric response which encompasses wide variations in soil texture, moisture content and temperature over a wide frequency range has been developed, and 2) Existing theoretical models of the dielectric behavior of moist soils were tested and a general overall theoretical perspective on the response has been developed.

The dielectric properties of soils are of considerable practical and theoretical interest. Because of this a number of researchers have made dielectric measurements in moist soils. A partial list is as follows: Smith-Rose, 1933; Scott, et. al., 1967; Hoekstra and O'Brien, 1969; Geiger and Williams, 1972; Cihilar and Ulaby, 1974; Hipp, 1974; Hoekstra and Delaney, 1974; Selig and Mansukhani, 1975; Davis and Annan, 1977; Topp, et. al., 1980. In spite of the substantial body of previous work, there remains a need for an extensive and carefully collected data base in order to test various models for the dielectric response and to support the development of soil moisture sensing technology.

In the Background Section the desirability of soil moisture data is discussed. Various techniques for *in-situ* soil moisture measurement are reviewed including electromagnetic methods which relate the moisture content of a soil to its dielectric constant. A critique of various remote sensing approaches to the measurement of soil moisture is also included. The nature of the problem of

1

measuring and modeling the dielectric response of moist soils is also discussed.

The basic properties of dielectrics in static and time dependent fields are reviewed in the Discussion on Dielectrics Section. The very commonly encountered Debye relaxation mechanism is also considered in some detail.

The theoretical basis, as well as the experimental technique of resonant cavity dielectric measurements is outlined in the Resonant Cavity Section . Data for a number of soils over a wide range of moisture contents is presented.

In the Coaxial Probe Measurements Section, the theoretical basis and experimental method for making RF dielectric measurements using a coaxial dielectric probe is discussed. The behavior of the dielectric constant as the sample size varies is also considered.

The bulk of the data in this thesis is contained in the Tempe Cell Measurements Section. The experimental procedure used to collect data from 1 to 50 MHz is discussed and a large collection of data for various soils is also presented.

In the Temperature Dependence of Dielectric Properties Section, the experimental procedure used to collect data using the coaxial dielectric probe as well as resonant cavity techniques is outlined. Experimental data and a discussion of its significance is presented.

The Mechanisms of Dielectric Loss Section reviews the various possible mechanisms resulting in dispersion and dielectric loss in moist heterogenous media. The possibility that the mechanism is

2

operating in moist soils is also discussed and compared to the experimental data.

In the Mixture Theory Section, various dielectric mixing theories are discussed and compared with the experimental data. An original fractal model is presented which appears capable of explaining many of the features of the experimental data.

Finally, in the Conclusions Section, generalizations regarding the data are put forward. Conclusions about the loss mechanisms operating in soils as well as the results of the mixture theory modeling are reviewed.

BACKGROUND

In this section, the importance of soil moisture is discussed. Numerous *in-situ* as well as remote sensing approaches to the measurement of soil moisture are reviewed. The need for soil dielectric response data is also presented. Finally, the difficulties involved in making dielectric measurements in moist soils is discussed.

NEED FOR SOIL MOISTURE DATA

According to Daniel Hillel, "The term *soil* refers to the weathered and fragmented outer layer of the earth's terrestrial surface" (Hillel, 1980). Soil is an extremely important part of man's environment. We grow our crops in it; build and travel on it; and it is an integral part of the hydrological cycle which affects weather and a whole host of human activities. One fundamental property of a soil is it's water content. The moisture content of soil is of great interest in the fields of agriculture, the military, meteorology, and hydrology. Furthermore the physical structure and chemical content of soil is complex and varied. Hence any evaluation of its electromagnetic response touches on fundamental questions in the behavior of heterogenous media.

Soil moisture is of importance in agriculture because of its dramatic effect on plant growth. A knowledge of water content of

4

agricultural lands is indispensable in scheduling irrigation, crop sowing, and dry land farming activities. The water content of soils (particularly if temperatures are below freezing) dramatically affects the trafficability of off-road areas. This is of major military interest in trying to adapt to limits in mobility due to soil moisture. Soil moisture is a significant variable in weather forecasting and modeling. The moisture content of soil greatly affects how incoming solar radiation is partitioned into sensible and latent heat fluxes. which in turn strongly affects weather. Of course, soil moisture data is of critical importance to hydrological studies. Soil moisture is intimately involved in determining how incident precipitation is divided into evapotranspiration, run-off, infiltration into the soil, and percolation into the water table. Finally, soil moisture is of great interest in construction and engineering activities. Soil moisture affects the properties of soil as a building material in dams and other structures. Soil moisture is also of interest in flood control as well as in the management of waste and contaminants in the environment.

For these reasons, as well as others, considerable effort has been expended in efforts to measure and study the effects of moisture, in this very important part of man's environment, soils

REMOTE SENSING OF SOIL MOISTURE

The desirability of having a remote sensing soil moisture system has been appreciated for a number of years. The advantages of a remote sensing system include relatively low manpower

requirements, the possibility of automated data collection, and data collection on a planetary scale in near real time. A number of remote sensing approaches have been attempted (Schmugge, et. al., 1979).

One of the most simplistic approaches is the measure of the surface albedo in the near UV to near IR spectral region (Condit, 1965). This technique exploits the change in the albedo of soils with moisture. However, this approach to the remote sensing of soil moisture is fraught with great difficulty. The albedo of soils is very soil dependent as well as moisture dependent. The measured albedo is also greatly affected by surface roughness, vegetative cover, and angle of solar illumination. In addition this technique can be used only under daylight and good weather conditions and is sensitive to soil moisture only at the surface of the soil.

It is also possible to exploit the thermal IR region of the spectrum. One technique involves using thermal IR measurements to determine the difference in temperature between the crop canopy and the surrounding air which is a reflection of the amount of water available for plant transpiration (Sabins, 1987). Unfortunately, the measured temperature difference is dependent on the crop and the growth stage of the crop. Also, the temperature differential can be quite insensitive to soil moisture over a wide range of soil moisture values. This technique is also responsive to soil moisture only in the root zone of the crop. For these reasons, this approach is of generally only of agricultural utility. Another related technique is the measurement of the surface soil temperature which is influenced by the amount of water present at the surface for evaporative cooling (Sabins, 1987). However the observed soil temperature depends on

6

factors such as vegetative cover and meteorological conditions such as humidity, wind speed, and solar flux as well as soil type.

A more sophisticated technique involves measuring the diurnal temperature variation of soils (Idso, et al.,1975; Schmugge, et al., 1978; Reginato, et al., 1976). The thermal response of soil depends on the thermal inertia of the soil and the "thermal driving forces" such as solar energy and evaporation. The thermal inertia of soil, P, is given by $P=(KC)^{1/2}$ where K=the thermal conductivity and C= the heat capacity of the soil. Due to water's high heat conductivity and heat capacity, the thermal inertia is highly dependent on the moisture content of the soil. Typically moist soils undergo much smaller diurnal temperature variations then dry soils. Under certain conditions, the correlation between the observed diurnal temperature range and soil moisture present in the soil can be quite good. Unfortunately the diurnal temperature variation is influenced by wind, humidity and solar radiation as well as the water content of the soil. Besides these difficulties, this technique cannot be used where a vegetative cover exists or in bad weather. This approach requires both day and night measurements which can be difficult to obtain from a satellite platform.

The use of the near IR spectral region allows for a qualitative determination of soil moisture (Sabins, 1987). As plants undergo water stress, the cell structure of the plants change resulting in a marked decrease in the near IR reflectance. The water stressed condition of the vegetation is indicative of relatively low soil moisture values in the root zone. However there are a number of serious drawbacks to this approach. Vegetation may undergo water

7

stress due to disease as well as drought. This technique is quite insensitive to moisture content over a wide range of soil moisture values. The point at which vegetation becomes water stressed depends markedly on species and the prevailing meteorological conditions.

Extensive effort has been devoted to the development of a remote sensing system based on using microwave measurements. The passive method uses the microwave radiation emitted as the tail end of thermal blackbody radiation. The emissivity of soil strongly depends on the dielectric profile of the soil which is very moisture dependent. A number of ground, airborne, and satellite microwave radiometer studies have shown a good correlation between the observed soil emissivity and soil moisture (Newton, 1977; Schanda, et. al.,1978; Burke, et. al., 1979; Eagleman and Lin, 1976). The observed microwave emission is affected by soil temperature, surface roughness, and vegetation which acts to reduce the emissivity of the soil. Due to the relatively weak signal, resolution is limited to about a 10 km scale from satellite based systems.

Active microwave techniques which involve measuring the backscatter of a microwave source off soil have been investigated. The observed backscatter is strongly influenced by the dielectric properties of the soil which are influenced by the moisture content of the soil. Good correlations between ground, airborne, and satellite based scatterometer measurements and soil moisture have been obtained (Blanchard, et. al., 1981; Batlivala and Ulaby, 1977; Ulaby, et. al., 1982). However the observed backscatter is also dependent

8

on such factors as surface roughness, vegetative cover, and the observation angle.

Microwave based approaches to the remote sensing of soil moisture offer a number of important advantages over the other techniques mentioned. Microwave data can be obtained day or night, and in inclement weather. Microwaves also have the ability to penetrate a significant amount of vegetative cover. Microwaves penetrate soil to a considerable degree, on the order of 10 cm, and hence thin surface anomalies are not as important as in visible and IR based measurements.

IN SITU MEASUREMENT OF SOIL MOISTURE

Considerable work has also been done to develop *in-situ* soil moisture instrumentation for meteorological, hydrological, agricultural and engineering applications. The various *in-situ* measurement techniques include gravimetric, nuclear, tensiometric, hygrometric, and electromagnetic (Schmugge, et. al.,1979).

The gravimetric technique consists of collecting a sample of soil to be analyzed, and comparing the weight of the sample before drying for 12 hours at 105º C, and after. From these two weights, the soil moisture expressed as grams of water per gram of dry soil can be calculated. The advantages of this approach are low cost, simplicity, and the lack of required calibration. Disadvantages include a high manpower requirement, a considerable lag between sample collection and soil moisture determination, and that the

9

procedure can be quite destructive to a site where long term monitoring of soil moisture is attempted. Despite these difficulties, this technique is typically used to calibrate other soil moisture measurement techniques.

A neutron scattering approach exploits the fact that neutrons are strongly scattered by light nuclei as compared to heavy nuclei (Belcher, et al., 1950, 1952). Hydrogen nuclei, present in the form of water molecules, are very effective in scattering and thermalizing neutrons from high energy neutrons produced by various isotopes. Soil moisture is then related to the number of slow thermal neutrons which return to the detector. Unfortunately, this method requires careful calibration for each soil type. There are numerous advantages to this system including responsiveness to water in a frozen state, the measurement is quick, and the system can be automated. Disadvantages include high cost, possible health hazard from radioactive isotopes, the fact that the volume of soil contributing to the signal depends on the soil and its moisture state, and the relatively large sensing volume precludes near surface measurements.

Another nuclear method exploits the scattering and absorption of isotopically produced gamma rays which depends on the moisture content of the soil (Gurr, 1962; Ferguson and Gardner, 1962). This technique has the advantage that through beam collimation of the source and detector, high spatial resolution can be obtained. This approach has a number of drawbacks such as cost and complexity, the complicated calibration caused by significant variations in the

bulk density of soils, and the possible health risks from the radioactive source.

Tensiometric techniques for the determination of soil moisture are based on measuring the energy or capillary tension which with water is held in the soil (Richards and Gardner, 1936). This capillary tension is highly moisture dependent. Typically, a tensiometer consists of a porous ceramic cup, in contact with the soil of interest, connected to a column of water with a vacuum gauge. The vacuum measured at the top of the water column is indicative of the capillary tension with which water is being held in the soil. This approach has a number of advantages. The system is relatively inexpensive, simple to use and install, and through the use of pressure transducers, data collection can be automated. One major drawback to this system is that for a given moisture content, the tensiometer reading depends very strongly on soil type. Additionally, the tensiometer is capable of reading tensions from about 0 to 0.9 bar which in clays may correspond to only a very small range of soil moisture values.

Hygrometric methods determine the relative humidity of the immediate atmosphere and relate it to soil moisture (Bouyoucos and Cook, 1965; Phene, et al., 1971). A number of sensors have been developed to make relative humidity measurements. The primary advantage to this approach is very low cost and simplicity. The primary limitation is the extensive calibration required for each soil.

Considerable work has been done to develop a soil moisture measurement system based on measurement of the electromagnetic properties of soils (Schmugge, et al.,1979). Since the magnetic

11

permeability of soil is near that of free space, this reduces to the measurement of the dielectric constant of soils. The dielectric constant of most dry soils is around 4 while that of water is around 80. This large difference makes the dielectric constant of a soil a sensitive indicator of soil moisture. In general the dielectric constant of moist soil is a complex number reflecting not only the polarization of the media but also energy dissipation which may result from either a phase lag in the polarization or to ionic conductivity. It is possible to correlate both the real and imaginary parts of the dielectric constant with soil moisture. There are a number of advantages to this approach. The technique is relatively simple, inexpensive, and well suited to the routine, long term monitoring of a site. In addition the dielectric constant of water falls from about 85 to 4 as it freezes which allows for the determination of freezing in soils which is of great interest in numerous applications. The primary disadvantages include the significant variation in dielectric response between soil types, dependence on effects due to salinity, and the fact that the dielectric behavior is frequency dependent. In spite of the difficulties, this approach is well suited to a number of engineering applications and this is in part the motivation for the present work.

IMPORTANCE OF THE DIELECTRIC PROPERTIES OF SOILS

A knowledge of the dielectric properties of soils is important for a number of reasons. A firm understanding of the dielectric

behavior of soils is needed to further investigate the feasibility of a remote sensing of soil moisture based on direct electromagnetic observation of soils. The dielectric properties of soil are of critical importance in determining the reflectivity or emissivity of moist soils. The response of *in-situ* electromagnetic soil moisture sensors is, of course, directly tied to the dielectric behavior of moist soils. Finally, soils form a complex, heterogeneous, dielectric and the dielectric behavior of such a media is of considerable theoretical interest.

SCOPE OF THE PROBLEM

The measurement, or theoretical prediction, of the dielectric behavior of moist soils is a difficult problem. Soils are very complex media containing dissolved ionic salts, organic material, air, water and a huge range of soil particle and pore sizes. The geometric arrangement of air spaces, water and soil particles is of such a complex nature that an analytic description of this arrangement is nearly impossible. In the progression gravel, coarse sand, fine sand, silt, and clay, the average particle size changes by many orders of magnitude. Naturally occurring soils typically are stratified, with marked change in composition with depth. Natural soils also often exhibit structure produced by organisms such as worms, or by physical processes such as cyclical freezing and thawing. Soils, particularly clays, may have such a small average particle size that a significant fraction of the water present in the soil is adsorbed onto

the surface of the soil particles. Water which has been adsorbed exhibits markedly different behavior than "free water" which is present in a nonadsorbed state in the soil.

The chemical composition of soils varies significantly and can be generally described as follows (Hillel, 1980). Sands, classified by the U.S.D.A. as soils with particle diameters of .05 to 2 mm, are most often composed of quartz. Feldspar, mica, zircon, tourmaline, and horneblende are also commonly found as a minor constituent in sands. Although jagged, most individual sand particles are roughly spherical in shape.

Silt soils, classified as soils with particle diameters of .002 to .05 mm, are mineralogically quite similar to sands. The silt particles are roughly spherical and shape, but due to their increased surface area they may become coated with clay particles. Thus, to some extent, silts may display some of the physiochemical attributes of clays.

Clays soils, classified as soils with particle diameters smaller than .002 mm, are composed of secondary minerals. These secondary minerals are produced when the primary minerals present in rocks undergo chemical reaction with air, water and dissolved chemical agents. The major constituents of these secondary minerals are the alumino-silicates, although some clays may have a considerable content of minerals such as calcium carbonate or iron oxide. The shape of clay particles departs greatly from spherical and may assume plate-like or needle shapes. This, combined with their small sizes, gives clays very large surface areas on a per volume basis. Clays then can exhibit swelling upon wetting

14

due to water adsorption and hydration of the soil particles. Clays may also become plastic or sticky upon wetting. Because of these properties, the clay fraction of a soil often determines, to a large extent, the physiochemical properties of a soil.

From a measurement standpoint, the determination of the dielectric behavior of soil is quite challenging. One concern is that the sample volume being measured may not be representative of the soil as a whole and thus that the measured dielectric constant is not a function of the sample size. The physical preparation of a soil sample in itself is not trivial. The packing of a sample and the introduction, or removal, of water in the soil requires considerable care. Clays, which often exhibit significant swelling upon the addition of water, can greatly exacerbate these problems. Since many soils contain soil particles with shapes departing greatly from that of spherical, it is quite possible that in the sample preparation, a preference for a certain particle orientation may develop. This could possibly manifest itself in an anisotropy in the observed dielectric constant and hence the measured dielectric constant would depend on how the dielectric probe was aligned in the sample.

Besides questions regarding sample preparation, there are a number of problems associated with making the electrical measurements of the sample. At the low frequency end (below about 10 MHz) electrode polarization effects as well as energy loss due to ionic conductivity can make measurements increasingly difficult. Also the design of a dielectric probe that allows for moisture movement through the sample, while also possessing a well defined electrical volume, requires care. At the high frequency end

(above about 100 MHz) wave guide or resonant cavity techniques must be used. Due to energy absorption from ionic condictivity or water dipole relaxation, wave guide or resonant cavity measurements can be difficult.

EMPHASIS OF THE RESEARCH

The dielectric properties of soils have been extensively investigated by numerous researchers. However, there still is a need for a data base of carefully collected measurements over a wide range of soil types to be used in theoretically modeling the observed dielectric behaviors. It is largely the intent of this work to address this need as well as attempt to contribute to the theoretical knowledge of soil dielectric behavior.

DISCUSSION ON DIELECTRICS

In this section, the basic concepts of dielectric response are reviewed including Debye relaxation. Those readers familiar with real and imaginary dielectric constants, loss tangents, and dispersion resulting from Debye relaxation may wish to skip this section.

BACKGROUND

Following the approach of Fröhlich (1949), consider a plate capacitor with a total charge of $+\sigma A$ on one plate and a total charge of $-\sigma A$ on the other plate where σ is the surface free charge density, and A is the area of one plate. This is shown schematically in the figure #1. In part A) the case of a dielectric with a dielectric constant of unity (such as a vacuum) is shown.

A)

$+\sigma A$

$+ + + + + + + + + + +$

$E=4\pi\sigma \quad D=E \quad P=0$

$-\sigma A$

$\varepsilon=1$

B)

$+\sigma A$

$+ + + + + + + + + + +$

$E=\dfrac{4\pi\sigma}{\varepsilon} \quad D=\varepsilon E \quad P$

$-\sigma A$

$\varepsilon>1$
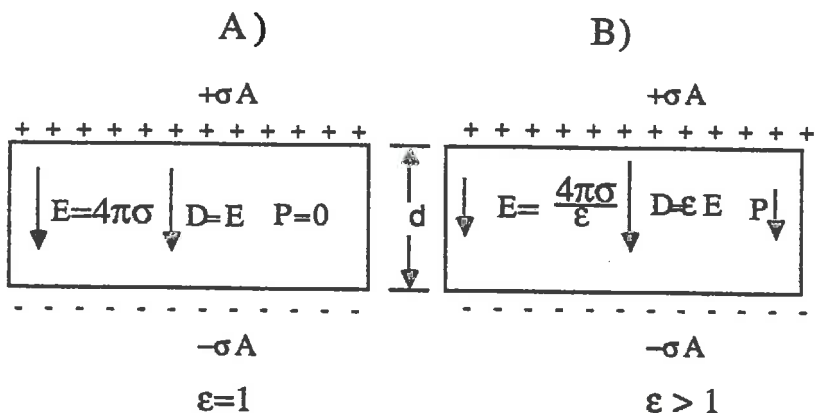
FIG. 1 ELECTRIC AND POLARIZATION FIELDS IN DIELECTRICS

In this instance, E (the electric field) $=4\pi\sigma$, and D (the electric displacement) $=\varepsilon E=E$, and there is no polarization, P. If no charge is allowed to move between plates and a dielectric is inserted between the plates as in   B), the electric field is reduced by a factor of $1/\varepsilon$ and a polarization, which is the effective surface bound charge density developed at the surface of the dielectric opposing the applied electric field, is given by $P=\sigma(\varepsilon-1)/\varepsilon$.

The above discussion applies when there is no time dependence in the electric field.   When an electric field is suddenly applied to a dielectric, the polarization will typically not assume its static value immediately.   One usually considers the important case where the electric field is a sinusoidal periodic function e.g.

$$E=E_0 Cos(\omega t) \tag{1}$$

where E_0 is independent of time and ω is the angular frequency. After a sufficient length of time, the electric displacement, D, must also be periodic, but may show some phase shift, ϕ, i.e.

$$D = D_0 Cos(\omega t - \phi) = D_1 Cos(\omega t) + D_2 Sin(\omega t) \qquad (2)$$

where for a linear dielectric at a given frequency, D_0 is proportional to E_0 and $D_1 = D_0 Cos\phi$, $D_2 = D_0 Sin\phi$. We can introduce two different frequency dependent dielectric constants ε_r and ε_i where:

$$D_1 = \varepsilon_r E_0 \ , \quad D_2 = \varepsilon_i E_0 \quad and \quad Tan\phi = \varepsilon_i/\varepsilon_r \qquad (3)$$

the reason for choosing subscripts i, r for the dielectric constants will become clear shortly. In the limit as the frequency goes to zero, we must recover the static case and if we assume no dielectric loss (it will be shown later that ε_i is proportional to energy loss in dielectrics) then we must have $\varepsilon_r(\omega)$ going to the static dielectric constant, and $\varepsilon_i(\omega) = 0$. We also assume that ε_r is well behaved in the high frequency limit, i.e. $\varepsilon_r(\omega)$ goes to ε_∞ as ω becomes very large. We may define a complex dielectric constant

$$\varepsilon = \varepsilon_r - i\varepsilon_i \qquad (4)$$

with real a real part ε_r and imaginary part ε_i, and then replace eq. (1) with

$$E = E_0 e^{-i\omega t} \qquad (5)$$

19

where we consider only the real part of the above equation. Using eqs. (4) and (5) we can then replace eq. (2) with

$$D = \varepsilon E \qquad (6)$$

where it is understood that we consider only the real part of the above equation.

If the temperature of the dielectric is held fixed, it can be show that the energy flux per unit volume into the dielectric, W, is given by

$$\delta W = \frac{1}{4\pi} E \, \delta D \qquad (7)$$

The average energy lost per unit volume per unit time, L, is then given by

$$L = \frac{\omega}{2\pi} \frac{1}{4\pi} \int_{\frac{2\pi}{\omega}}^{0} E \frac{\partial D}{\partial t} dt \qquad (8)$$

Using eq (5) and (6) in the above integral gives

$$L = \frac{\varepsilon_i E_0^2 \omega}{8\pi} \qquad (9)$$

The above equation can be arranged to give

20

$$L = \frac{\varepsilon_r E_0^2 \omega}{8\pi} \text{Tan}\phi \qquad (10)$$

where $\text{Tan}\phi$ is defined in eq. (3). Since the loss in the dielectric is proportional to $\text{Tan}\phi$ this is often referred to as the loss tangent.

DIPOLE RELAXATION

The polarization induced in a media by an applied field is produced, in part, by the three mechanisms- atomic polarization, molecular polarization, and permanent dipole orientation. In moist soils, the large permanent dipole moment of water allows the permanent dipole orientation mechanism to be important. At high enough frequencies, all of these mechanisms are no longer capable of responding to the applied field. In the case of molecular polarization and atomic polarization, these frequencies lie in the infrared to ultraviolet part of the spectrum. At frequencies well below these values such as those used in the experimental work described herein, these polarization mechanism show no frequency dependence. However the frequency at which the permanent dipole relaxation mechanism begins to fade (the dipole relaxation frequency) is about 14 GHz for pure water at room temperature (Hastead, 1973). This is close enough to the employed experimental measurement frequencies, that the dynamics of this dipole relaxation must be

21

considered. The following discussion follows the presentation of Debye (Debye, 1929).

First consider a dilute collection of dipoles (this restriction allows us to neglect near field effects) with permanent dipole moment μ, in a static electric field of magnitude E. In the absence of an electric field, the dipole moments of the molecules, are on average, distributed with equal probability in all directions and hence there is no net polarization. When an electric field is applied, the energy of each dipole, U, becomes

$$U = -\mu E \cos\theta \qquad (11)$$

where θ is the angle the dipole makes with respect to the applied field. In response to this field, there is now a preferred orientation and the number of dipoles, dZ, found in a given solid angle $d\Omega$, is obtained according to Boltzmann's Law,

$$dZ = A e^{-\left(\frac{U}{KT}\right)} d\Omega \qquad (12)$$

where K is Boltzmann's Constant, T is the absolute temperature, and A is a constant dependent on the number of molecules being considered. The average dipole moment in the direction of the electric field is then given by

$$m = \frac{\int A\,e^{(\mu E/KT)\cos\theta}\,\mu\cos\theta\;d\Omega}{\int A\,e^{(\mu E/KT)\cos\theta}\;d\Omega} \qquad (13)$$

where the integration is to be performed over all angles. On performing the integration we have

$$m = L\left(\frac{\mu E}{KT}\right) \equiv \cotanh\left(\frac{\mu E}{KT}\right) - \frac{KT}{\mu E} \qquad (14)$$

where $L(x)$ is Langevin's Function which appears in magnetic moment calculations. In the limit where the argument of Langevin's Function is much smaller than unity (typical values of $\mu E/KT$ for water at room temperature in moderate fields are on the order of 10^{-5}) the net dipole moment becomes

$$m = \left[\frac{\mu^2}{3KT}\right]E \qquad (15)$$

and is linear in the applied field and exhibits a reciprocal temperature dependence. The derivation, and its results, are analogous to the the well known Curie Law of magnetic susceptibility.

Having considered the dipole's response to a static field, we now turn to its behavior in a dynamic field. Qualitatively, one can think of the dipole tending to align itself to the changing field but being opposed by the finite moment of inertia of the dipole. A better

23

description of this process is that the varying field continually changes the probability of finding the dipole aligned or unaligned with the applied field (Smyth, 1955; Fröhlich, 1949). At low frequencies, there is sufficient time for the population of dipoles to achieve the distribution required by Boltzmann statistics and the polarization response is at its maximum. As the frequency increases, there is no longer sufficient time for the dipoles to achieve an equilibrium distribution and the polarization begins to fall. At very high frequencies, there is no time for the dipoles to react to the applied field and the contribution to the polarization due to permanent dipole orientation drops to zero. The inability of the dipoles to instantaneously respond to applied fields, will lead to a complex dielectric constant.

The quantitative calculations of the dynamic behavior of dipoles were first done by Debye (Debye, 1929). The following discussion has been condensed from Fröhlich (Fröhlich, 1949). The derivation is based upon the hypothesis that in constant external fields equilibrium is attained exponentially with time. We thus introduce a decay function, $\alpha(t)$, such that

$$\alpha(t) = A e^{-\left(t/\tau\right)} \qquad (16)$$

where A and τ are time independent but may be temperature dependent. The electric displacement, D(t), is then given in terms of the electric field, E(t), and the decay function as follows,

24

$$D(t) = \varepsilon_\infty E(t) + \int_{-\infty}^{t} E(u)\alpha(t-u)\, du \qquad (17)$$

where ε_∞ is the contribution to the dielectric constant due to mechanisms other than permanent dipole relaxation. The above equation can be transformed into a differential equation by exploiting the fact that

$$\frac{d\alpha(t)}{dt} = -\frac{1}{\tau}\alpha(\tau) \qquad (18)$$

and by differentiating eq. 17 with respect to time, and then multiplying by τ, to give

$$\tau\frac{dD(t)}{dt} = \varepsilon_\infty\tau\frac{dE(t)}{dt} + \tau\alpha(0)E(t) - \int_{-\infty}^{t} E(u)\alpha(t-u)\, du \qquad (19)$$

Adding eqs. 17 and 19 then gives

$$\tau\frac{d}{dt}(D-\varepsilon_\infty E) + (D-\varepsilon_\infty E) = \tau\alpha(0)E \qquad (20)$$

The constant $\alpha(0)$ can be determined by considering the special case of equilibrium in a static field where we have

$$\frac{d}{dt}(D-\varepsilon_\infty E) = 0, \qquad D = \varepsilon_s E \qquad (21)$$

25

where ε_s is the static dielectric constant. Using these relations in eq. 20 then gives

$$\tau \alpha(0) = \varepsilon_s - \varepsilon_\infty \qquad (22)$$

Using eq. 22 in eq. 20 then produces

$$\tau \frac{d}{dt}(D - \varepsilon_\infty E) + (D - \varepsilon_\infty E) = (\varepsilon_s - \varepsilon_\infty)E \qquad (23)$$

Eq. 23 then is the differential equation connecting the electric displacement and the electric field assuming an exponential decay function

$$\alpha(\tau) = \left(\frac{\varepsilon_s - \varepsilon_\infty}{\tau}\right)e^{-\left(t/\tau\right)} \qquad (24)$$

It can be shown (Fröhlich, 1949) that the approach to equilibrium of a capacitor, for either constant charge on the capacitor plates or constant voltage across the plates, will result in an exponential decay function when eq. 23 is applied. If we assume E is a periodic field of the form

$$E = E_0 e^{-i\omega t} \qquad (25)$$

and thus

26

$$\frac{dE}{dt} = -i\omega E \ , \ D = \varepsilon(\omega)E \ , \ \frac{dD}{dt} = -i\omega\varepsilon(\omega)E \qquad (26)$$

Using the relations in eq. 26 in eq. 23 then gives

$$\varepsilon(\omega) - \varepsilon_\infty = \frac{\varepsilon_s - \varepsilon_\infty}{1 - i\omega t} \qquad (27)$$

Eq. 27 can be separated into real and imaginary parts

$$\varepsilon_r(\omega) = \varepsilon_\infty + \frac{\varepsilon_s - \varepsilon_\infty}{1 + \omega^2\tau^2} \quad \text{and} \quad \varepsilon_i(\omega) = \frac{(\varepsilon_s - \varepsilon_\infty)\omega\tau}{1 + \omega^2\tau^2} \qquad (28)$$

The above equations are known as the Debye relaxation equations and are pervasive in the literature of dielectrics. The maximum imaginary dielectric loss, $\varepsilon_i(max)$, is given by

$$\varepsilon_i(max) = \frac{\varepsilon_s - \varepsilon_\infty}{2} \qquad (29)$$

The dielectric behavior predicted by these equations is shown in figure #2. It can be easily shown that when the imaginary
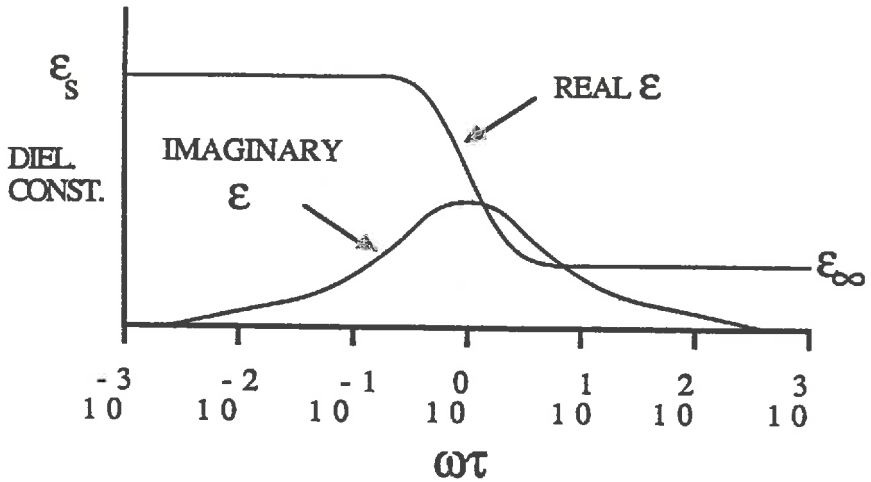
FIG. 2 GENERALIZED DEBYE RESPONSE

dielectric constant is plotted against the real dielectric constant (a Cole-Cole diagram) a semicircular plot will be generated (see figure #3). This forms a useful test of Debye Relaxation in a sample.
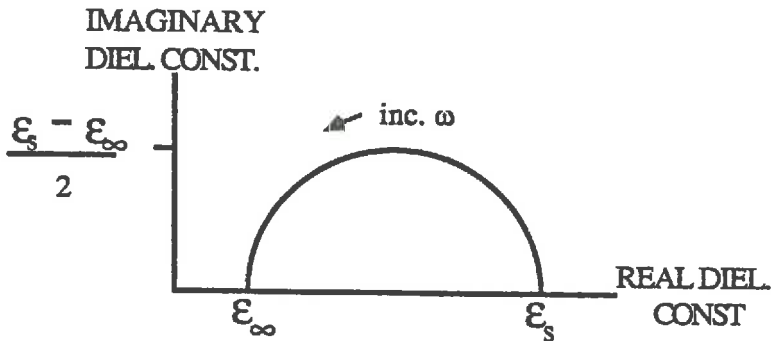
FIG. 3 GENERALIZED COLE-COLE DIAGRAM

The preceding derivation contains a number of important assumptions. One of the most restrictive is that the sample must be a dilute media so that there are no near field effects. Although liquid water has a strong intermolecular interaction and thus undergoes aggregation and other interactions, the Debye Relaxation equations fit the observed dielectric response to a surprising degree of accuracy (Hastead, 1973).

In general, the dipole moments in liquids and solids are not completely free to rotate. If one adopts the simple model that (in the absence of electrical fields) the dipole can assume two different orientations of equal energy and of opposite direction separated by an energy barrier, ΔE, then a temperature dependence in the relaxation time develops. This dependence is given by (Meakins, 1961) as

$$\tau = A e^{\left(\frac{\Delta E}{RT}\right)} \qquad (30)$$

where A is a constant, T is the absolute temperature, and R is the universal gas constant. Thus we see that the temperature dependence of the dielectric behavior of a media can help to elucidate the mechanism of dielectric relaxation.

Debye dipole relaxation type behavior is an extremely important concept in the study of dielectrics. A number of different phenomena besides the response of the permanent dipole moment of water molecules can be modeled as relaxation processes.

29

In many physical situations including mixtures of liquids and heterogeneous media, it has been found that a single relaxation time is unable to satisfactorily explain the observed data. The Cole-Cole equation (Cole and Cole, 1949) which has the following form

$$\varepsilon(\omega) - \varepsilon_\infty = \frac{\varepsilon_s - \varepsilon_\infty}{1 + (j\omega\tau)^{1-\alpha}} \qquad (31)$$

has been used to model experimental data in a variety of systems. This equation corresponds to a distribution in the relaxation times of the dipoles

$$f(\tau) = \frac{\sin\alpha\pi}{2\pi \cosh\left[(1-\alpha)\ln\left(\dfrac{\tau}{\tau_0}\right)\right] - \cos\alpha\pi} \qquad (32)$$

which represents a symmetrical distribution about the principal relaxation frequency, τ_0, of width α. Eq. 31 rationalizes to give

$$\varepsilon_r = \varepsilon_\infty + \frac{\left(\varepsilon_s - \varepsilon_\infty\right)\left[1 + (\omega\tau)^{1-\alpha}\sin\dfrac{\alpha\pi}{2}\right]}{1 + 2(\omega\tau)^{1-\alpha}\sin\dfrac{\alpha\pi}{2} + (\omega\tau)^{2(1-\alpha)}} \qquad (33)$$

and

$$\varepsilon_i = \frac{\left(\varepsilon_s - \varepsilon_\infty\right)\left(\omega\tau\right)^{1-\alpha}\cos\frac{\alpha\pi}{2}}{1 + 2\left(\omega\tau\right)^{1-\alpha}\sin\frac{\alpha\pi}{2} + \left(\omega\tau\right)^{2(1-\alpha)}} \qquad (34)$$

RESONANT CAVITY MEASUREMENTS

In this section, the theoretical basis of resonant cavity dielectric measurements is discussed as well as the experimental configuration used to make these measurements in this work. Fixed temperature resonant cavity dielectric response data for a number of soils is also presented.

RESONANT CAVITY EXPERIMENTAL PROCEDURE

A cavity consisting of conducting walls allows only a discrete set of electromagnetic waves to exist in its interior. The allowed frequencies of the cavity are dependent on the cavity geometry as well as the dielectric properties of the media filling the cavity. when a sample with a complex dielectric constant is placed in a resonant cavity, the observed set of resonances with air filling the cavity are observed to change. The resonant frequencies shift to lower values while the breadth (at half maximum) of the resonances increases. The shift in the resonances can be quantitatively related to the dielectric constant of the media in the cavity.

For a cylindrical cavity with perfectly conducting walls containing electromagnetic waves with a time dependence of $e^{-i\omega t}$, the discrete set of allowed resonance TM mode frequencies is given by

$$\omega_{mnp} = \frac{C}{\sqrt{\mu\varepsilon}}\left[\frac{X_{mn}^2}{R^2} + \frac{P^2\Pi^2}{D^2}\right] \qquad (35)$$

where m,n, and p are mode indices, c =the speed of light, X_{mn} = the nth root of the mth Bessel Function, R = the radius of the cavity, D = the length of the cavity, and μ,ε are, respectively, the magnetic permitivity and the dielectric constant of the material filling the cavity (Jackson, 1975). The indices m and p can take on integral values including 0 while the index n must be a positive integer. When 2.03R>D, the lowest frequency mode of the cavity is the TM_{010} mode, i.e. m=0, n=1, p=0. and has a resonant frequency of

$$\omega_{010} = \frac{2.405\,C}{\sqrt{\varepsilon}\,R} \qquad (36)$$

where μ has been taken to be unity. Now in general, ε may be complex which in turn causes the resonant frequency to be a complex number. This manifests itself in an exponential damping of the electric and magnetic fields within the cavity, i.e.

$$E(t) = E_0 e^{\left(\frac{-\omega_s t}{2Q}\right)} e^{(-i\omega_s t)} \qquad (37)$$

where ω_s is the peak resonance frequency of the cavity filled with a dielectric sample (a real number) and Q (the quality factor, also a real number) is indicative of the frequency spread of the resonance

peak and is equal to the resonance frequency divided by the width at half maximum.

Using eq. 36, and taking the ratio of the the complex resonance frequencies in air, ω_A (which can be taken to be real since the cavity has a very sharp resonance in air), and in a sample, ω_R (a complex number), gives

$$\frac{\omega_A}{\omega_R} = \sqrt{\varepsilon_s} \qquad (38)$$

where ε_s is the dielectric constant of the sample in the cavity, and the dielectric constant of air has been taken as unity. Furthermore we can relate the complex dielectric constant, ε_s, to the peak resonance frequency, ω_s (a real number), and the width at half maximum, Γ, as follows,

$$\omega_R = \omega_s - i\frac{\Gamma}{2} , \quad Q = \frac{\omega_s}{\Gamma} \qquad (39)$$

Substituting eq. 39 into eq. 38 and solving for the real and imaginary dielectric constants gives

$$\varepsilon_r = \frac{\omega_a^2\left(\omega_s^2 - \left(\Gamma/2\right)^2\right)}{\left(\omega_s^2 - \left(\Gamma/2\right)^2\right)^2 + \Gamma^2\omega_s^2} \qquad (40)$$

$$\varepsilon_i = \frac{\omega_a^2 \, \omega_s \, \Gamma}{\left(\omega_s^2 - \left(\Gamma\big/2\right)^2\right)^2 + \Gamma^2 \omega_s^2} \qquad (41)$$

In order to make resonant cavity measurements, a cylindrical cavity of height 2.55 cm, diameter 12.70 cm, and volume 322.2 cm^3 was constructed out of brass. The dimensions of the cavity were chosen in order to maximize the frequency spread between resonant modes of the cavity and thus facilitate measuring the width of the resonances. With a lossy dielectric sample in a cavity with a height approximately equal to the diameter, the individual resonances overlap greatly making it difficult or impossible to resolve individual resonances. The resonant cavity has a lid that can be removed or bolted down to insure good electrical contact with the rest of the cavity. Two straight antennas (electric field coupling) of 2 cm length were placed at opposites ends of a diameter, half way up the wall of the cavity. The fundamental mode of the cavity, TM_{010} , with air as a dielectric, has a frequency of 1812.5 MHz and a Q value (ratio of the resonance frequency to the width at half maximum) in excess of one thousand With various soils in the cavity the resonance frequency ranges from about 1200 MHz at the dry end to 400 MHz near saturation, and the Q value from about 50 to 6.

The experimental configuration (see figure #4) consists of a resonant cavity filled with a soil sample connected to a network analyzer.

35
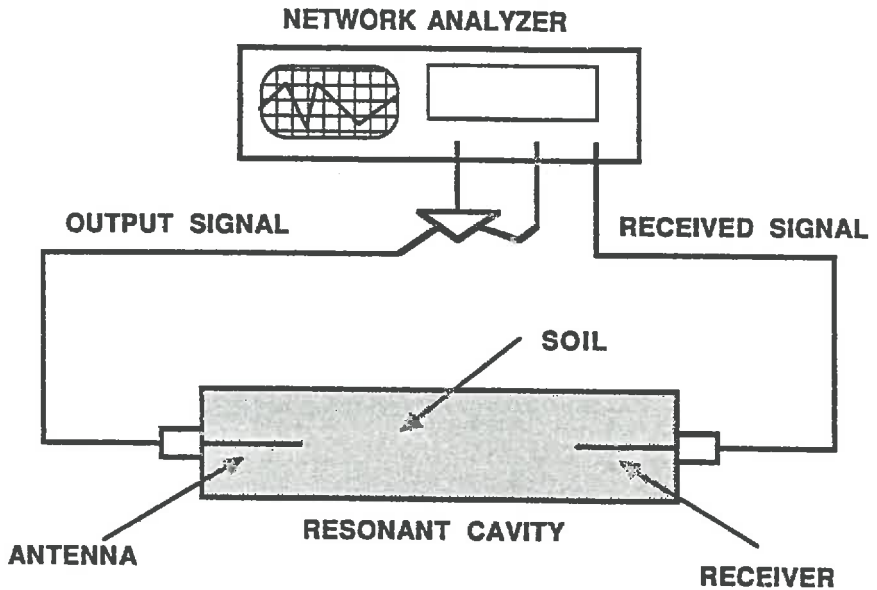
FIG. 4 SCHEMATIC OF RESONANT CAVITY EXPERIMENTAL
CONFIGURATION

The HP 8753A Network Analyzer is used to sweep an output signal
to an antenna and when the frequency is such that the cavity is near
resonance, the network analyzer receives a signal from the antenna
connected to the input port. This input is shown schematically in the
following figure. The resonance frequency and Q value were then
recorded.
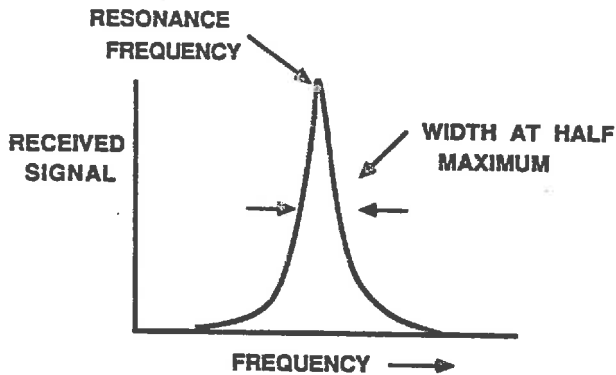
FIG. 5 TYPICAL RESONANCE RESPONSE

The dielectric behavior of a soil as a function of water content is evaluated in the following manner. First the weight of the empty cavity is recorded. A water saturated slurry of the soil to be studied is carefully packed into the cavity. Care must be exercised to insure that the sample completely fills the cavity. The cavity lid is then bolted back in place and the weight of the resonant cavity with soil is then recorded. The resonant cavity is then connected to the network analyzer and the resonance frequency and Q value are recorded.

The lid is then removed and water is allowed to evaporate (a heat lamp was used in some cases to speed this process). The lid is then bolted back in place and approximately two hours is allowed for the moisture in the sample to equilibrate following which the resonance frequency and Q value are recorded. This equilibration can be observed by monitoring the observed resonance. In a number of cases, the resonance was measured in the evening and again in the morning. The agreement in the calculated dielectric constant is typically better than 1%. In one case a sample was left

37

undisturbed for 35 days and the dielectric constant then agreed within 1.1% with the value obtained 2 hours after sealing the cavity. The procedure of drying, weighing the cavity, and measuring the resonance frequency is continued until the sample is dry. The soil was assumed to be dry when the weight of the cavity did not change over several hours of exposure to temperatures of approximately 100 ºC. Using the weight of the empty cavity, weight of the cavity filled with dry soil, cavity volume and weight at each reading allows one to compute a volumetric water content for the sample and the bulk density of the soil in the cavity.

RESONANT CAVITY DATA

A total of four different soil samples were analyzed using a resonant cavity technique. The soils used were Ottawa Sand, Hart Sand, Manchester Silt, and Wilder Silt. The soil samples were obtained, as were all the samples in this work, from the Army's Cold Regions Research and Engineering Laboratories (CRREL) located in Hanover, New Hampshire. The soils were packed in the resonant cavity to the following bulk densities Hart Sand 1.439 g/cm^3, Ottawa Sand 1.675 g/cm^3, Manchester Silt 1.607 g/cm^3, Wilder Silt 1.590 g/cm^3. An attempt to collect resonant cavity data using a fifth soil, Fort Edwards clay, was unsuccessful. The sample underwent extensive shrinking and cracking during drying. Since the analysis of the resonant cavity data depends on the cavity being uniformly and completely filled, reliable data for this sample could not be obtained. The following graphs show the measured real and imaginary

dielectric behavior of the four samples (figures #6 and #7). To the right of each graph is a plot symbol key with the corresponding plot symbol for each of the soils with obvious abbreviations. A number of interesting features are readily apparent.

REAL DIELECTRIC CONSTANT VS. WATER CONTENT FOR FOUR DIFFERENT SOIL TYPES
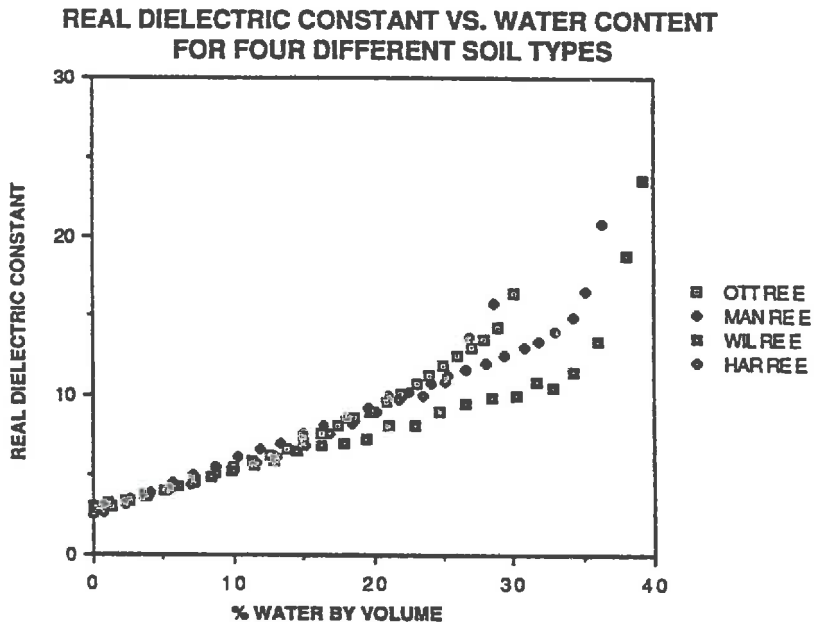
FIG. 6 REAL DIELECTRIC CONSTANT RESONANT CAVITY DATA FOR
FOUR SOILS

39

IMAGINARY DIELECTRIC CONSTANT VS. WATER CONTENT FOR FOUR DIFFERENT SOIL TYPES
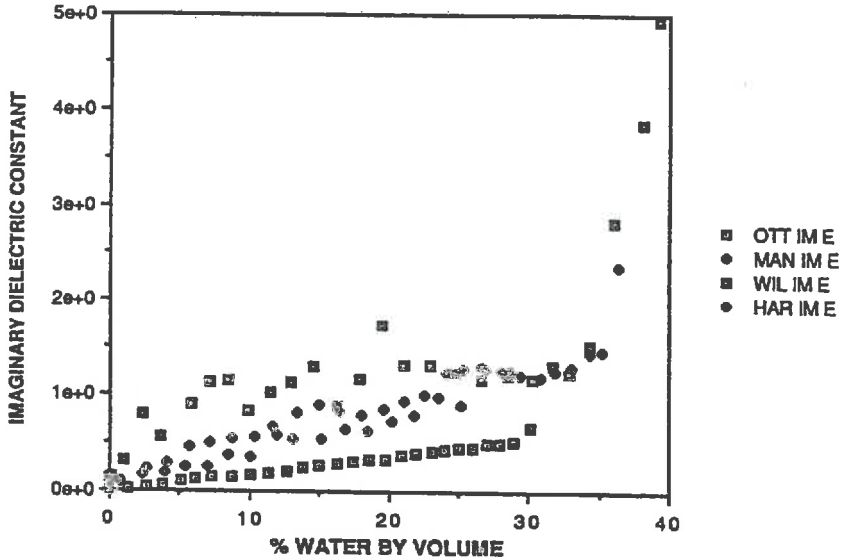
FIG. 7 IMAGINARY DIELECTRIC CONSTANT RESONANT CAVITY DATA FOR FOUR SOILS

The plot of real dielectric constant versus water content shows a striking lack of dependence on soil type, particularly at low water contents. At higher water contents the curves for the four different soil types begin to diverge. In addition, the two sands have a higher dielectric constant than the two silts at higher moisture contents. The anomalous behavior of the highest moisture content points for each soil are, I believe, not accurate. This erratic behavior stems from standing water in the bottom of the cavity for these oversaturated conditions. The plot of the imaginary dielectric

40

constant versus water shows a marked linear trend, particularly for Hart Sand, Ottawa Sand, and Manchester Silt. In addition, the imaginary dielectric constant falls to near zero for all completely dry soil samples. Finally, the imaginary dielectric constants of these four different soils are in order of magnitude agreement.

As will be seen in the section dealing with the temperature dependence of the dielectric properties of moist soils, the loss in Ottawa sand appears to be due to the relaxation of the free water present in the soil. The other soil samples have dielectric losses that are much greater than can be accounted for by this loss mechanism. If the mechanism of dielectric loss in the Tempe Cell measurements presented in a later section is due to ionic conductivity, interpolation to the higher frequencies used in the resonant cavity measurement gives dielectric losses that are in order of magnitude agreement with the resonant cavity dielectric losses. It is also possible that the dielectric loss is due to the relaxation of surface adsorbed water. Measurements of surface adsorbed water in Na-montmorillonite (Hoekstra and Doyle, 1971) indicates that adsorbed water relaxes at a frequency of approximately 1 GHz and is of the right order of magnitude to account for the dielectric loss in the resonant cavity data.

One considerable complication to the theoretical analysis of the resonant cavity data is the inherent lack of control over the frequency at which the measurement is made. As the soil drys in the cavity, the frequency at which resonance occurs changes considerably. The following graph (figure #8) shows the dependence

4 1

on water content of the resonance frequency for Ottawa Sand and is representative of the behavior of the other samples as well.

RESONANT FREQUENCY OF CAVITY VS. OTTAWA SAND WATER CONTENT
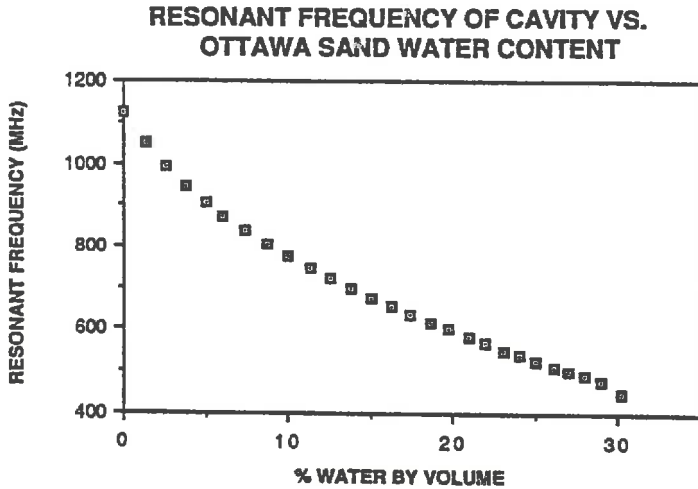
FIG. 8 FREQUENCY OF RESONACE FOR OTTTAWA SAND

COAXIAL PROBE MEASUREMENTS

In this section, the theoretical basis and experimental procedure for dielectric probe measurements at RF frequencies is discussed. A number of possible obscuring effects such as scaling and electrode polarization are considered and shown to be unimportant. The coaxial probe technique will be used in the Tempe Cell Measurements section to collect the bulk of the data in this work.

COAXIAL PROBE EXPERIMENTAL PROCEDURE

Due to the size of the required cavity, radio frequency measurements of soils with resonant cavity techniques are not practical. Through the use of a coaxial probe technique, RF measurements in soils can be made. In addition, direct control over the measurement frequency can be obtained. In the resonant cavity measurements described earlier, it was not possible to vary the moisture content while the resonant frequency was held fixed.

In order to make RF frequency (1-50 MHz) dielectric measurements of soil, a coaxial probe was constructed. A coaxial design has a number of advantages including a well specified electrical volume with very little fringing outside of the probe. The coaxial probe was constructed using tines instead of a solid outer conductor. This design has the advantage of allowing for the free movement of moisture into and out of the sensing volume. A coaxial

43

probe design also simplifies the analysis of the data because the probe behaves, to a large extent, as a coaxial wave guide for which electrical parameters such as the impedance have relatively simple closed forms. Figure # 9 shows the design and important dimensions of the coaxial probe. The probe has six metal tines in hexagonal pattern on the outside.

TOP VIEW   **SIDE VIEW**
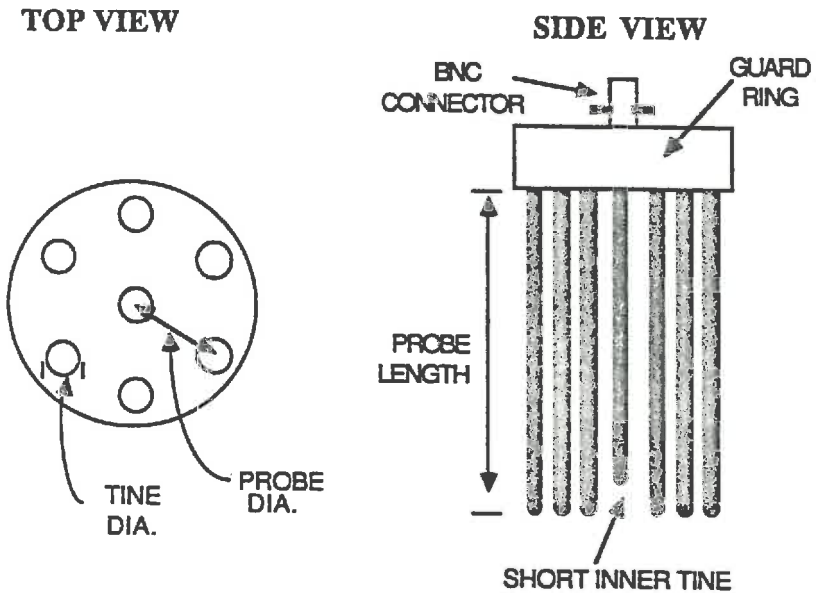
FIG. 9 COAXIAL PROBE CONFIGURATION

These are in electrical contact with a metal guard ring. The inner tine is connected to a BNC connector and is electrically insulated from the guard ring by a teflon insert. The inner tine is shorter than the outer tines in order to eliminate field fringing through the end of the probe.

44

Three different coaxial probes with different dimensions were constructed. The large and medium coax probes are fabricated out of brass while the small coax probe has a copper guard ring and stainless steel tines. The table below shows the relevant parameters for each probe.

Parameter	Small Coax	Medium Coax	Large Coax
Inner Tine Length	5.92 cm	7.87 cm	8.13 cm
Probe Length	6.35 cm	8.70 cm	8.89 cm
Tine Diameter	.470 cm	.635 cm	.635 cm
Probe Radius	1.14 cm	1.91 cm	3.81 cm
Capacitance of Sensing Vol.	2.38 pF	2.67 pF	1.84 pF
Stray Capacitance	2.38 pF	3.00 pF	2.92 pF

Using a HP 8753A network analyzer and a HP 8721A directional bridge, a signal can be sent down a 50 ohm coaxial cable into the probe and the reflected signal can be measured. The reflected signal depends on the impedance mismatch between the probe and the 50 ohm coaxial cable. The network analyzer, through the use of an internal conversion feature, can be configured to display the probe impedance directly. The impedance mismatch in turn is dependent on the dielectric properties of the sample in the probe. The network analyzer was configured to average over ten sweeps with a bandwidth of 10 Hz. Full S11 port calibration was performed in order to compensate for the finite directivity of the

directional bridge, cable length and crosstalk between cables. The experimental configuration is illustrated in figure #10.
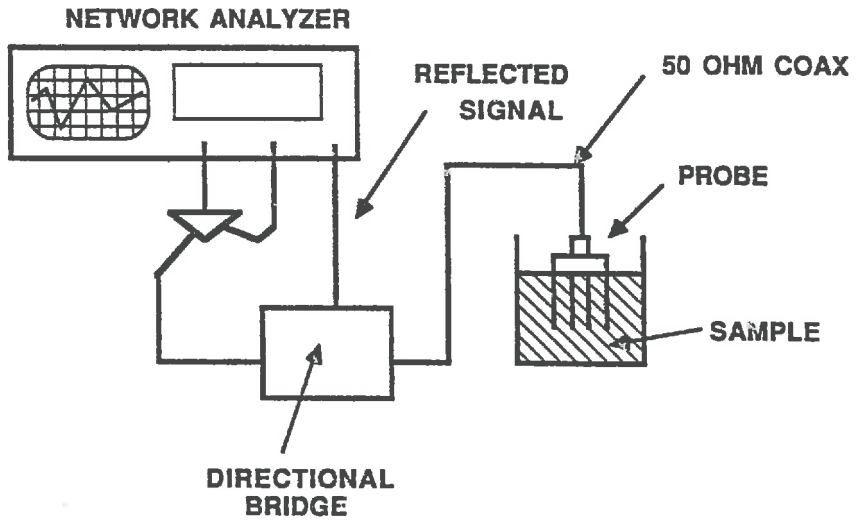
FIG. 10 EXPERIMENTAL CONFIGURATION OF COAXIAL PROBE
DIELECTRIC MEASUREMENTS

The impedance mismatch between the probe and the coaxial cable gives rise to, in general, a complex voltage reflection coefficient, Γ, (Collins, 1966) given by

$$\frac{Z_p}{Z_c} = \frac{1+\Gamma}{1-\Gamma} \qquad (42)$$

where Z_p = the impedance of the probe, and Z_c = the impedance of the coaxial cable which was 50 ohms in the experimental configuration used. The design of the coaxial probe is such that, to a

47

good approximation it can be treated as a concentric coaxial wave guide of a certain length terminated by a open circuit in parallel with a stray capacitance. The impedance of a coaxial waveguide of length, L, inner diameter, A, outer diameter, B, filled with a material of dielectric constant ,ε, is given by (Collins, 1966)

$$Z_p = \frac{2}{c\sqrt{\varepsilon}} \log\left(\frac{B}{A}\right) \cotanh\left(\frac{\omega\sqrt{\varepsilon}L}{c}\,i\right) \qquad (43)$$

where c is the speed of light. To solve for ε requires graphical techniques. However using the power series expansion of cotanh, i.e.,

$$\cotanh(x) = \frac{1}{x} + \frac{x}{3} + \ \text{..........} \qquad (44)$$

and for x smaller than unity, this series converges quickly. The argument of cotanh in eq. 43 is the length of the waveguide divided by the wavelength of the signal in the medium. For the experimental setup used, this quantity is significantly less than unity for frequencies up to about 50 MHz. Keeping only the first two terms in the expansion of cotanh in eq. 43 gives

$$Z_p = \frac{2 \log\left(B/A\right)}{\omega\varepsilon Li}\left[1 - \frac{\varepsilon\omega^2 L^2}{3c^2}\right] \qquad (45)$$

The first term in the brackets is the impedance of a coaxial capacitor filled with a dielectric in the limit that the wavelength is large compared to the length of the waveguide. The second term in the brackets is the term due to the second order expansion of cotanh and includes the effects of decreasing wavelength. The total impedance of the probe, Z_T, is

$$Z_T = \frac{1}{\frac{1}{Z_p} + \frac{1}{Z_s}} \quad \text{and} \quad Z_s = \frac{1}{\omega C_s i} \tag{46}$$

where Z_s = the stray impedance due to the BNC connector and guard ring contributing a stray capacitance, C_s . Using eqs. 45 and 46 and solving for ε gives

$$\varepsilon = \left(\frac{\frac{L}{2 \log\left(\frac{B}{A}\right)}}{\frac{1}{Z_T \omega i} - C_s} + \frac{\omega^2 L^2}{3 c^2} \right)^{-1} \tag{47}$$

In practice, the values B, A, and L are adjusted to give the best agreement between the calculated value of ε and the experimentally known value for water. The optimum values of B, A, and, L are in reasonable agreement with the physical dimensions of the probe. Without the use of this first order correction, the measured dielectric

49

constant of water at 50 MHz deviates from the known value by about 15%.

The BNC connector and guard ring contribute a stray capacitance, C_S, to the capacitance of the probe. In order to correct for this stray capacitance and measure the capacitance of the sensing volume, C_0, (the electrical volume into which a sample is placed) a simple procedure is followed. Each probe is immersed in distilled water and air at a known temperature. At all of the frequencies of interest, the probe impedance is measured and the total probe capacitance is calculated. The capacitance of the sensing volume, C_0, and the stray capacitance, C_S, are then given by

$$C_0 = \frac{C_W - C_A}{\varepsilon_W - \varepsilon_A} \quad \text{and} \quad C_S = C_A - C_0 \qquad (48)$$

where C_w, C_A, ε_W, ε_A are, respectively, the measured real capacitance in water, the measured real capacitance in air, the real dielectric constant of water at the specified temperature, and the real dielectric constant of air which is taken to be unity. The measured capacitance is defined by,

$$C_{meas.} = \frac{1}{\omega Z_T i} \qquad (49)$$

This expression includes the second order terms of eq. 43.

50

As a test of the above analysis, the probe was used to measure the dielectric constant of methanol. The experimentally measured value agreed with the literature value to within 1.5 %.

SCALING TEST

In order to determine if probe size influences the measured dielectric constant, a scaling experiment was performed. Using air and distilled water, the stray capacitance and the capacitance of the sensing volume for the large, medium, and small coaxial probes was determined. Using dry Ottawa Sand of known volume (approximately 2 liters), the impedance of all three probes was measured at 1, 2, 5, 10, 20, and 50 MHz. Care was taken to insert the probes in as uniform manner as possible. The sample was then removed from the beaker and a measured volume of water was added to the soil which was then mixed. This was placed back into the beaker in approximately six portions with moderate tamping between layers. From the measured packed volume and the known volume of added water, a volumetric water content could be calculated in the following manner

$$\Theta_w = 100 \times \frac{V_w}{V_s} \qquad (50)$$

where Θ_w = the volumetric water content in percent by volume, V_w = the total volume of water contained in the sample, and V_s = the total volume of soil and water. This procedure was repeated twice in

51

order to give impedance measurements for all three probes at the specified frequencies for four water contents. The water contents were roughly completely dry, slightly moist, moist, and near saturation. This entire procedure was repeated for two additional soil types- Manchester Silt and Varved Clay.

In the following graphs (figures #11-#16), the experimentally determined probe size dependence of the real dielectric constant and loss tangent for four different soil water contents is shown for Ottawa Sand, Manchester Silt and Varved Clay.

REAL DIELECTRIC CONSTANT VS. FREQUENCY FOR THREE
DIFFERENT PROBE SIZES IN OTTAWA SAND
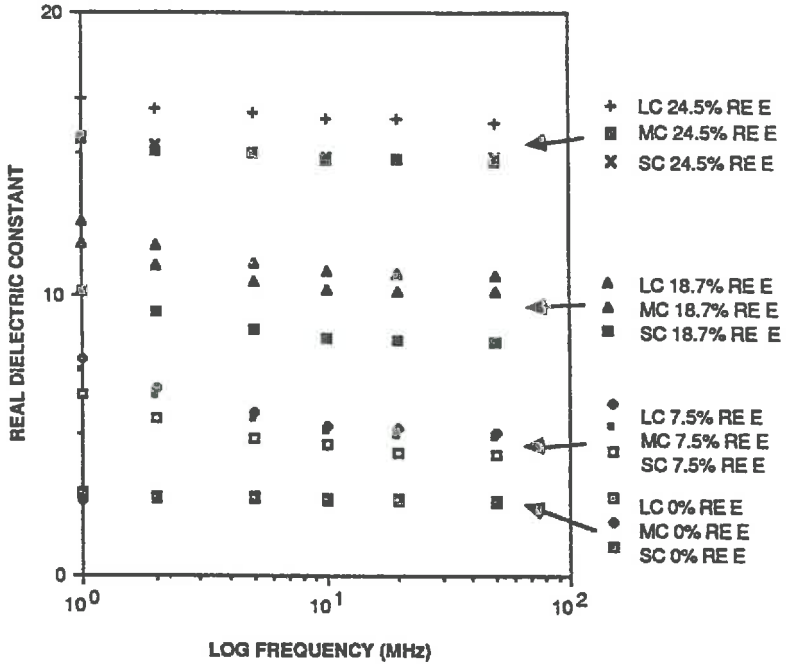
FIG. 11 REAL DIELECTRIC CONSTANT DATA FOR SCALING
EXPERIMENT IN OTTAWA SAND

53

REAL DIELECTRIC CONSTANT VS. FREQUENCY FOR THREE
DIFFERENT PROBE SIZES IN MANCHESTER SILT
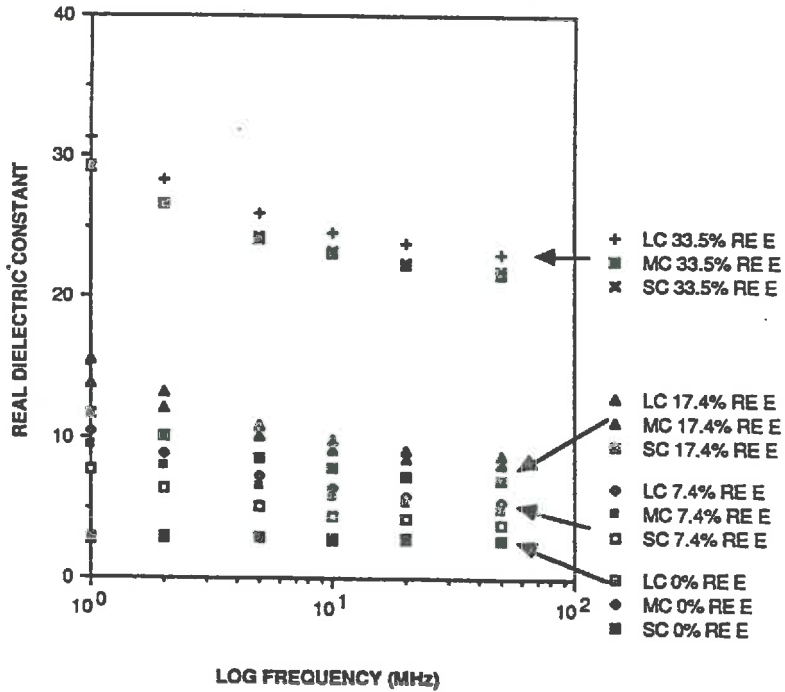
FIG. 12 REAL DIELECTRIC CONSTANT DATA FOR SCALING
EXPERIMENT IN MANCHESTER SILT

REAL DIELECTRIC CONSTANT VS. FREQUENCY FOR THREE
DIFFERENT PROBE SIZES IN VARVED CLAY
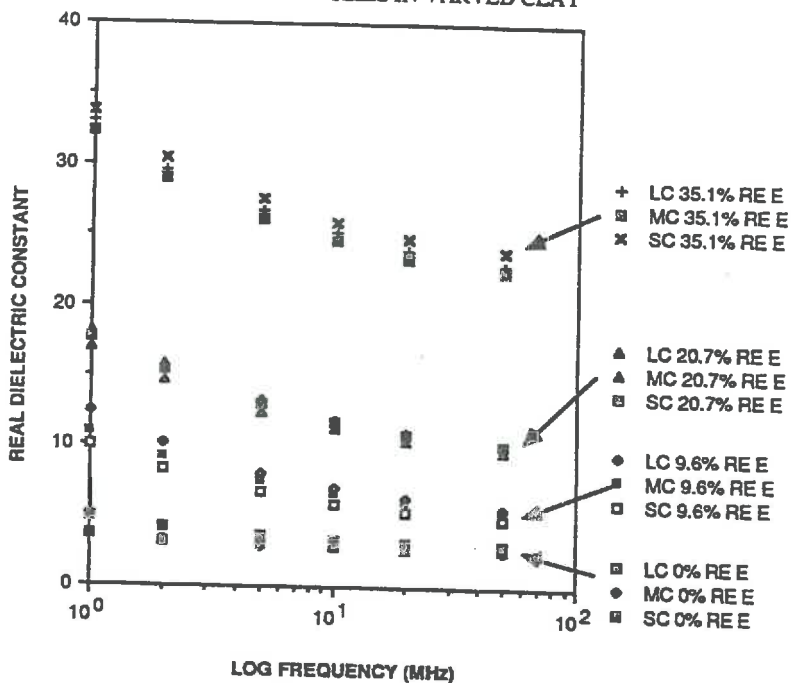
FIG. 13 REAL DIELECTRIC CONSTANT DATA FOR SCALING
EXPERIMENT IN VARVED CLAY
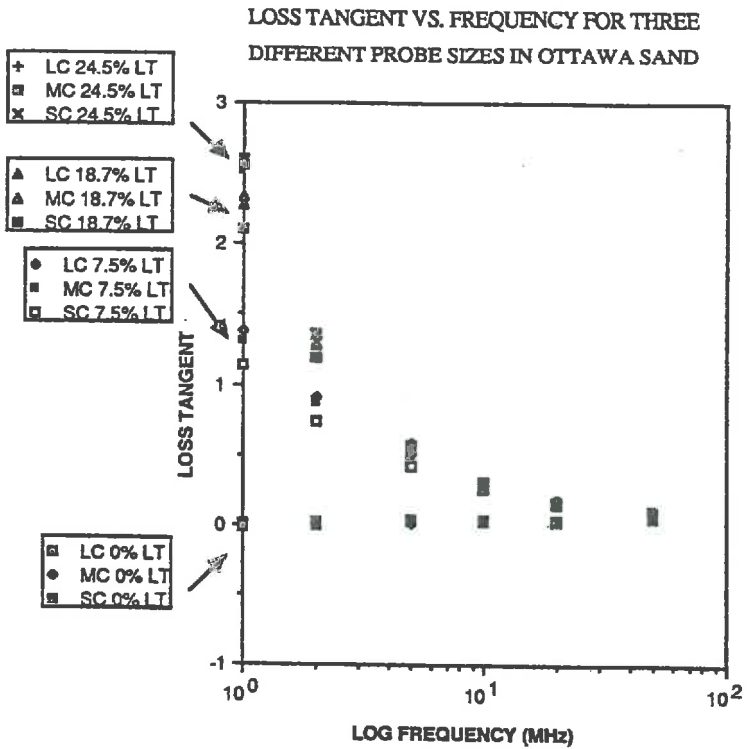
FIG. 14 LOSS TANGENT DATA FOR SCALING EXPERIMENT IN
OTTAWA SAND

LOSS TANGENT VS. FREQUENCY FOR THREE
DIFFERENT PROBES IN MANCHESTER SILT
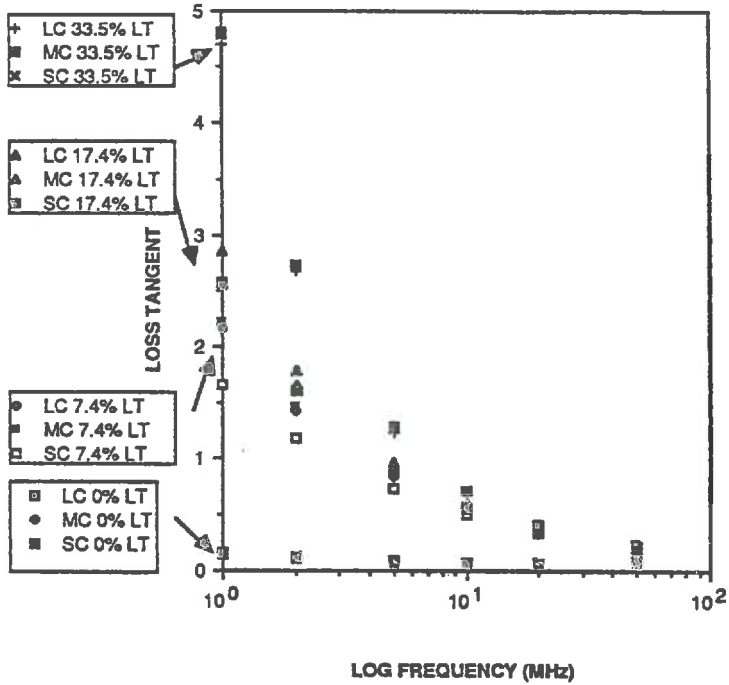
FIG. 15 LOSS TANGENT DATA FOR SCALING EXPERIMENT IN
MANCHESTER SILT

57
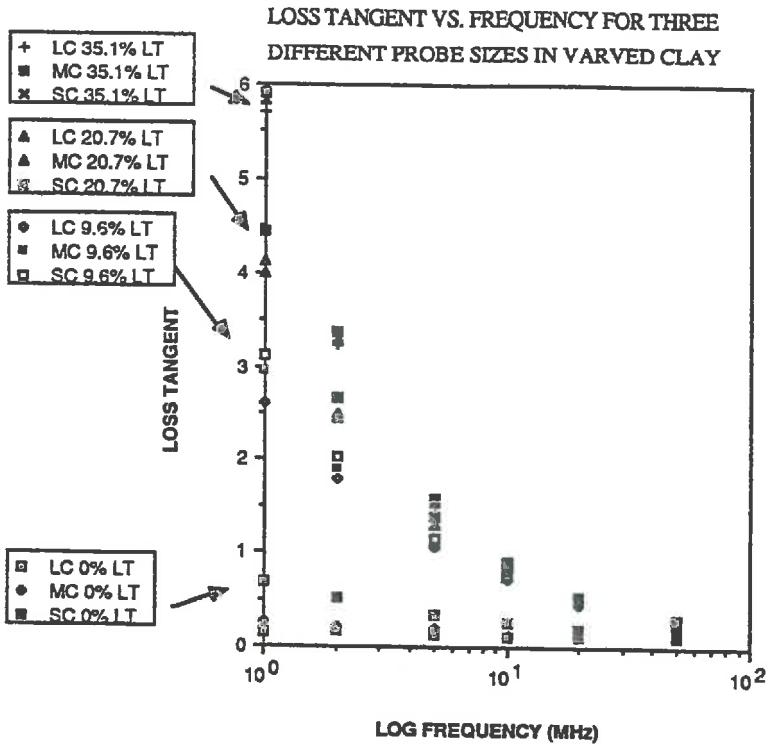
FIG. 16 LOSS TANGENT DATA FOR SCALING EXPERIMENT IN VARVED
CLAY

In the legend to the right of the graphs, LC, MC, and SC stand
respectively for large, medium, and small coaxial probes. The
numbers refer to the volumetric water content of the sample.

For a given moisture content, some dependence on probe size is
observed, particularly in the real dielectric constant. However when
all three soil samples are considered (Ottawa Sand, Manchester Silt,
and Varved Clay) there is no consistent dependence on probe size.

The observed dependence of the measured dielectric properties of the moist soil samples does not, in my opinion, reflect an intrinsic size scaling in these soils. I believe the differences between probes reflects the difficulty in 1) preparing a homogeneous soil sample by the crude preparation technique employed and, 2) The difficulties involved in inserting these probes into soil samples in a non-disruptive manner.

ELECTRODE POLARIZATION

Moist soil may contain dissolved salts which in contact with metal coaxial probe surfaces could give rise to the possibility of electrolytic action and subsequent electrode polarization. In response to an applied electric field, ions may migrate to an electrode and accumulate there to mimic dielectric polarization charge. In addition, the adsorption of polar molecules onto the electrode can also contribute to electrode polarization (Bard, 1980). This effect can result in anomalous dielectric behavior. Apparent dielectric constants rise to values as high as 10^7 at 10 Hz in some soils (Heim, 1984). Electrode polarization phenomena typically display a number of characteristics (Bard, 1980). First, electrode polarization effects tend to be nonlinear, i.e. the measured impedance of a system undergoing electrode polarization is highly dependant upon the voltage, or power, used to perform the measurement. Also electrode polarization effects are accentuated at lower frequencies where there is sufficient time to allow for charge buildup at the electrode surface.

59

In addition, they are very dependent on the surface state of the electrode; thin layers of contaminants such as oils can have a dramatic effect on electrode polarization. Finally, electrode shape, surface size and composition is of extreme influence in electrode polarization effects.

In order to preclude the existence of significant electrode polarization effects in the coaxial probe data, a number of observations can be used. The data presented in the previous section shows no systematic probe size dependence. However, between the three different probes there is a considerable variation in both probe composition and electrode size which if electrode polarization effects were significant should lead to a significant, systematic trend in the observed dielectric behavior between probes.

In an attempt to verify that the measured probe impedance is not a function of the power used to make the measurement, a number of power sweeps were performed. The network analyzer was configured to sweep the measurement power from -10 to 25 dBm at a frequency of 1 MHz. This frequency was used because it is the lowest used in any data collection, and if there are any significant electrode polarization effects they should be most apparent at lower frequencies. The experimental setup and instrument configuration was identical to that used in the scaling experiment except that the frequency was held fixed while the power was swept.

Power sweep measurements were made with five different samples- air, distilled water, .01M NaCl in distilled water, methanol, and nearly saturated wilder silt (chosen because of the dispersive

60

nature of this soil shown in subsequent data). Three important points can be made from the data of this experiment.

First, the measured power dependence of the impedance of the coaxial probe in all of the samples was very small. Typically, there was less than a .3% range of the impedance over the entire power sweep. Thus, for these samples, no significant nonlinear behavior was observed. Second, the determined dielectric constants for the distilled water and methanol are within less than 1% of their static values (Malmberg and Maryott, 1956; Weast, 1978). The good agreement with the known dielectric constants is strong evidence that surface adsorption or surface contamination is not affecting the coaxial probe data. Third, the impedance measurements in .01M NaCl produce a change of less than 3% in the calculated real dielectric constant as compared to pure distilled water. The loss tangent of this saline solution is approximately 30, far higher than measured loss tangents in any soil (reflecting the relatively high conductivity of this solution). In saline solutions the possibility arises of an interfacial structure, composed of ions and water molecules, between the electrode surface and the bulk solution (Bard, 1980). This interfacial zone can act as a capacitor in series with the bulk solution and thus markedly affect dielectric measurements of the bulk solution (Bard, 1980). The absence of any significant change in the real dielectric constant of the .01M NaCl solution is very strong evidence that this process is not occurring.

As a final test of the possibility that electrode effects are significantly perturbing the data, the following experiment was performed. A plexiglass box of approximate dimensions 15 cm x 15

61

cm x 15 cm was prepared with two circular ports. Into these two ports, two different probes were mounted and sealed. The two probes were then calibrated using air and distilled water at a known temperature. One probe was a standard small coaxial probe with 6 outer prongs while the other probe was identical except that every other outer tine had been removed to produce a 3 outer tine probe.

The box then was partially filled with saturated Manchester silt. The soil was then vibrated and tamped in an effort to insure uniform packing. This procedure was repeated until the soil occupied a volume of 1900 ml in the box. The two probes were then buried (with their tines parallel to the soil surface) a depth of 6 cm which was about one-half the depth of the soil in the box.

The probes buried in the soil form two different electrode configurations with very different surface areas. If electrode polarization is present, the two probes should produce markedly different dielectric behavior.

In turn each probe was connected to the network analyzer, and the impedance at 1, 2, 5, 10, 20, and 50 MHz was measured. The plexiglass box was then weighed which allows the volumetric water content to be determined. The sample was then exposed to air until a sufficient amount of moisture evaporated and then the box was sealed for at least 24 hours in order to remove moisture gradients in the soil. At moisture levels below about 5% by volume, a heat lamp was required to remove water in a reasonable amount of time. The soil was assumed to be completely dry when the weight changed less than .2 g after 4 hours of heating at approximately 50^0 C. This

procedure required three months to remove all the water from the sample. Figures #17 and #18 show the results obtained.

REAL DIEL. CONST. VS. WATER CONT. FOR TWO PROBES
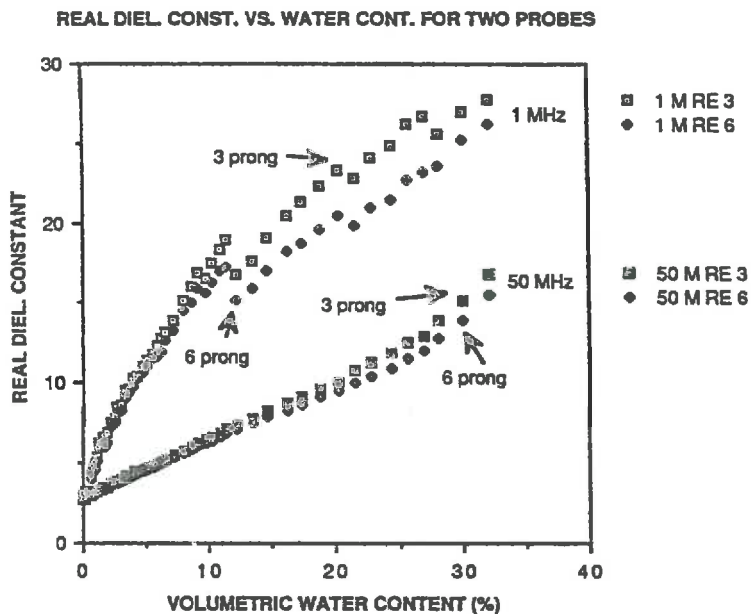
FIG. 17 REAL DIELECTRIC CONSTANT DATA FROM ELECTRODE
POLARIZATION EXPEREIMENT

63

IMAGINARY DIEL. CONST. VS. WATER CONTENT FOR TWO PROBES
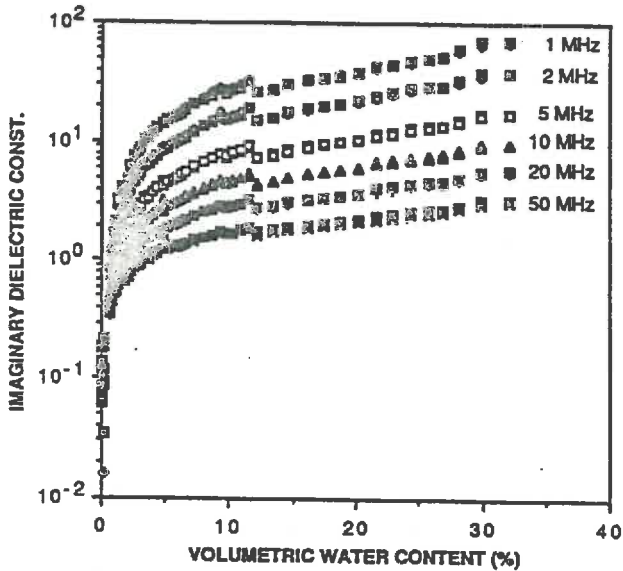
FIG. 18 IMAGINARY DIELECTRIC CONSTANT DATA FROM ELECTRODE
POLARIZATION EXPEREIMENT

A number of features are worthy of comment. The plot of real
dielectric constant vs. volumetric water content shows a significant
difference between the two probes at both 1 and 50 MHz.   The
difference is greatest at lower frequencies and at high volumetric
water contents.   At low moisture contents, the difference becomes
quite negligible.   Of interest is the observation that the difference
between probes increases with frequency, however it does not
increase with frequency as fast as one would expect if electrode
polarization was present.   The discontinuity in the 1 MHz data

probably reflects a 10 day interruption in data collection which was also accompanied by a considerable change in the ambient room temperature. The plots of imaginary dielectric constant vs volumetric water content show almost no difference between probes throughout the entire frequency range. Although care was taken to insure that the soil packing and moisture conditions were identical in both probes sensing volume, it is possible that variations in the sample contributed to the discrepancy between probes. The data from this simple experiment supports the claim that electrode polarization effects are of negligible importance.

The preceding arguments based on the scaling, power sweep, saline solution, and varying electrode surface data form a strong body of evidence precluding electrode polarization effects. It is of paramount importance to eliminate this possibility because the behavior of the soil data that has been collected could be mimicked by electrode polarization effects.

TEMPE CELL MEASUREMENTS

In this section, the experimental procedure (based on the coaxial probe technique) that was used to collect the majority of the data in this work is discussed. In addition, a subset of the data collected is presented, and the prominent features are outlined.

TEMPE CELL EXPERIMENTAL PROCEDURE

A number of serious difficulties plague the experimental procedure employed in the scaling experiments. One of the most severe is that encountered when one tries to prepare soils with a specified moisture content. At low water contents, particularly in clays, it can be extremely difficult to prepare a homogeneous, uniformly wetted sample. In addition, as the moisture content of the soil varies it is practically impossible to pack the sample to a fixed bulk density. It is also difficult to insert a coaxial probe into a soil sample in a reproducible manner and in a way such that there is no gap between the soil and probe tines. For these reasons a different experimental setup was developed.

In order to avoid the difficulties involved in the manual mixing of soil samples and the insertion of the coaxial probe, a special sample holder was designed. The design is a modification of a standard Tempe cell design (Reginato and Bavel, 1962). The sample holder consists of a plexiglass cylinder of length 8.51 cm and diameter 7.62 cm. Midway up the cylinder, a small coaxial probe

was epoxied into a hole in the plexiglass cylinder in order to form an airtight seal. One of the outside tines of the coaxial probe was hollow and into this tine, a Omega Engineering Inc. F3101 precision platinum resistance thermometer was placed. This was connected to an ohmeter which allowed, through the use of the manufacturer's calibration table, the soil temperature to be measured. Each end of the cylinder was equipped with a circular plexiglass disk with approximately 50 holes of 1.5 mm diameter placed in uniform pattern over the disk. This formed a sample holder with a total volume of 384.4 cm^3.

Two plexiglass endcaps were constructed in order to fit snugly over the ends of the sample holder and to hold the perforated disks firmly onto the cylinder. The endcaps were equipped with O-rings in order to form an airtight seal against the sample holder. A clearance of approximately .8 cm was maintained between the indented portion of the endcaps and the perforated disk in order to allow water and air to move freely. A screw fitting to allow the endcaps to be connected to a water or vacuum system was placed on the top on the endcaps. Around the periphery of the endcaps, five clearance holes for bolts were drilled. The two endcaps can then be placed on the sample holder and bolted together to sandwich the sample holder and form an airtight system with a vacuum connection at each endcap. This combined sample holder has the advantage of being symmetrical, i.e. the top and bottom of the sample holder are identical.

The experimental configuration of the system is shown in the following diagram (figure #19)

67
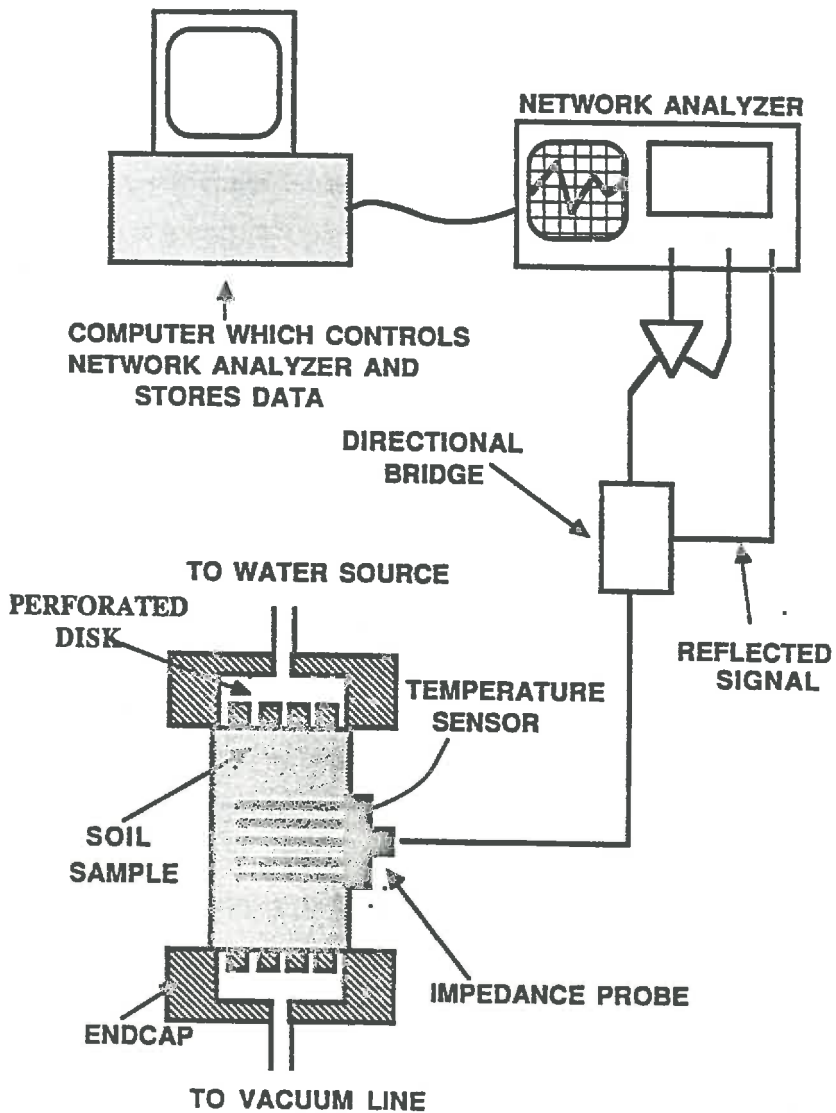
FIG. 19 TEMPE CELL EXPERIMENTAL CONFIGURATION

The RF portion of the experimental configuration; the network analyzer and the directional bridge, is identical to that employed in the previous section, Coaxial Probe Measurements, with one exception. Through the use of a HP 82990A controller card, an IBM XT Personal Computer was interfaced to the network analyzer to facilitate data collection and analysis. The analysis of the subsequent output is identical to that described in the Coaxial Measurements Section. The controller card, through the use of software written by Bayrd Johnson (a undergraduate research assistant) allowed the computer to configure the network analyzer for data collection and to store on floppy disk the data collected by the network analyzer. The data were then transferred to another computer for data reduction.

The network analyzer was configured with internal software to convert the measured signal reflection directly to a magnitude and phase of the probe impedance. Full S11 port calibration was employed. A sweep averaging factor of ten as well as a bandwidth of 10 Hz was employed to reduce noise. The frequency range from 1 to 50 MHz was swept at 1 MHz intervals. Data for all these frequencies could then be transferred to the controlling computer.

The soil was placed in the sample holder using the following procedure. The combined sample holder weight was measured and recorded. A piece of filter paper was then placed on the perforated disk facing the interior of the sample holder. The filter paper prevents soil from moving through the holes in the disk while still allowing the free movement of air and water. The bottom endcap was then placed on the sample holder to firmly hold the perforated

disk to the sample holder. A vacuum source was then attached to the endcap and a suspension in distilled water of the soil to be studied was prepared. This was poured in small increments into the open top of the sample holder. The vacuum being pulled on the bottom of the sample holder facilitates an even sample packing. After about every cm of sample was added to the sample holder, moderate tamping was employed. Although tamping in and around the coaxial probe tines presents some difficulty, the soil appeared to be of a uniform nature throughout the sample holder. Upon packing to the top of the sample holder, the other perforated disk equipped with filter paper was put in place. The other endcap was then attached and the the two endcaps were then bolted together using moderate force to insure that the two O-rings formed a tight seal with the endcaps. The combined sample holder filled with the near saturated soil sample to be studied was then connected to a vacuum source and checked for leaks.

Great care was taken during filling the sample holder. As much as two days were spent in preparing one sample. A sloppily filled sample holder results in hollow cavities forming in the sample and the sample pulling away from the walls of the sample holder. One advantage of the plexiglass sample holder is that it allows the investigator to continuously monitor the sample during the measurement process and verify that the sample is homogeneous. Of the six soils studied, only Fort Edwards Clay presented any problems during the measurement runs. As the sample was dried, this clay exhibited obvious shrinking and cracking. During drying of all the other samples, only slight cracking or shrinking developed.

After the soil to be studied has been placed in the sample holder, a measurement run can be started. The network analyzer is allowed to warm up and it is then calibrated. The controlling computer is started and loaded with the data collection software. The bottom endcap of the sample holder is connected to a mechanical vacuum pump equipped with a water trap and a anhydrous calcium sulfate water vapor trap with a valve between the traps and the sample holder. The top endcap of the sample holder is connected to a distilled water reservoir with a valve placed between the sample holder and the water reservoir.

The valve to the water reservoir is closed and the valve to the vacuum line is then opened. After a near vacuum has been achieved in the sample holder, the valve to the vacuum line is closed and the valved to the water reservoir is opened. This completely and uniformly saturates the soil sample completely filling all the pore spaces. The valve to the water reservoir is then closed and the sample holder is disconnected from both the water and vacuum lines. Water present in the space between the sample holder and the endcaps is removed as well as water present in the vacuum and water lines.

The sample holder is then weighed. From the weight of the empty sample holder, the weight of the sample holder filled with completely dry soil, and the volume of the soil sample a volumetric water content for the sample and the fixed bulk density can be determined. When the temperature of the sample reaches 20-23 ^0C (as determined by the resistance thermometer in the probe), the 50 ohm coaxial cable leading to the network analyzer is then connected

and the data collection software is run. The data (in the form of the magnitude and phase of the probe impedance) for all 50 frequencies is collected and displayed on the controlling computer's screen. The user is asked if the data is to be stored. If the answer is yes, the user is prompted for the soil type, weight of the sample holder, and any comments he would like to attach to the data. The data are then stored on a floppy disk.

The water reservoir is then removed which allows air to be pulled through the sample if desired. The vacuum and air lines are then reconnected and the air valve is closed while the vacuum line is opened. Typically because the sample is overly saturated initially, liquid water is pulled out of the sample holder. When approximately 4 ml of water has been removed corresponding to a change in volumetric water content in the sample of about 1%, the vacuum line is closed.

Approximately two hours is allowed for the sample to equilibrate with respect to temperature and moisture movement. This appeared to be an ample length of time for equilibration. A number of samples were left overnight with a typical change in the measured impedance of less than 1% between evening and morning. One sample of about 15% water by volume was left in the sample holder for two weeks. The measured impedance had drifted only .5% over the period.

The sample holder is then weighed and the data collection software is run. After removing water from the sample, the sample holder is flipped before reconnecting to the vacuum and air lines. This helps to avoid the formation of any moisture gradients within

the soil. The process of removing water, allowing equilibrium to be achieved, and collecting the data is then repeated. As the sample drys, liquid water is no longer removed but rather water vapor. As the sample drys, it can take greater than one hour to remove what amounts to 1% volumetric water content. The vacuum drying of the sample causes the temperature of the soil to drop sharply. This necessitates care in insuring that when the data are collected the sample has reached room temperature throughout the sample.

When the data collection run has been finished, the soil sample is completely dry. The soil was considered dry when four hours of vacuum pumping produced less than a .1% change in the percentage volumetric water content. The weight of the sample holder filled with the dry sample is then recorded. The floppy disk contains a file with 30-50 sets of data for all 50 frequencies. Each set has an associated sample weight which allows the corresponding volumetric water content to be calculated.

TEMPE CELL DATA

A total of six different soil types were investigated. The soils and the bulk densities to which they were packed to are as follows-Hart sand 1.656 g/cm^3, Ottawa sand 1.699 g/cm^3, Manchester silt 1.536 g/cm^3, Wilder silt 1.601 g/cm^3, Varved clay 1.488 g/cm^3, and Fort Edwards clay 1.213 g/cm^3. Due to the shrinking and cracking accompanying drying of the Fort Edwards Clay, data for this soil type are of questionable validity. The following graphs (figures #20 - #30) show both the real dielectric constant and the loss tangent for

73

each soil at 1, 2, 5, 10, 20, and 50 MHz with one exception. Loss tangent data for Ottawa sand is not shown. The loss tangent data is not reliable due to a problem with the instrument calibration that was not noticed until towards the end of the data collection run. However, based on a number of checks, the real dielectric constant values were not appreciably affected.

REAL DIELECTRIC CONSTANT VS. WATER CONTENT FOR FIVE DIFFERENT FREQUENCIES IN OTTAWA SAND

Legend:
- □ 1 MHZ RE E
- ● 2 MHZ RE E
- ■ 5 MHZ RE E
- ◉ 10 MHZ RE E
- ■ 20 MHZ RE E
- □ 50 MHZ RE E
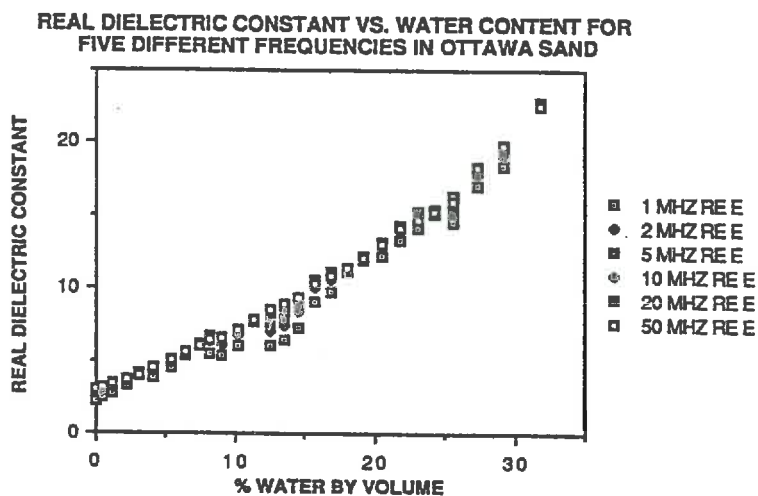
FIG. 20 REAL DIELECTRIC CONSTANT TEMPE CELL DATA FOR OTTAWA SAND

**REAL DIELECTRIC CONSTANT VS. WATER CONTENT FOR
FIVE DIFFERENT FREQUENCIES IN HART SAND**

Legend:
- 1 MHZ RE E
- 2 MHZ RE E
- 5 MHZ RE E
- 10 MHZ RE E
- 20 MHZ RE E
- 50 MHZ RE E
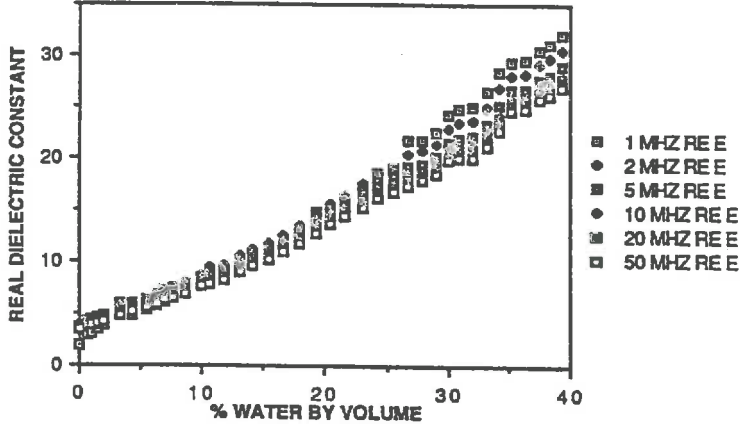
FIG. 21 REAL DIELECTRIC CONSTANT TEMPE CELL DATA FOR HART

SAND

**REAL DIELECTRIC CONSTANT VS. WATER CONTENT FOR
FIVE DIFFERENT FREQUENCIES IN MANCHESTER SILT**

Legend:
- 1 MHZ RE E
- 2 MHZ RE E
- 5 MHZ RE E
- 10 MHZ RE E
- 20 MHZ RE E
- 50 MHZ RE E
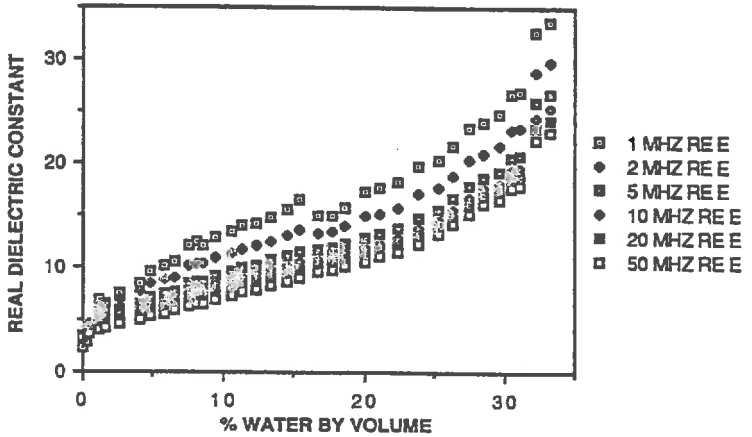
FIG. 22 REAL DIELECTRIC CONSTANT TEMPE CELL DATA FOR

MANCHESTER SILT

75
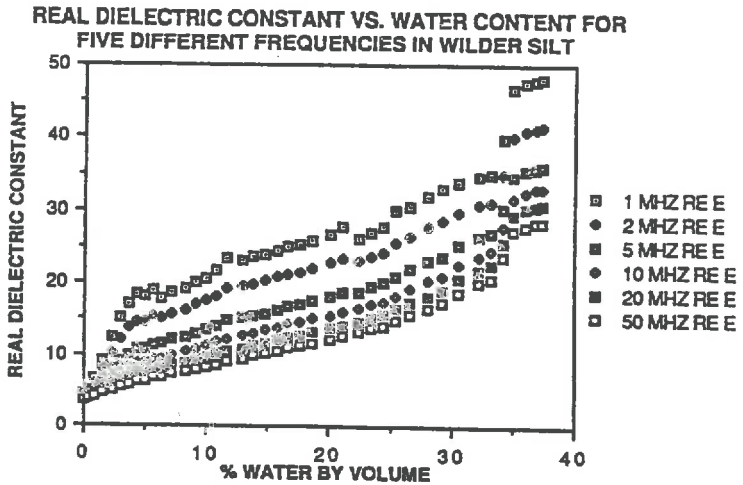
FIG. 23 REAL DIELECTRIC CONSTANT TEMPE CELL DATA FOR WILDER

SILT
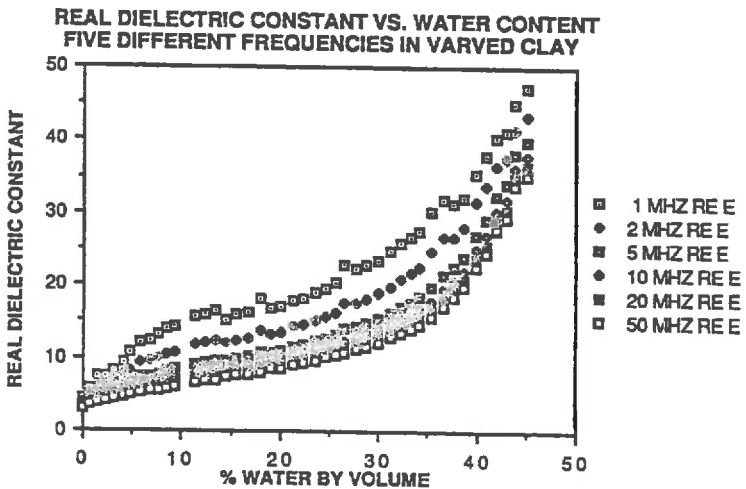
FIG. 24 REAL DIELECTRIC CONSTANT TEMPE CELL DATA FOR

VARVED CLAY

REAL DIELECTRIC CONSTANT VS. WATER CONTENT FOR FIVE DIFFERENT FREQUENCIES IN FT. EDWARDS CLAY
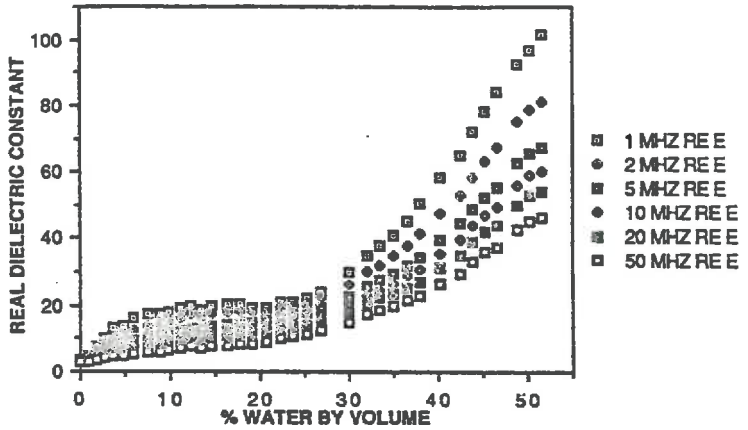
FIG. 25 REAL DIELECTRIC CONSTANT TEMPE CELL DATA FOR FT. EDWARDS CLAY
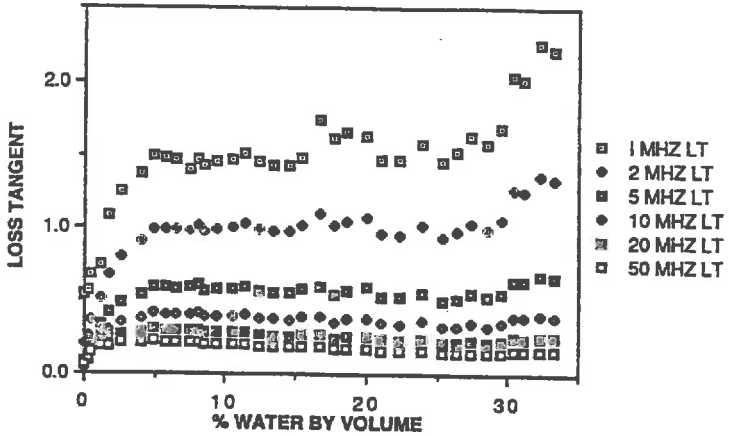
LOSS TANGENT VS. WATER CONTENT FOR FIVE DIFFERENT FREQUENCIES IN HART SAND

FIG. 26 LOSS TANGENT TEMPE CELL DATA FOR HART SAND

77

FIG. 27 LOSS TANGENT TEMPE CELL DATA FOR MANCHESTER SILT
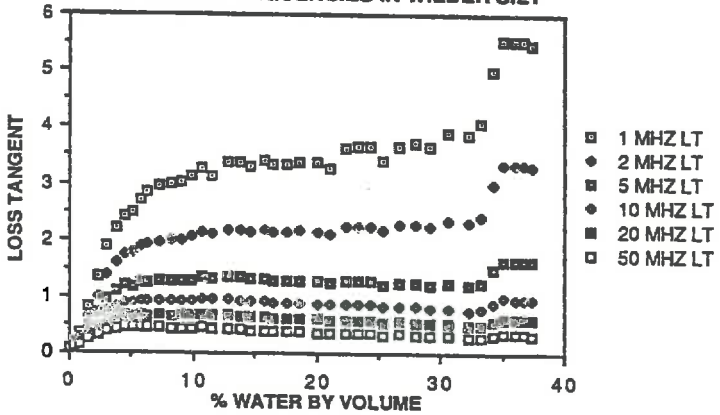
FIG. 28 LOSS TANGENT TEMPE CELL DATA FOR WILDER SILT
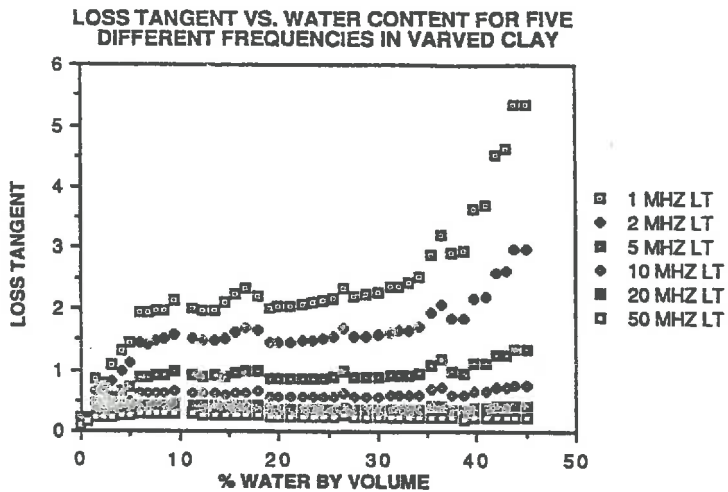
FIG. 29 LOSS TANGENT TEMPE CELL DATA FOR VARVED CLAY
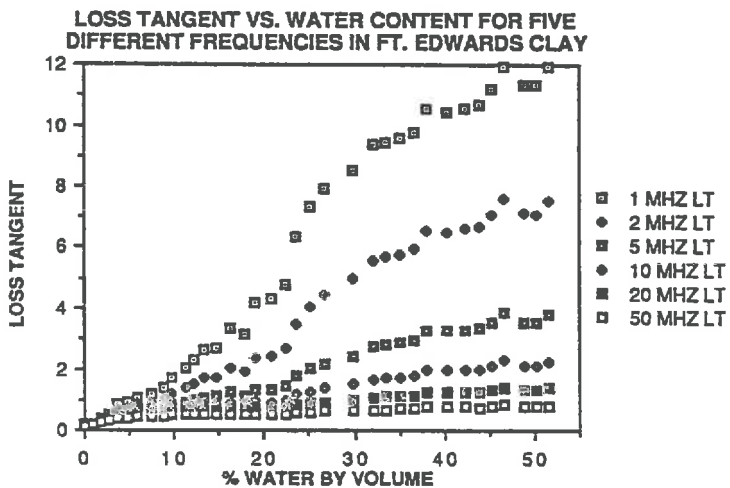
FIG. 30 LOSS TANGENT TEMPE CELL DATA FOR FT. EDWARDS CLAY

79

The above graphs have a number of striking features. One of the most apparent is the marked frequency dependence of the dielectric properties of the soils investigated. In all the samples, except Ottawa Sand, at all water contents the real dielectric constant is highest at 1MHz and lowest at 50 MHz. The frequency dependence of the real dielectric constant also is greatest at high water contents and drops as the water content of the sample is reduced. Between a water content of 10% to 0% by volume, the frequency dependence almost completely disappears. The frequency dependence of the dielectric constant also shows a significant variation between soil types. The dependence on frequency increases as the soil type changes from sand through silts to clays.

The graphs of the loss tangent versus water content illustrate that for all the soil types except Fort Edwards Clay, the loss tangent is relatively independent of water content for intermediate moisture values. There is also an even more dramatic frequency dependence than for the real dielectric constant. There also appears to be a very strong correlation between the range of the loss tangent and the range of the real dielectric constant For example, Fort Edwards clay has a very large spread in the loss tangent at high water contents, approximately 1 to 12 as the frequency varies from 50 to 1 MHz. The real dielectric constant varies from about 40 to 100 as the frequency changes from 50 to 1 MHz. The corresponding spread in the loss tangent and real dielectric constant for high water content Hart sand is .1 to 1 and 25 to 30. At very low water contents this is even more apparent. For example, the frequency dependence in the real dielectric constant of Wilder silt begins to dramatically decrease

at about 5% water by volume. At this same water content, the loss tangent of Wilder silt begins to drop precipitously.

One other important observation is that, particularly in the clays, the real dielectric constant assumes very high values at the wet end of the curves. Dielectric constants as high as a hundred are observed in Fort Edwards clay at 1 MHz

As the following graphs shows (figures #31 and #32), the frequency dependence of the measured dielectric properties is striking and quite smooth for all the soils investigated. The volumetric water content of the sample is indicated, in %, in the key next to the abbreviation of the soil type.

FREQ. DEP. OF THE REAL DIEL. CONST. FOR SIX SOILS

Legend:
- □ HAR 30.81 RE
- ● OTT 30.76 RE
- ▣ MAN 31.10 RE
- ● VAR 31.22 RE
- ▦ EDW 29.89 RE
- □ WIL 30.61 RE
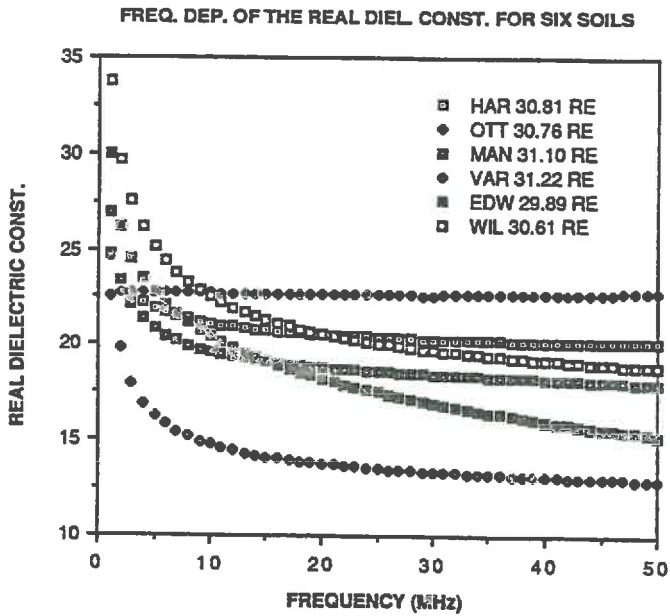
FIG. 31 FREQUENCY DEPENDENCE OF REAL DIELECTRIC CONSTANT
TEMPE CELL DATA FOR MOIST SOILS

82

FREQUENCY DEP. OF THE IM. DIEL. CONST. OF FIVE SOILS

Legend:
- HAR 30.81 IM
- MAN 30.10 IM
- VAR 31.22 IM
- EDW 29.89 IM
- WIL 30.61 IM
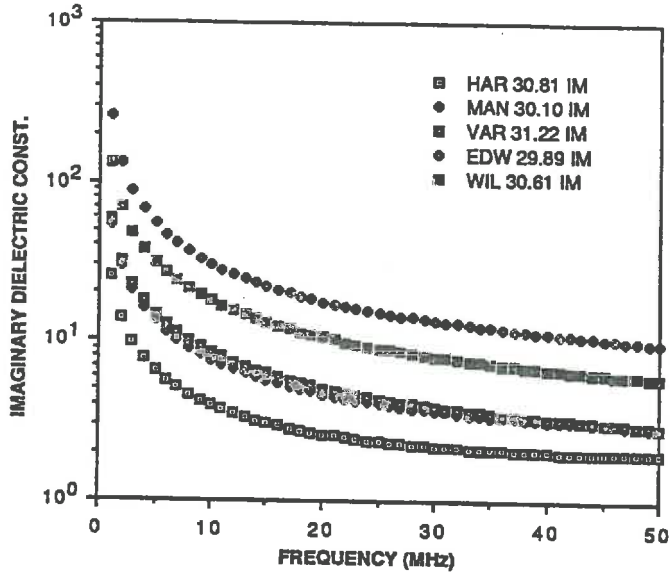
FIG. 32 FREQUENCY DEPENDENCE OF IMAGINARY DIELECTRIC
CONSTANT TEMPE CELL DATA FOR MOIST SOILS

The magnitude of the observed imaginary dielectric losses differ
widely but the frequency dependence of both the real and imaginary
dielectric constants are surprisingly similar between soils.   The
following graphs (figures #33 and #34) of the frequency dependence
of the dielectric properties of Manchester silt for various water
contents are typical.

8 3
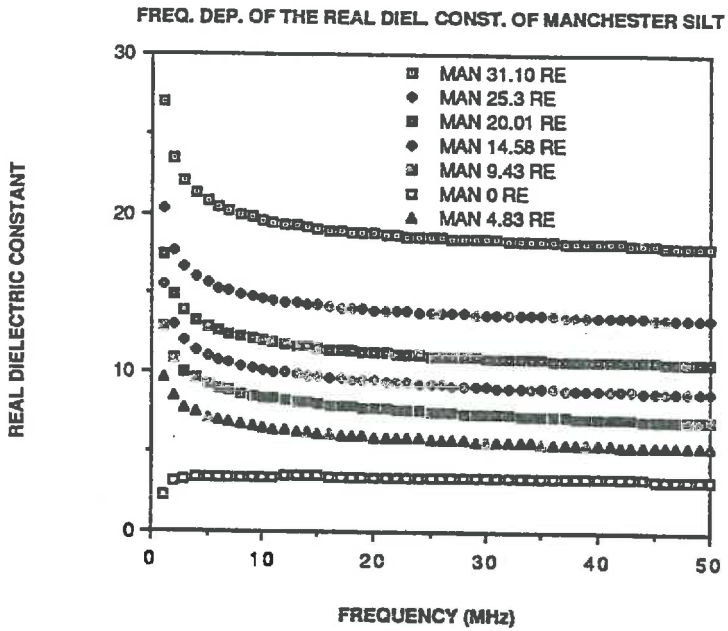
FIG. 33 FREQ. DEP. OF MANCHESTER SILT REAL DIEL. CONSTANT
TEMPE CELL DATA AS A FUNCTION OF MOISTURE CONTENT

FIG. 34 FREQ. DEP. OF MANCHESTER SILT IMAG. DIEL. CONSTANT
TEMPE CELL DATA AS A FUNCTION OF MOISTURE CONTENT
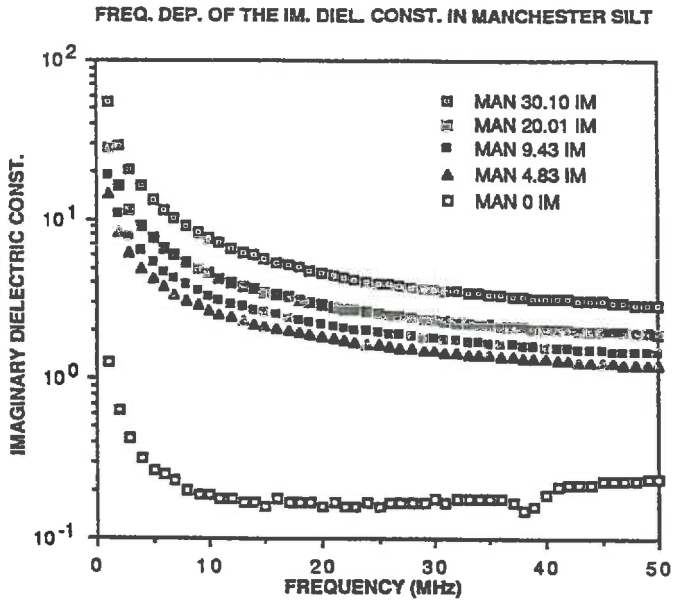
A number of interesting features are revealed in the above two
graphs. The real dielectric constant shows considerable frequency
dependence, decreasing with decreasing water content. At 0% water
there is almost no frequency dependence in the real dielectric
constant. The frequency behavior of the imaginary dielectric
constant is also very independent of moisture content except at 0%
water. As the soil drys, the magnitude of the imaginary dielectric
constant steadily falls but it retains its basic frequency dependence.

The following graph (figure #35) shows that over the frequency range studied in the Tempe cell measurements, the dielectric behavior follows a simple power law dependence on the frequency.

FREQUENCY DEPENDENCE OF THE DIELECTRIC
PROPERTIES OF 30.61%W WILDER SILT

REAL E $y = 31.684 * x^{-0.14}$ $R = 0.99$
IM E $y = 109.2347 * x^{-0.7643}$ $R = 1.00$
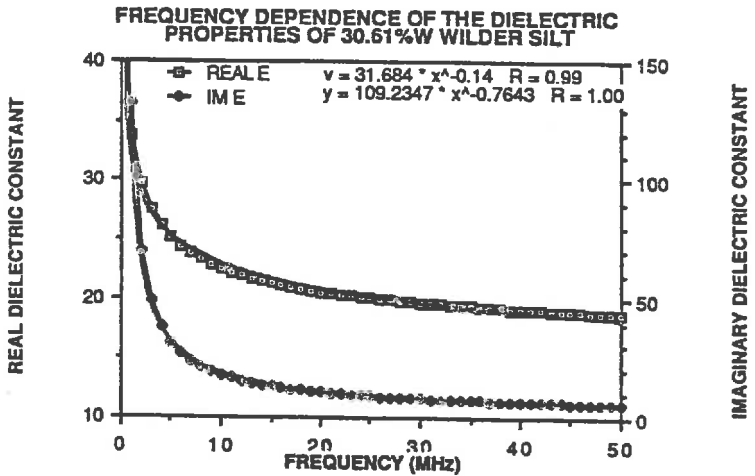
FIG. 35 FREQUENCY DEPENDENCE OF THE DIELECTRIC PROPERTIES OF
MOIST WILDER SILT

A Cole-Cole diagram (figure #36) for this same soil sample does not show the characteristic circular shape associated with simple Debye Dipole Relaxation. This unusual, but quite smooth and regular dispersion curve, requires further investigation.

COLE-COLE PLOT FOR 30.61% WATER WILDER SILT

150

IMAGINARY DIELECTRIC CONSTANT

FREQ. = 1 MHz

100

50

FREQ.= 50 MHz

0

0   25   50   75   100   125   150

REAL DIELECTRIC CONSTANT
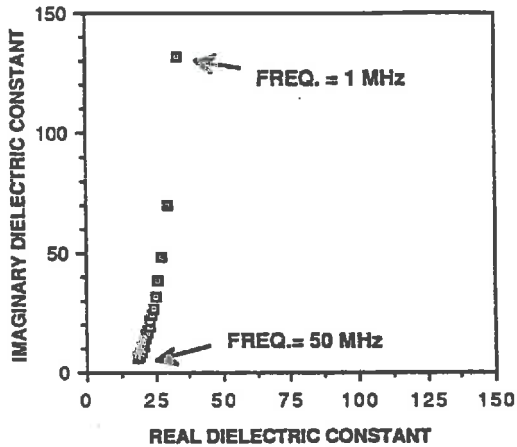
FIG. 36 COLE-COLE PLOT FOR MOIST WILDER SILT

The similarity in the frequency dependence of the dielectric properties of the soils investigated is striking. This behavior is indicative that the same mechanism is giving rise to the observed dispersion in all the soils.

TEMPERATURE DEPENDENCE OF THE DIELECTRIC PROPERTIES

In the following section, the temperature dependence of the dielectric response is investigated with coaxial probe and resonant cavity techniques. The collected data are presented and general trends are noted. The temperature dependence data are also used to calculate an activation energy for the relaxation mechanism at low frequencies (1 - 50 MHz) as well as to test a simple model of dielectric loss in moist soils at resonant cavity frequencies.

COAXIAL PROBE MEASUREMENTS

The temperature dependence of the dielectric constant of soils is of practical and theoretical interest. How the dielectric constant of moist soils depends on temperature can help to elucidate the mechanism of dielectric loss as well as test various dielectric models. Basic relaxation mechanisms are temperature dependent and hence dependence on temperature can be used to differentiate among competing possibilities. The significant temperature dependence observed in the dielectric response of moist soils is of practical interest since electromagnetic *in-situ* or remote sensing measurements will encounter moist soils with a wide range of temperatures.

In order to make these varying temperature measurements the following experimental setup was used. A small coaxial probe was

placed in a plexiglass tube of diameter 2.54 cm and length 9 cm. The probe was epoxied to the plexiglass tube to form a watertight seal. The plexiglass tube was then filled with the soil sample to be studied and a watertight endcap was then used to seal the tube. An approximately 15 cm long plexiglass tube was then slipped over the probe head containing the BNC connector in order to keep water from entering the coaxial cables connected to the probe. This entire setup was then placed in a circulating temperature controlled water bath. After allowing approximately 10 minutes for the sample holder to equilibrate to the bath temperature of $-.5$ ^0C , impedance measurements were made using the same network analyzer and controlling computer configuration described in the section on Tempe Cell measurements. The temperature of the circulating bath was then increased by about 2 ^0C and after waiting approximately 10 minutes impedance measurements were collected. This process was repeated until the sample reached a temperature of approximately 85 ^0C.

The results shown in the following three graphs (figures #37-#39)for a sample of moist Manchester Silt (34.2% volumetric water content) show a number of interesting features. The graph of real dielectric constant vs temperature shows a relatively small dependence on the temperature for the 2 and 5 MHz data but a rather significant dependence on temperature for the other frequencies.

REAL DIELECTRIC CONSTANT VS. TEMPERATURE FOR FIVE DIFFERENT FREQUENCIES IN MOIST MANCHESTER SILT

Legend:
- 1 MHZ RE E
- 2 MHZ RE E
- 5 MHZ RE E
- 10 MHZ RE E
- 20 MHZ RE E
- 50 MHZ RE E
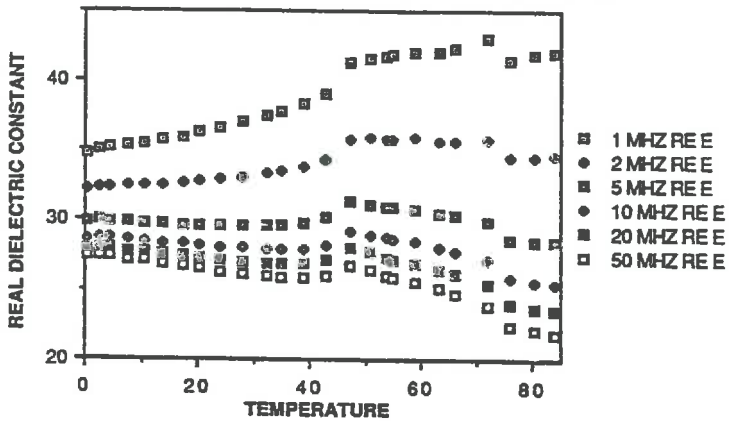
FIG. 37 REAL DIELECTRIC CONSTANT DATA AS A FUNCTION OF TEMPERATURE FOR MOIST MANCHESTER SILT

IMAGINARY DIELECTRIC CONSTANT VS. TEMPERATURE FOR FIVE DIFFERENT FREQUENCIES IN MOIST MANCHESTER SILT

Legend:
- 1 MHZ IM E
- 2 MHZ IM E
- 5 MHZ IM E
- 10 MHZ IM E
- 20 MHZ IM E
- 50 MHZ IM E

FIG. 38 IMAGINARY DIELECTRIC CONSTANT DATA AS A FUNCTION OF TEMPERATURE FOR MOIST MANCHESTER SILT

90
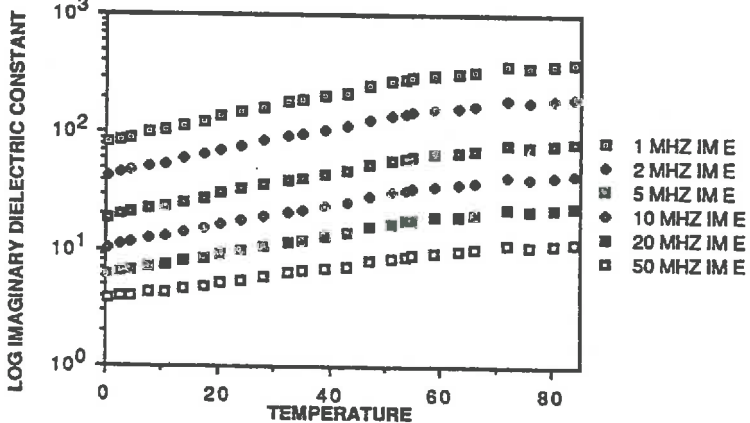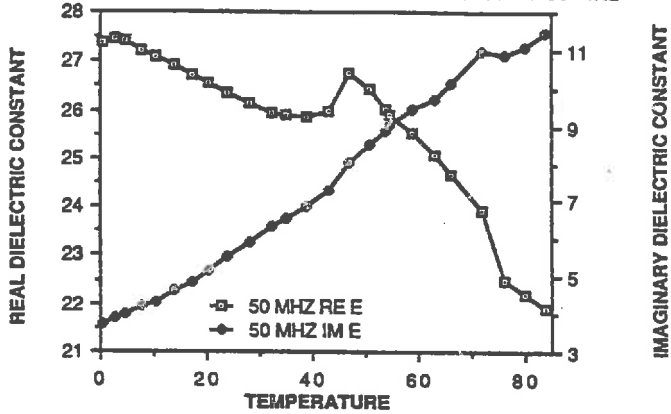
FIG. 39 RELATIONSHIP BETWEEN REAL AND IMAGINARY DIEL. CONST. FOR MOIST MANCHESTER SILT AS A FUNCTION OF TEMP.

The graph of the imaginary dielectric constant vs. temperature illustrates the uniform and significant increase in the imaginary dielectric constant with temperature. The last graph illustrates the correlation between the real and imaginary dielectric constants at 50 MHz. At lower frequencies, both the real and imaginary dielectric constants fall with temperature. As in other data presented, there is a marked correlation between changes in the real and imaginary dielectric constants.

Recalling eq. 30 which was presented earlier

$$\tau = A e^{\left(\frac{\Delta E}{RT}\right)} \qquad (51)$$

91

we see that the temperature dependence of the dielectric behavior is indicative of the activation energy, ΔE, of the relaxation mechanism. The experimental data indicate that the measurement frequencies are much higher than the relaxation frequency, so we have

$$\varepsilon_i = \frac{(\varepsilon_s - \varepsilon_\infty)\,\omega\tau}{1 + \omega^2\tau^2} \rightarrow \frac{(\varepsilon_s - \varepsilon_\infty)}{\omega\tau} \quad \text{for } \omega\tau \gg 1 \quad (52)$$

Thus at a fixed frequency

$$\varepsilon_i = Ce^{-\left(\frac{\Delta E}{RT}\right)} \qquad (53)$$

where C is some constant. Thus a plot of $\log(\varepsilon_i)$ vs $\log(1/T)$ should yield a straight line of slope $-\Delta E/R$. A plot of these quantities for Manchester silt is shown in figure #40.

TEMP. DEP. OF THE IM. DIEL. CONST AT 1 MHz
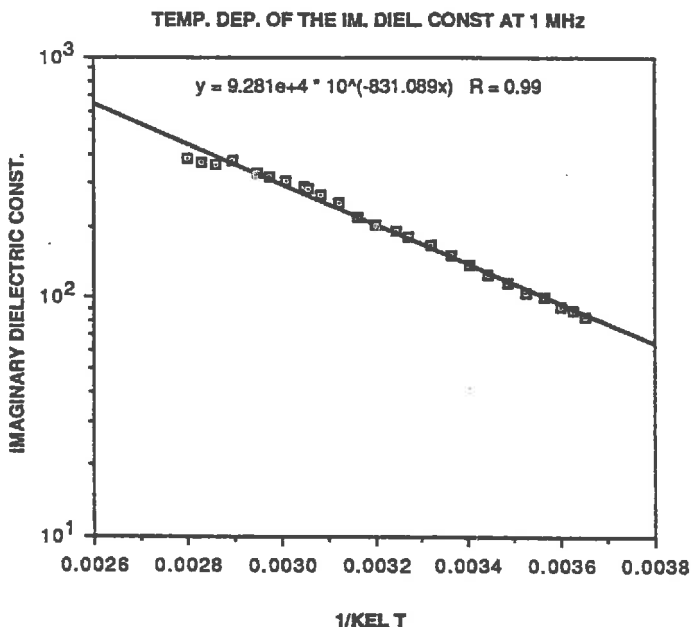
FIG. 40 PLOT OF IMAGINARY DIELECTRIC CONST VS. 1/T FROM
WHICH A RELAXATION ACTIVATION ENERGY CAN BE DEDUCED

The slope of this line gives an activation energy of approximately 7 kcal/mole.

RESONANT CAVITY MEASUREMENTS

Temperature measurements using the resonant cavity technique were also undertaken. The experimental technique employed was identical to the one described in the Resonant Cavity Experimental Procedures Section except for the following differences.

93

An Ottawa Sand sample containing 26.7% water by volume was placed in the cavity by placing a wet slurry in the cavity and allowing the sample to dry. The lid to the cavity was then bolted into place for the duration of the experiment in order to prevent further drying of the sample. At the end of the data collection run, the volumetric water content had changed less than .1%.

A thermocouple thermometer unit was attached using special heat conducting graphite paste to the lid of the resonant cavity. The entire cavity was then wrapped in an approximately 1 inch thick insulating styrofoam padding with a removable lid. The readout cables from the thermocouple protruded outside of the insulated cover which allowed the temperature of the cavity to be measured without opening the insulating cover.

The entire cavity was then heated to approximately 85 ^{0}C and placed in the insulating wrap. The cavity, in the insulating wrap, cooled at a rate of about 4 ^{0}C per hour. It was assumed that the rate of temperature change was slow enough that the entire cavity was in near equilibrium with the highly thermally conductive brass cavity lid. At approximately 2 ^{0}C intervals, the resonant frequency and Q value of the cavity was recorded. When the temperature of the resonant cavity approached the ambient room temperature, the cavity was placed in a refrigerator overnight. In the morning the procedure was repeated except that the cavity was allowed to warm instead of cool.

The results of the experiment are shown in the following graphs (figures #41 and #42). Immediately apparent is the discontinuity in the real dielectric constant at the temperature which

corresponds to the point at which the cooling and warming legs of the experiment meet. Curiously, this discontinuity is absent in the plot of imaginary dielectric constant versus temperature.

REAL DIELECTRIC CONSTANT VS. TEMPERATURE FOR 26.7% WATER OTTAWA SAND
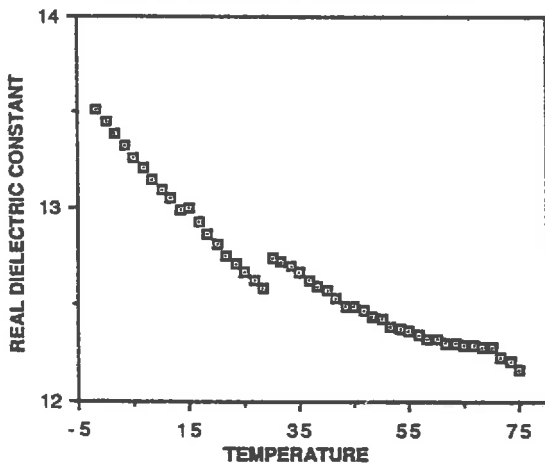
FIG. 41 TEMPERATURE DEPENDENCE OF RESONANT CAVITY REAL
DIELECTRIC CONSTANT DATA

EXP. AND THEOR. IMAGINARY DIEL. CONST. VS TEMP.
FOR 26.7% WATER OTTAWA SAND
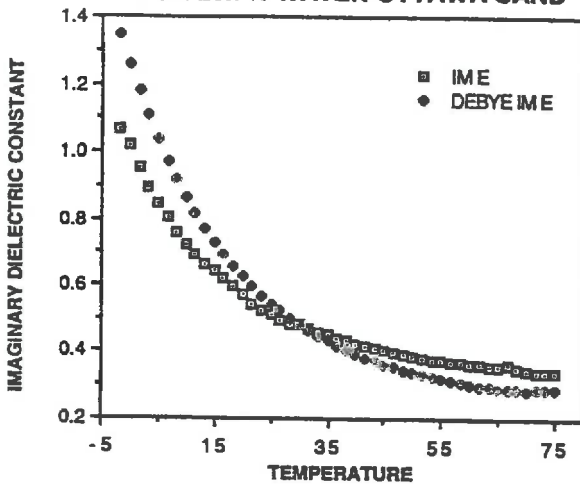
FIG. 42 TEMPERATURE DEPENDENCE OF RESONANT CAVITY
IMAGINARY DIELECTRIC CONSTANT DATA

The observed moderate decrease in the real dielectric constant with temperature is consistent with RF coax temperature measurements mentioned previously. The fall in real dielectric constant with temperature makes intuitive sense in that the real dielectric constant of bulk water decreases considerably with increasing temperature.

Of particular interest is the behavior of the imaginary dielectric constant with rising temperature (the experimentally measured curve is IM E in the plot key; the other curve will be discussed shortly). Unlike RF coax measurements, the imaginary dielectric constant decreases with increasing temperature.

96

The plot with symbol key DEBYE IM E is a theoretical description of the observed data based on the simple model

$$\varepsilon_i(\text{theor.}) = \theta_v \frac{\left(\varepsilon_s - n^2\right)\omega\tau}{1 + \omega^2\tau^2} \qquad (54)$$

where θ_v is the volumetric water content, ε_s is the temperature dependent static dielectric constant of water, n is the index of refraction, and τ is the temperature dependent (Hastead, 1973) Debye Relaxation Constant for water. In this model it is assumed that all of the dielectric loss is due to water in the sample and that the soil matrix does not affect this loss.

In the theoretical expression for loss one sees that the loss changes with temperature because 1) the static dielectric constant is temperature dependent, 2) the relaxation frequency is temperature dependent, and 3) the resonance frequency changes with temperature because of the change in dielectric constant of the cavity media. The theoretical curve in the preceding graph takes these factors fully into account.

Despite the crude nature of the model, it follows the observed temperature dependence of the imaginary dielectric constant quite well. This presents a fairly strong argument for a simple Debye Relaxation model for dielectric loss at the frequency of these measurements, approximately 500 MHz.

MECHANISMS OF DIELECTRIC LOSS

In the following section, the dielectric relaxation mechanisms appropriate to moist heterogenous media are reviewed and compared to the dielectric response data base. Heterogeneous materials containing water (such as soils) can possibly display a dielectric relaxation response due to a number of different mechanisms (Hastead, 1973). These different relaxation phenomena span the frequency range of Hz to hundreds of GHz. The principal relaxation mechanisms include ionic conductivity, ice relaxation, relaxation of free water (considered in a previous sections), charged double layers, Maxwell-Wagner effect, surface conductivity, and bound water relaxation (Hastead, 1973). The characteristics of these relaxations will be considered in the following discussion and compared to the dielectric response data. It is concluded that the predominant loss mechanism observed at low frequencies (1 - 50 MHz) in the Tempe Cell data is due to ionic conductivity.

RELAXATION OF ICE

The dielectric response of ice can be understood as a Debye type relaxation phenomena with a relaxation frequency in the low kilohertz region due to the limited mobility of the water molecules in the crystalline structure of ice (Auty and Cole, 1952). At the frequencies employed in this thesis, the real dielectric constant of ice is approximately 3.5 while the imaginary dielectric constant is less

than .1. As the temperatures employed in the experimental work were such that frozen water was not present in the samples, this mechanism will not be considered further.

CHARGED DOUBLE LAYERS

It has been observed that colloidal particle suspensions can display extremely high dielectric constants. For sphere-like particles with diameters of 1μ , the real dielectric constant can rise to values over 10,000 at frequencies below 1 KHz (Schwan, et. al., 1962). Colloidal particles are electrically charged by adsorbed ions and have a counterion atmosphere. This structure forms a charged double layer. The counterions adsorbed on the particle are tightly bound by electrostatic forces. However, along the surface of the particle, the ions are relatively free to move. The deformation of this ion atmosphere by an electric field is what gives rise to a high dielectric constant as well as dielectric loss. A theoretical model for this effect has been developed (Schwarz, 1962).

In Schwarz's theory, a colloidal particle of radius R and complex conductivity K_i is suspended in an electrolyte with complex conductivity K_a. The sphere is electrically charged by adsorbed ions of charge e_0 giving rise to a uniform surface charge density σ_0 in the absence of external electric fields. The adsorbed ions are assumed to be able to move only in a direction parallel to the surface of the particle and have a mechanical mobility (velocity per unit force) u. Schwarz proceeds to calculate a surface dielectric constant, ε_{su} , of the form

particles (about the size of the smallest particles found in soil) the relaxation frequency was well under a KHz. Thus according to Schwarz's theory the relaxation frequency of the charged double layers should be well below 1 MHz which is the lowest frequency at which measurements were taken. Thus if this relaxation mechanism is operating, we are in the regime where $\omega\tau \gg 1$ and the relaxation equations are, in this limit,

$$\varepsilon_i = \frac{(\varepsilon_s - \varepsilon_\infty)}{\omega\tau} \quad \text{and} \quad \varepsilon_r = \varepsilon_\infty + \frac{(\varepsilon_s - \varepsilon_\infty)}{\omega^2\tau^2} \quad (61)$$

From the dependence on R of $\varepsilon_s - \varepsilon_\infty$ and τ as shown in eqs. 59 and 60, we see for high but fixed frequencies that in a colloidal suspension of particle size R

$$\varepsilon_i = \frac{A}{R} \quad \text{and} \quad \varepsilon_r = \varepsilon_\infty + \frac{B}{R^3} \quad (62)$$

all other factors being equal. Thus we see that at a fixed frequency, the charged double layer mechanism requires a small particle size to significantly influence the dielectric properties of the medium. The imaginary dielectric constant, at say 1 MHz, should be much higher in clays than in sands due to the smaller particle size. The increase in the real dielectric constant above its "infinite frequency" value should depend very strongly on particle size. As an estimate of this dielectric increment we can take the difference between the real dielectric constant at 1 MHz and at 50 MHz. For Varved clay this

102

difference is about 10 while in Hart sand the difference is approximately 5. The median particle size changes by approximately 2 orders of magnitude between the sand and the clay. Eq. 62 then predicts a change in the dielectric increment of six orders of magnitude. One also predicts that the imaginary dielectric constants should differ by a factor of about 100. The observed difference is approximately 10.

Due to the very strong dependence on particle size of the dielectric increment, one can make the argument that the dielectric properties of the soil at high frequencies are completely dominated by the smallest particle present in the soil. Hart sand is composed of approximately 2% by weight of particles with diameters less than 1μ, while for Varved clay this figure is roughly 25%. Even using these figures, one can not account for the relatively small difference in the dielectric increment between Varved clay and Hart sand. Other soils in the data set also present strong arguments for the inapplicability of this loss mechanism.

Based on the relatively high relaxation energy and the relatively weak dependence of the dielectric properties on soil particle size, a charged double layer relaxation mechanism is not a significant factor in the dielectric response of moist soils.

MAXWELL-WAGNER EFFECT

When the frequency behavior of a suspension of a conducting dielectric in a nonconducting dielectric is investigated, a dispersion is observed. The origin of this dispersion, which under certain

conditions follows the Debye relaxation equations, is the Maxwell-Wagner effect (Wagner, 1914). Following the approach of Hastead, this can most easily be understood by considering the simple case of two parallel slabs of dielectric with equal widths, d, and dielectric constants ε_1, ε_2 and conductivities σ_1 and zero placed between two parallel capacitor plates. It is assumed that the dielectric constants and conductivities are frequency independent. The complex capacitances of the two capacitors in series are then given by (M.K.S. units)

$$C_1 = \left(\varepsilon_1 - \frac{j4\pi\sigma_1}{\varepsilon_0\omega} \right) \frac{\varepsilon_0}{4\pi d} \quad , \quad C_2 = \frac{\varepsilon_2\varepsilon_0}{4\pi d} \qquad (63)$$

The total capacitance, C, of the system is given by

$$C = \frac{C_1 C_2}{C_1 + C_2} \qquad (64)$$

which gives rise to an apparent permittivity for the combined system of

$$\varepsilon = \frac{\varepsilon_0}{4\pi} \frac{2\varepsilon_2 \left(\varepsilon_1 - j{4\pi\sigma}/{\omega\varepsilon_0} \right)}{\left(\varepsilon_1 - j{4\pi\sigma}/{\omega\varepsilon_0} \right) + \varepsilon_2} \qquad (65)$$

In the limits of infinite frequency and zero frequency the above equation has the following limits

$$\omega \rightarrow \infty \,, \ \varepsilon \rightarrow \frac{2\varepsilon_1 \varepsilon_2}{\varepsilon_1 + \varepsilon_2} \equiv \varepsilon_\infty \qquad (66)$$

and

$$\omega \rightarrow 0 \,, \ \varepsilon \rightarrow 2\varepsilon_2 \equiv \varepsilon_s \qquad (67)$$

We can then recast our equation for the apparent permittivity of the system into the form

$$\varepsilon = \varepsilon_\infty + \frac{\left(\varepsilon_S - \varepsilon_\infty\right)}{1 + j\omega\tau} \qquad (68)$$

where

$$\tau = \frac{\varepsilon_1 + \varepsilon_2}{\sigma_1} \frac{\varepsilon_0}{4\pi} \qquad (69)$$

Thus we see that this simple system is capable of producing a dispersion of a Debye relaxation type.

Since most heterogeneous media do not conform to a simple parallel plate geometry it is advantageous to have expressions for

the Maxwell-Wagner effect for more representative geometrical configurations. The case of a suspension of dielectric spheres in a surrounding dielectric has been solved (Schwan, et. al., 1962). The results are accurate only in the limit as the volume fraction occupied by the spheres approaches zero. The Debye relaxation parameters are

$$\tau = \frac{\varepsilon_2 + 2\varepsilon_1 - p(\varepsilon_2 - \varepsilon_1)}{\sigma_2 + 2\sigma_1 - p(\sigma_2 - \sigma_1)} \varepsilon_0 \qquad (70)$$

$$\varepsilon_\infty = \frac{\varepsilon_2 + 2\varepsilon_1 + 2p(\varepsilon_2 - \varepsilon_1)}{\varepsilon_2 + 2\varepsilon_1 - p(\varepsilon_2 - \varepsilon_1)} \qquad (71)$$

$$\varepsilon_s - \varepsilon_\infty = \frac{9p(1-p)(\varepsilon_1\sigma_2 - \sigma_1\varepsilon_2)^2}{\left[\varepsilon_2 + 2\varepsilon_1 - p(\varepsilon_2 - \varepsilon_1)\right]\left[\sigma_2 + 2\sigma_1 - p(\sigma_2 - \sigma_1)\right]^2} \quad (72)$$

where ε_1, σ_1 characterize the surrounding medium and ε_2, σ_2 the spherical inclusions which occupy a volume fraction p. For moist soils, with spherical inclusions composed of soil particles, and the surrounding media being air and water, the conductivity of the soil particles is negligible and the Debye relaxation parameters become

$$\tau = \frac{\varepsilon_2 + 2\varepsilon_1 - p(\varepsilon_2 - \varepsilon_1)}{(2+p)\sigma_1} \varepsilon_0 \qquad (73)$$

$$\varepsilon_\infty = \frac{\varepsilon_2 + 2\varepsilon_1 + 2\,p(\varepsilon_2 - \varepsilon_1)}{\varepsilon_2 + 2\varepsilon_1 - p(\varepsilon_2 - \varepsilon_1)} \qquad (74)$$

$$\varepsilon_s - \varepsilon_\infty = \frac{9\,p(1-p)(\varepsilon_2)^2}{[\varepsilon_2 + 2\varepsilon_1 - p(\varepsilon_2 - \varepsilon_1)][2+p]^2} \qquad (75)$$

Although the above equations were derived in the limit that the volume fraction of the spherical inclusions goes to zero, the experimental data (Kharadly and Jackson, 1953 ; Dryden and Meakins, 1957) has shown that the above equations give much better than order of magnitude agreement to inclusion volume values as high as 40%.

Experimental work by Hamon (Hamon, 1953) with spheres of discrete copper phthalocyanine (a moderately good conductor) embedded in paraffin wax shows a good agreement with the predictions of the above equations. Of particular interest are experiments Hamon performed by coating paraffin particles with copper phthalocyanine and then pressing the particles in a mold to form a structure with conducting paths. The frequency of peak dielectric absorption increases steadily through the KHz frequency range as the concentration of copper phthalocyanine increases. Over a wide range of frequencies, the experimental data can be approximated by the empirical relation

$$\varepsilon_i = \kappa f^{-\alpha} \qquad (76)$$

(Hartshorn and Ward, 1935) where κ is a positive constant, α is a positive number, and f is the frequency. For a material displaying a frequency independent conductivity α equals unity.

Soils at saturation have values of p around 0.5, and the dielectric constant of the surrounding media which is water is approximately 80, while that of the soil particles is about 7. Under these conditions, eq. 75 predicts that the maximum change in the real dielectric constant should be less than .1 while the maximum dielectric loss should be less than .05. Using the conductivity measured in Manchester silt at 1 MHz (.0056 mho/m), eq. 223 predicts a relaxation frequency slightly in excess of 1 MHz. However, the experimental data support a relaxation frequency well below 1 MHz. We conclude that the Maxwell-Wagner effect can not account for the observed dielectric behavior of moist soils.

SURFACE CONDUCTIVITY

O'Konski (O'Konski, 1955 ; O'Konski, 1960) has proposed that a frequency independent tangential surface conductivity on the surface of colloidal particles would result in dielectric dispersion. Schwan (Schwan, et. al., 1962) has investigated the implications of surface conductivity on the dielectric behavior of colloidal suspensions. In the regime of dielectric constants appropriate for

soil particles and water, he found that the following Debye relaxation parameters resulted (M.K.S. units)

$$\tau = \frac{\varepsilon_a}{\kappa_a} \varepsilon_0 \qquad (77)$$

$$\varepsilon_0 - \varepsilon_\infty = 9\,p\frac{1-p}{(2+p)^3}\frac{\varepsilon_i^2}{\varepsilon_a} \qquad (78)$$

$$\varepsilon_\infty = \varepsilon_a \frac{\varepsilon_i + 2\varepsilon_a + 2\,p(\varepsilon_i - \varepsilon_a)}{\varepsilon_i + 2\varepsilon_a - p(\varepsilon_i - \varepsilon_a)} \qquad (79)$$

where p is the volume fraction occupied by the colloidal particles with dielectric constant ε_i immersed in an aqueous solution of dielectric constant ε_a and conductivity κ_a. One of the interesting features of these relations is the independence of the Debye relaxation parameters on particle size.

For saturated soils, p is approximately .5 and the dielectric constant of the soil inclusions is about 7 while the dielectric constant of water is about 80. Eq. 78 then predicts a maximum change (with increasing frequency) in the real dielectric constant of less than .1 with a maximum imaginary dielectric constant of less than .05. The experimental data show dispersion more than two orders of magnitude greater than surface conductivity predicts. In addition, imaginary dielectric constants as high as one hundred have been

109

observed which is three orders of magnitude greater than surface conductivity can account for. Using the conductivity observed in Manchester silt at 1 MHz (.0056 mho/m), eq. 77 predicts a relaxation frequency in excess of 1 MHz while the data support a relaxation frequency well below 1 MHz. Thus we conclude that surface conductivity can not explain the observed data.

BOUND WATER RELAXATION

Water may be present in unfrozen heterogeneous moist materials in two states "free" and "bound". Free water has the structure and electrical properties of bulk water. Bound water can be either physically adsorbed or chemisorbed. Physically adsorbed water is bound by intermolecular forces such as hydrogen bonding while chemisorbed water bound by chemical bonds to form hydrated compounds.

Relatively little is known about the dielectric properties of adsorbed water, but the observed activation energies for bound water appear to be between that of bulk water (activation energy 4.5 Kcal./mole) and ice (activation energy 13 Kcal./mole) (Hastead, 1961).

Experimental data (Muir, 1953) indicates that a dispersion in the dielectric constant due to adsorbed water exists for clay minerals. In Muir's work, the dielectric behavior of kaolinite, halloysite, metahalloysite and talc were investigated. These silicate minerals display significant dielectric loss in the frequency range of 2.5 KHz to 25 MHz. The known surface areas of these minerals combined with

measured weights of the samples allowed Muir to calculate the number of adsorbed water layers present on the sample of interest. The largest imaginary imaginary dielectric constant attributed to adsorbed water relaxation encountered over the above frequency range was that for metahalloysite with a value of less than two. The maximum absorption for talc and kaolinite was less than .2. Muir also found that the frequency at which peak dielectric loss occurred rose steadily with increasing adsorbed water layer thickness. For example, the frequency of peak absorption for kaolinite rises from 100 KHz to approximately 25 MHz as the adsorbed layer increases from two to four water molecules.

In a study of sands exposed to humid atmospheres (Shahidi, et. al., 1975) the dielectric properties of a number of sands were investigated over the frequency range of .1 Hz to 5 MHz. Dry sands were exposed to humidity controlled atmospheres and allowed to absorb water. At high humidities, water in excess of 2% by weight was absorbed by the samples.

For Libyan sand exposed to 94% humidity, the real dielectric constant increases to a value in excess of 10,000 at one hertz. In the low MHz frequency range the real dielectric constant appears to show little frequency dependence. The imaginary dielectric constant is less than unity at 1 MHz for this same sample, and decreases rapidly with increasing frequency in the range of .1 Hz to 5 MHz.

The relaxation frequency for a number of inorganic compounds including quartz, are in the low KHz range (Hastead, 1973). This, combined with the above experimental data, appears to preclude bound water relaxation as the principle relaxation observed in the

111

Tempe Cell experimental data. The large dispersion in the real dielectric constant as well as the very high imaginary dielectric constants encountered in the low MHz frequency range can not be explained by an absorbed water relaxation mechanism.

CONDUCTIVITY

The effects of conductivity and dielectric polarization are indistinguishable from a measurement standpoint. The electrical response of any given dielectric can be duplicated by an appropriate conductivity. Following the approach of Jackson (1975) consider the Maxwell-Ampere equation

$$\nabla \times H = \frac{4\pi}{c}J + \frac{1}{c}\frac{dD}{dt} \qquad (80)$$

If we then assume the media obeys Ohm's law, i.e. $J = \sigma E$, and a harmonic time dependence for H, J, and E then the preceding equation becomes

$$\nabla \times H = -i\frac{\omega}{c}\left(\varepsilon + i\frac{4\pi\sigma}{\omega}\right)E \qquad (81)$$

were σ, ε are the conductivity and dielectric constant of the media (possibly complex) and ω is the frequency of the electric field. The term in the brackets can be considered as a generalized dielectric constant and one can lump the effects of conductivity and dielectric

112

constant into a pure dielectric constant. In fact one is free to pick either conductivity or the dielectric constant as the fundamental electrical property of the media. Typically one refers to, in the presence of an electric field, polarization as due to a non-zero dielectric constant while the motion of free charges results from a non-zero conductivity. The transformations in the following equation show how the conductivity and dielectric constant can be interrelated.

$$\varepsilon \rightarrow i\frac{4\pi\sigma}{\omega} \quad \text{or} \quad \sigma \rightarrow -i\frac{\omega\varepsilon}{4\pi} \qquad (82)$$

From these interrelations, one can see that a real conductivity can appear as a imaginary dielectric constant while an imaginary conductivity can manifest itself as a real dielectric constant. The reciprocal dependence on frequency of the apparent dielectric constant for a given conductivity is of importance. By going to higher and higher frequencies, the relative effects of conductivity, all things else being the same, can be reduced.

Dispersion in conductivity can occur in a number of simple systems. Consider the simple equation of motion for a charged particle (Jackson, 1975)

$$m\left[\ddot{x} + \gamma\dot{x}\right] = -eE(x,t) \qquad (83)$$

where m is the mass of the particle which carries a charge of -e, E is the electric field, and γ is a drag constant. This equation might be

113

appropriate in the modeling of the motion of an ion and its solvent cloud in an electric field. The drag force, proportional to the velocity, may arise from viscous forces or some other mechanism. Solving this equation for a harmonic electric field leads to a conductivity of

$$\sigma(\omega) = \frac{Ne^2}{m(\gamma - i\omega)} \qquad (84)$$

or equivalently

$$\epsilon(\omega) = \epsilon_0 + \frac{4\pi Ne^2}{m\omega(\gamma - i\omega)} \qquad (85)$$

where N is the volume density of ions and ϵ_0 is the contribution to the dielectric constant from other mechanisms than "conductivity".

This rather simple example showing a dispersive conductivity, or dielectric constant, illustrates some of the complexities in the study and modeling of dielectrics. Soils, which can contain dissolved salts, can thus display conduction effects which can complicate the observed dielectric response.

Eq. 84 thus gives rise to a Debye-like relaxation equation for the conductivity with a relaxation time of $1/\gamma$. If one assumes the drag force on an ion and its solvent cloud is due to viscosity, then a relaxation frequency on the order of 1000 GHz arises. This is so far above the frequencies employed in this thesis to be of complete insignificance.

However, the mechanism of ion atmosphere relaxation can produce a dispersion in both the real dielectric constant and the real conductivity (Falkenhagen, 1934). Following the presentation of Falkenhagen, ions of the opposite charge tend to congregate around an ion in solution giving rise to a net "atmosphere" of opposite charge surrounding the ion. It can be shown that in dilute electrolytes, the electric potential, Ψ, due to an ion and its atmosphere has the following form (c.g.s. units)

$$\Psi = \frac{e_1}{\varepsilon_{so}} \frac{e^{-\kappa r}}{r} \qquad (86)$$

where r is the distance from an ion of charge e_1, ε_{so} is the dielectric constant of the solvent, and $1/\kappa$ is a parameter known as the Debye thickness of the ion atmosphere (Debye, 1929) and is given by

$$\frac{1}{\kappa} = \left(\frac{\varepsilon_{so} k T}{4\pi e^2 \sum n_i z_i^2} \right)^{\frac{1}{2}} \qquad (87)$$

where e is the electronic charge, k is Boltzmann's constant, z_i is the valency of the ion, and n_i is the number of ions per cubic centimeter. For a 1-1 valent electrolyte such as NaCl at a concentration of .001 moles/liter, the ion atmosphere has a thickness of about 100 Å. Due to the limited mobility of the ions in the electrolyte, the ion

115

atmosphere is not able to respond instantaneously to electric fields, but exponentially approaches the new equilibrium distribution over a period of time characterized by the relaxation time, τ_i . The relaxation time, in seconds, is given by

$$\tau_i = \frac{|z_1||z_2|}{|z_2|l_1 + |z_1|l_2} \frac{15.34 \times 10^{-8}}{kTq} \frac{1}{\kappa^2} \quad (88)$$

$$q \equiv \frac{|z_1||z_2|}{|z_2|l_1 + |z_1|l_2} \frac{l_1 + l_2}{|z_1| + |z_2|} \quad (89)$$

where z_1 , z_2 are the charge, in electronic charge units, and l_1 , l_2 are the ionic mobilities of the ions of the electrolyte which is assumed to be 1-1 valent in the above equation. The extension to other valencies is straightforward.

The ionic mobilities are defined by

$$\Lambda_\infty^* = \sum l_i \quad (90)$$

$$\Lambda_\infty^* = \lim c^* \to 0 \quad \text{of} \quad \frac{1000 L^*}{c^*} \quad (91)$$

where Λ_∞ is the equivalent molar conductivity at infinite dilution, L^* is the specific conductivity of electrolyte solution and c^* is the equivalent concentration of the electrolyte. One equivalent of an electrolyte produces one mole of both positive and negative charges upon disassociation. For KCl at a concentration of .001 moles/liter,

116

the relaxation time is approximately .1 μs. It is this finite relaxation time of the ionic atmosphere which gives rise to dispersion in the dielectric properties of electrolytes.

Falkenhagen has derived the following equations for the frequency behavior of the conductivity and real dielectric constant of an electrolyte (Falkenhagen, 1934).

$$\Lambda_\omega = \Lambda_\infty - \Lambda_{I\omega} - \Lambda_{II} \qquad (92)$$

$$\varepsilon_e - \varepsilon_{so} = \frac{1.97 \times 10^6 z_1 z_2 \left(v_1 z_1^2 + v_2 z_2^2\right)^{\frac{1}{2}} \sqrt{q}}{\varepsilon_{so}^{1/2} T^{3/2} \omega \tau_i \left[\left(1 - 1/q\right)^2 + \omega^2 \tau_i^2\right]} \left[q\left(1 - \frac{1}{q}\right) - \omega \tau_i\left(R - \frac{1}{\sqrt{q}}\right)\right]\sqrt{\gamma} \quad (93)$$

where Λ_ω is the molar conductivity at an angular frequency ω, Λ_∞ is the molar conductivity at infinite dilution (mhos/cm^2), $\Lambda_{I\omega}$ is the contribution to the molar conductivity due to ion atmosphere relaxation, and Λ_{II} is the molar conductivity due to electrophoresis. ε_e is the dielectric constant of the electrolyte and γ the the molarity of the electrolyte expressed in total moles of ions/liter. The other terms are defined by the following relations

$$\Lambda_{I\omega} = \Lambda_{I0}\alpha(\omega\tau_i, q) \qquad (94)$$

$$\Lambda_{II} = \frac{29}{(\epsilon_{so}T)^{1/2}\eta_0}\left(\sum v_i z_i^2\right)^{3/2}\sqrt{\gamma} \qquad (95)$$

$$\Lambda_{IO} = \frac{9.85 \times 10^5}{(\epsilon_{so}T)^{3/2}}\frac{2q}{1+\sqrt{q}}|z_1 z_2|\left(\sum v_i z_i^2\right)^{1/2}\sqrt{\gamma} \qquad (96)$$

$$\chi(\omega\tau_i, q) = \frac{1+\sqrt{q}}{\sqrt{q}\left[(1-q^2)+\omega^2\tau_i^2\right]}\left[\left(1-\frac{1}{q}\right)\left(R\frac{1}{\sqrt{q}}\right)+\omega\tau_i Q\right] \qquad (97)$$

$$R = \frac{1}{\sqrt{2}}\left[\left(1+\omega^2\tau_i^2\right)^{1/2}+1\right]^{1/2} \qquad (98)$$

$$Q = \frac{1}{\sqrt{2}}\left[\left(1+\omega^2\tau_i^2\right)^{1/2}-1\right]^{1/2} \qquad (99)$$

where q, τ_i are defined in earlier equations while η_0 is the viscosity of water in c.g.s. units and T the temperature in degrees Kelvin.

The basic behavior produced by these relatively complex equations is as follows. As the measurement frequency approaches the relaxation frequency, the conductivity is observed to increase. At frequencies greatly in excess of the relaxation frequency, the conductivity approaches a high frequency value $\Lambda_\infty - \Lambda_{II}$. As $\chi(\omega\tau_i, q)$ is a function that varies between 0 and 1, the maximum variation in the conductivity is Λ_{IO} which is proportional to the

square root of the molarity, γ. The relaxation frequency is inversely proportional to γ. The frequency dependence of the function χ which determines the elevation of the conductivity with frequency is shown below in figure #43 for a 1-1 valent electrolyte such as NaCl for which q=.5.

FREQUENCY DEPENDENCE OF THE FUNCTION CHI
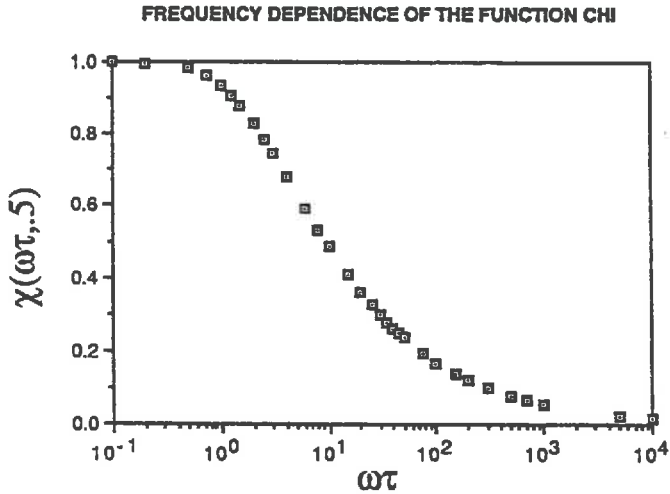
FIG. 43 FREQUENCY DEPENDENCE OF FALKENHAGEN'S CHI FUNCTION

The relaxation is quite broad, occurring over a much wider frequency band than in Debye relaxation.

For a .001M NaCl solution the magnitude of the dispersion of the conductivity is about 1.8% of the static conductivity value. However, the dispersion is strongly dependent on the valency of the ions and for .001M $Ca_2Fe(CN)_6$ the dispersion is approximately 20%. As the concentration varies from a typical soil salinity range of .01M to .0001M NaCl, the relaxation frequency varies from 28.3 to .283

MHz. Due to the broad relaxation in the conductivity, soils with salinities in this range can be expected to display significant dispersion in the conductivity over the frequency range of 1 to 50 MHz employed in much of the experimental work in this thesis.

Compared to the dispersion in the conductivity, the dispersion in the real dielectric constant is quite small. For NaCl, the magnitude of the dispersion is

$$\varepsilon_d(\omega=0) - \varepsilon_{so} = 3.79\sqrt{\gamma} \qquad (100)$$

as the elevation in the real dielectric constant falls to zero for frequencies much higher than the relaxation frequency. For a very saline soil with $\gamma = .01$ the dispersion in the real dielectric constant is less than .5% of the value of the real dielectric constant of water. The dispersion in the real conductivity will not be investigated further.

In order to explore the possibility that conductivity effects were present in the experimental soil data, a series of experiments were performed. In one experiment, the dielectric properties of saturated Manchester silt and the water component of this soil were measured. This was accomplished using an instrument and probe configuration identical to that used in the scaling experiment.

First, the dielectric constant of distilled water was measured to insure that the probe was clean and that a low imaginary dielectric constant which is associated with a low conductivity was obtained. A slurry consisting of 2700 g of Manchester silt and 840 g of distilled water was then prepared. After mixing and allowing the mixture to

sit for 30 minutes, a small coaxial probe was inserted into the soil and the dielectric properties of the soil were measured at 1, 2, 5, 10, 20, and 50 MHz. The values obtained were in relatively good agreement with the data collected at high moisture levels in the Tempe cell. An additional 500 ml of water was added, the sample stirred, and allowed to sit for 30 minutes. The excess water was then decanted and the dielectric properties of the Manchester silt were again measured and showed no significant difference from earlier.

A vacuum filtration setup was then prepared. In order to insure that there were no trace contaminants in the filter apparatus, distilled water was first filtered. The dielectric properties of this filtrate showed no appreciable change from that of distilled water. The decanted fluid was then filtered to yield a very-slightly turbid solution. The dielectric properties of this first filtrate were then measured. An additional two liters of distilled water was added to the Manchester silt slurry, the mixture stirred, and allowed to sit for 90 minutes. This mixture was then vigorously stirred and vacuum filtered. The slightly turbid filtrate was then filtered again to yield an almost clear solution. The dielectric properties of this second filtrate were then measured. In order to help eliminate the possibility of surface contamination of the probe surfaces, the probe was rinsed with distilled water and then re-inserted into the filtrate with no discernible change in the dielectric properties. As another check, the outer tines were coated with a thin layer of vacuum grease (in order to help eliminate electrode polarization or surface contamination phenomena) and re-inserted into the solution. Again there was no appreciable change. The dielectric constant of the

solutions were measured 48 hours after filtering with no discernible change. In all the filtrate measurements, the real dielectric constant was within 2% of the value obtained in distilled water. The results for the imaginary dielectric constant are shown below in figure #44.

IM. DIEL. CONST. VS. FREQ. FOR MAN. SILT AND ITS FILTRATES
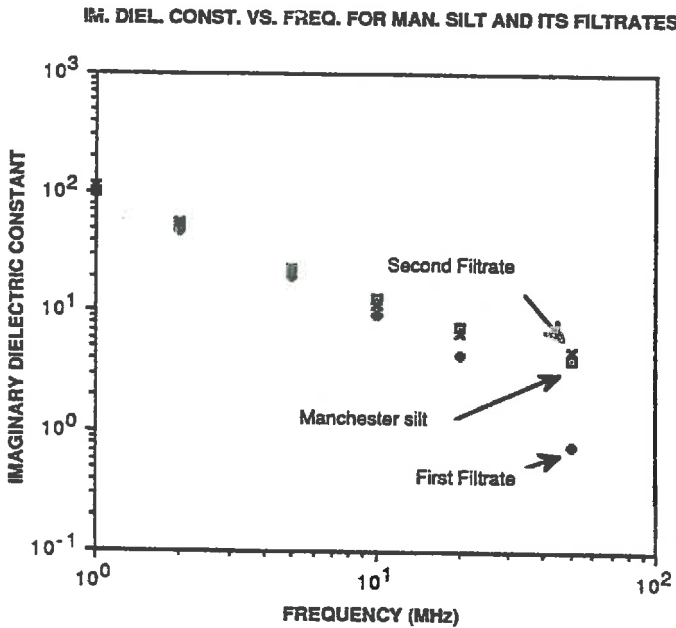
FIG. 44 FREQUENCY DEPENDENCE OF THE IMAGINARY DIELECTRIC CONSTANT FOR MANCHESTER SILT AND ITS FILTRATES

There is a striking agreement between the imaginary dielectric constants of the Manchester silt and its filtrate, particularly in the case of the second filtrate. This forms a strong argument for the presence of dielectric loss due to ionic conductivity. The imaginary

122

dielectric constant of 98 at 1 MHz corresponds to a conductivity of .0056 mho/m.

As a further test of a conductivity mechanism for dielectric loss in soils, the dielectric behavior of saline solutions was investigated. Using the same network analyzer and probe configuration as in the scaling experiment, the dielectric behavior of .001M NaCl was measured at 23.0 ^{0}C at 1 MHz intervals between 1 and 50 MHz. In addition a temperature controlled circulating water bath was used to measure the temperature dependence of the dielectric behavior of .001M NaCl at 1, 10, and 50 MHz. The real dielectric constant of these saline solutions agreed with the static value of distilled water at the appropriate temperature to within 1.5%.

The following graphs (figures #45-#47) show a comparison between the temperature dependence of Manchester silt (from an earlier section of this thesis) and the scaled imaginary dielectric constant (im. diel. const/1.40) of .001M NaCl at 23.0 ^{0}C for three frequencies.

IM. DIEL. CONST. VS. TEMP. FOR MANCHESTER SILT AND SALINE SOLUTION
AT 1 MHZ
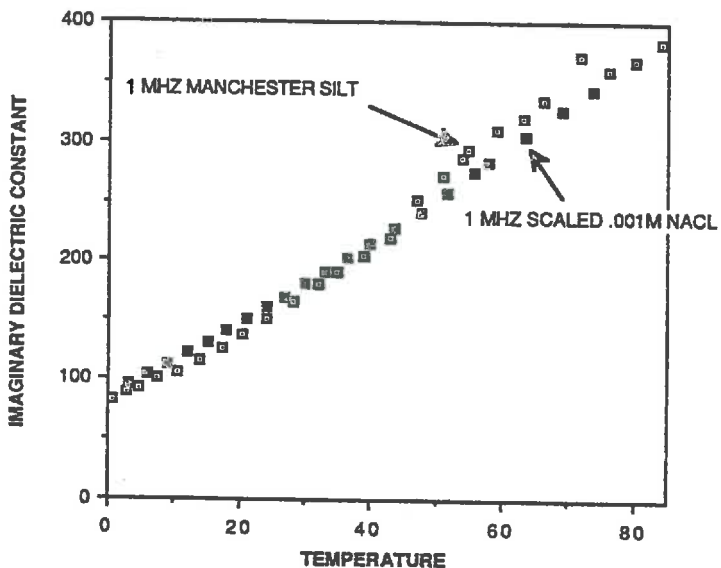
FIG. 45 TEMP. DEP. OF THE IMAG. DIEL. CONST. OF MANCHESTER SILT
AT 1 MHz COMPARED TO SALINE SOLUTION

IM. DIEL. CONST. VS. TEMP. FOR MANCHESTER SILT AND SALINE SOLUTION AT 10 MHZ
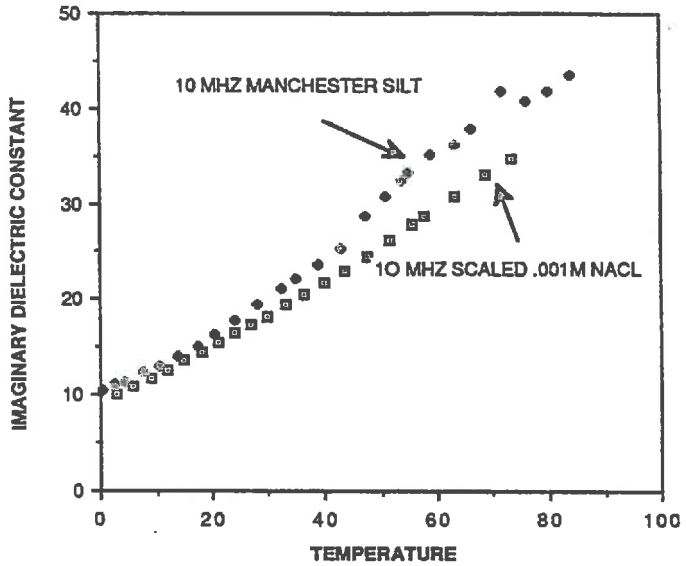
FIG. 46 TEMP. DEP. OF THE IMAG. DIEL. CONST. OF MANCHESTER SILT
AT 10 MHz COMPARED TO SALINE SOLUTION

125

IM. DIEL. CONST. VS TEMP. FOR MANCHESTER SILT AND SALINE SOLUTION
AT 50 MHZ

IMAGINARY DIELECTRIC CONSTANT

50 MHZ MANCHESTER SILT

50 MHZ SCALED .OO1M NACL
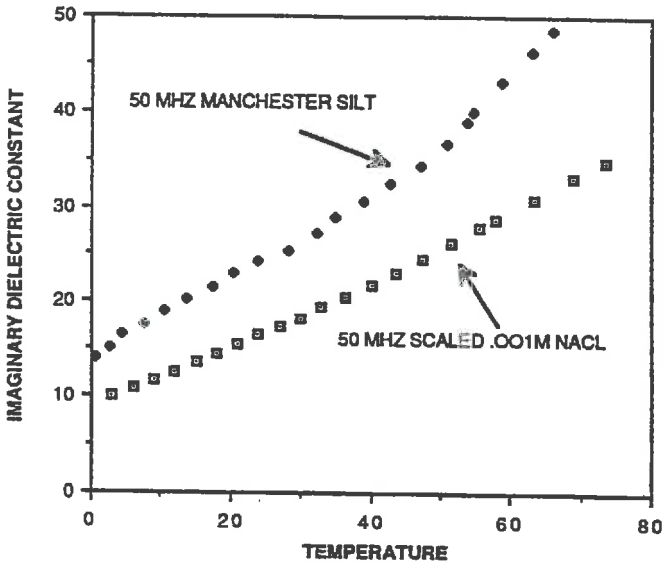
TEMPERATURE

FIG. 47 TEMP. DEP. OF THE IMAG. DIEL. CONST. OF MANCHESTER SILT
AT 50 MHz COMPARED TO SALINE SOLUTION

The temperature dependence of saline solution and Manchester silt is
almost identical at 1 MHz. As the frequency increases the agreement
deteriorates somewhat. This may be due to another loss mechanism
entering in at higher frequencies.

Another test of a conductivity loss mechanism is the
comparison of the frequency dependence of the imaginary dielectric
constant of Wilder silt (30.61% water) and that of 23 ⁰C .001M NaCl.
The following graph (figure #48) illustrates this comparison

126
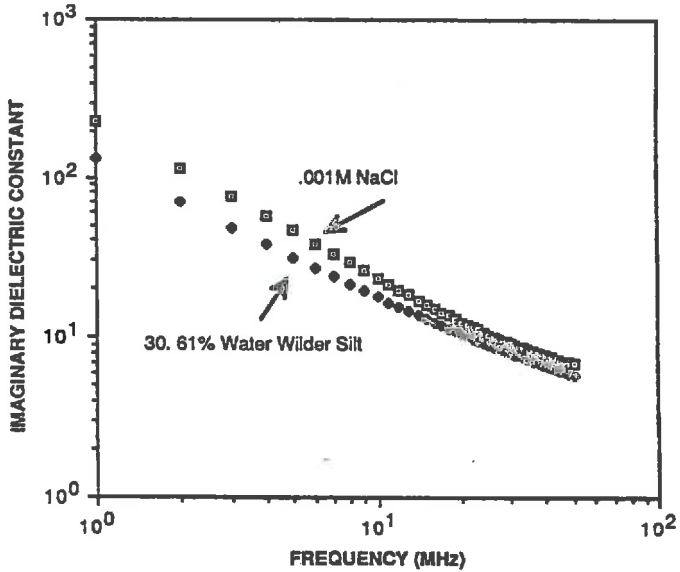
FIG. 48 COMPARISON OF THE FREQ. DEP. OF THE IMAGINARY DIEL.
CONSTANT FOR MOIST WILDER SILT AND SALINE SOLUTON

The very similar behavior of the these samples is again
noteworthy. In both the soil and the saline solution, the slopes are
not quite -1 which is indicative of a frequency independent
conductivity. The conductivity of the saline solution calculated from
the imaginary dielectric constant agrees with the static value of the
conductivity of .001M NaCl to within better than 1%. However, a plot
of the conductivity of .001M NaCl vs. frequency, shown in figure #49,
is difficult to understand.

127

CONDUCTIVITY VS. FREQUENCY FOR .001M NaCl
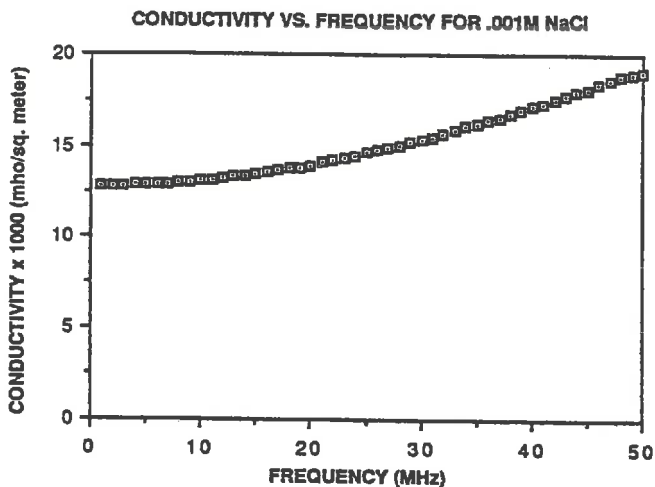
FIG. 49 FREQUENCY DEPENDENCE OF THE CONDUCTIVITY OF .001M
NaCl SOLUTION

The change in the conductivity is over an order of magnitude greater
than the dispersion equations of Falkenhagen predict as discussed
earlier. This is disturbing in that Falkenhagen's theory is apparently
in reasonably good agreement with experiment (Falkenhagen, 1934).
This anomalously high dispersion in the conductivity may be the
result of inadequate temperature control during data collection,
however I feel this is rather unlikely.

The dispersion produced by Falkenhagen's ion atmosphere
relaxation theory is of interest because it can predict the behavior of
the imaginary dielectric constant observed in soils. An increasing
conductivity with frequency manifests itself in an imaginary

dielectric constant which does not fall quite as fast as (frequency) $^{-1}$. Data presented in the section on Tempe cell measurements indicates that the imaginary dielectric constant in soils falls roughly as the (frequency) $^{-.8}$. This connection between the frequency behavior of the imaginary dielectric constant in soils and a possible ion atmosphere relaxation dispersion requires further investigation.

In conclusion, the experimental data strongly support the contention that an ionic conductivity loss mechanism is operating in the soils. The salinity which would be required to be present in the soil in order to account for the observed dielectric loss is of order .001M or 30 ppm NaCl. The experimental data also indicates that MHz frequency range dielectric measurements may be a practical technique for measuring soil salinity.

MIXTURE THEORY

In the following section, a number of existing mixing models are applied to moist soils in an attempt to arrive at a theoretical understanding of the dielectric response of moist soils. An original fractal model for moist soils is also presented which is able to explain many features of the observed dielectric response.

SCOPE OF THE PROBLEM

Mixture theory attempts to understand how the overall dielectric response of a heterogeneous mixture of dielectric media is determined by the constituent dielectrics and their geometrical distribution. Due to the considerable theoretical as well as practical interest, considerable effort has been extended in this field beginning with Maxwell in the mid eighteen hundreds. However, for all but the simplest cases, this problem is either quite difficult or completely intractable. A theoretical understanding of the dielectric properties of moist soils is a particularly challenging problem. As illustrated in figure #50, naturally occurring soils display an extremely complicated relationship between pore spaces (filled with both air and water which in general contains dissolved salts) and soil particles. The complexity of these interrelations is such that it often is problematic to merely characterize and describe the soils structure.

130
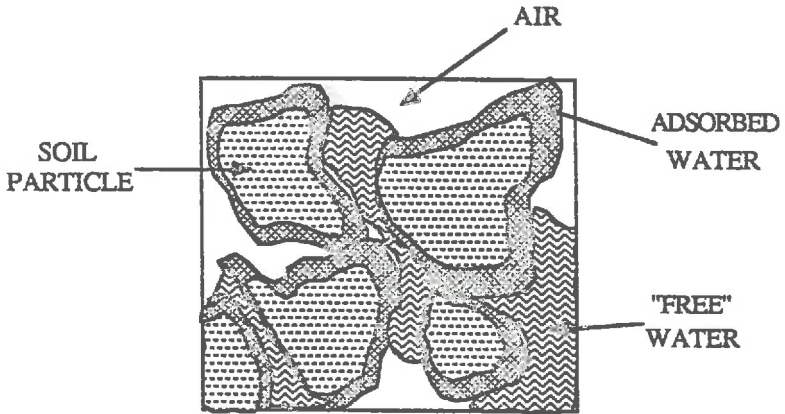
SOIL SCHEMATIC

FIG. 50 SOIL SCHEMATIC

In moist soils there are at least four distinctly different dielectrics present- air, free water, soil particles, and bound water. Free and bound water can display considerable variation in their dielectric behavior with changing temperature as well as changing dissolved salt concentration. In frozen soils, ice can be present with markedly different dielectric properties than liquid water.

SIMPLE PARALLEL AND SERIES MIXING

One simple but illustrative example of dielectric mixing theory considers the case of series and parallel dielectric slabs between a plate capacitor illustrated in the figure #51 for a tertiary system containing air, soil, and water as dielectrics.

131
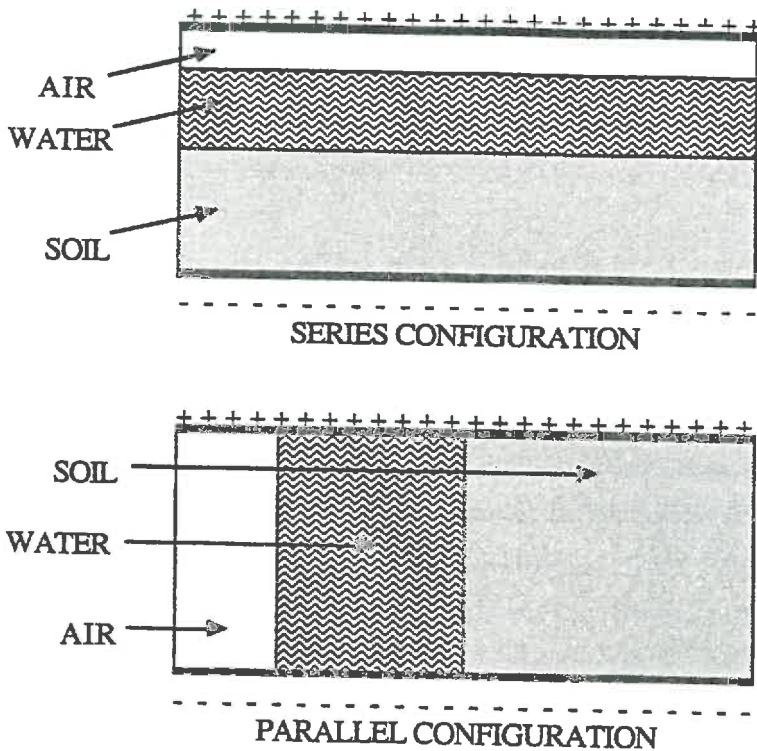
FIG. 51 PARALLEL AND SERIES MIXING FOR MOIST SOILS

For these two simple configurations, closed form solutions exist for the effective dielectric constant of the system. They are

$$\varepsilon_m = p_a\varepsilon_a + p_s\varepsilon_s + p_w\varepsilon_w \quad \text{in parallel} \quad (101)$$

$$\frac{1}{\varepsilon_m} = \frac{p_a}{\varepsilon_a} + \frac{p_s}{\varepsilon_s} + \frac{p_w}{\varepsilon_w} \quad \text{in series} \quad (102)$$

where ε_a , ε_s , ε_w and p_a , p_s , p_w are the dielectric constants and the occupied volume fractions of air, soil, and water and ε_m is the effective dielectric constant of the system. A more general form dielectric mixing has been proposed (Ansoult, et. al., 1984) of the form

$$\varepsilon_m^k = \varepsilon_a^k p_a + \varepsilon_s^k p_s + \varepsilon_w^k p_w \qquad (103)$$

where k can take on any value between -1 and +1. k=+1 corresponds to parallel mixing while k=-1 corresponds to series mixing. As expected, intermediate values of k give mixing results between the series and parallel result. A plot of the series and parallel model results and the dielectric profile of a typical soil (adapted from Ansoult, 1984) is shown in figure #52.
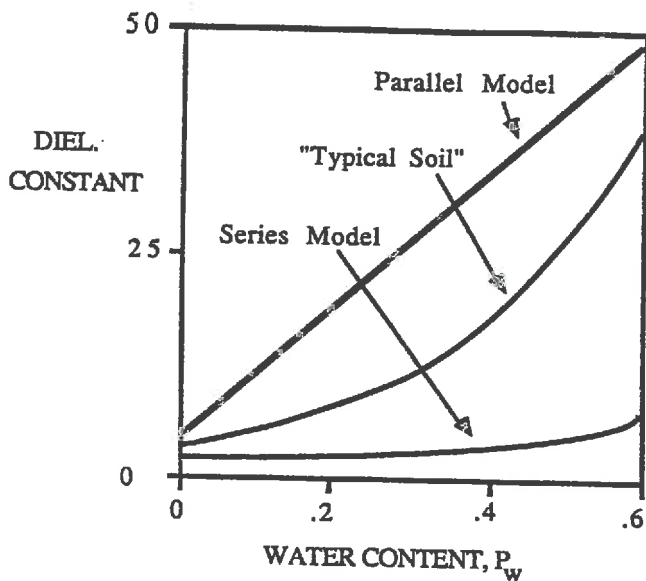
FIG. 52 COMPARISON OF SERIES AND PARALLEL MIXING MODELS TO "TYPICAL" SOIL BEHAVIOR

The very marked difference in the dielectric profile between the series and parallel models is illustrative. The effective dielectric constant of a heterogeneous media is very strongly dependent on the geometrical arrangement of the constituent dielectrics. It can be shown that series and parallel mixing models form lower and upper bounds to the possible dielectric response of an arbitrary mixture of different dielectrics (Milton, 1981). If the dielectric response of the composite medium is isotropic (simple series and parallel mixing models are not isotropic) slightly better limiting bounds for the dielectric response of the composite can be made (Milton, 1981; Hashin and Shtrikman, 1962).

134

The more generalized eq. 103 has been used to fit experimental data from moist soils (Ansoult, 1984). This approach is intellectually unsatisfying as all values of k between -1 and +1 are empirical in nature.

RANDOMLY ORIENTED ELLIPSOID MODELS

A number of studies have been undertaken to calculate the effective dielectric constant of a mixture of randomly distributed and oriented ellipsoidal particles in a host dielectric. For most heterogeneous dielectrics including soils, this is a much more realistic model than a simple series or parallel configuration. In the previous section on dielectric loss mechanisms, some of these mixing models were used to calculate dielectric relaxation parameters. A number of these mixing models are reviewed in the following discussion. Of the numerous randomly oriented ellipsoid models discussed, only the Looyenga model will be considered in detail in a later section.

In a classic work (Polder and Van Santen, 1946) the approximate effective dielectric constant of such a system was calculated. The approximation is as follows. First a special particle is assumed to be surrounded by an effective dielectric constant in which a uniform electric field exists far from the particle. It is then assumed that the mean field that exists in this special particle is representative of the mean field in the particles of the mixture. This allows one to overcome the insurmountable mathematical difficulties encountered when one tries to calculate the effect of each particle's polarization field on its neighbors. This is a fairly good

135

approximation when the volume fraction, p, occupied by the particles is small.

Polder derives (following the presentation of Hastead, 1973) an expression for the electric field along the axis a, E_a, when a field E is applied applied along the axis a of a ellipsoid with semi-axes a, b, c.

$$E_a = \frac{\varepsilon_h E}{\varepsilon_h + A_a(\varepsilon_i - \varepsilon_h)} \qquad (104)$$

where ε_h and ε_i are the dielectric constants of the host and ellipsoid constituents and A_a is a depolarization factor along the a-axis and is given by

$$A_a = \int_0^\infty \frac{ds}{\left(a^2 + s\right)^{3/2}\left(b^2 + s\right)^{1/2}\left(c^2 + s\right)^{1/2}} \qquad (105)$$

The depolarization factors satisfy the following relationship

$$A_a + A_b + A_c = 1 \qquad (106)$$

This gives rise to an induced polarization per unit volume, P_a, as follows

$$P_a = (\varepsilon_i - \varepsilon_h) E_a \qquad (107)$$

136

which gives rise to an induced dipole moment

$$\mu_a = \frac{4}{3}\pi abc P_a \qquad (108)$$

and thus to a polarizability

$$\alpha_a = \frac{\frac{4}{3}\pi abc \varepsilon_h (\varepsilon_i - \varepsilon_h)}{\varepsilon_h + A_a (\varepsilon_i - \varepsilon_h)} \qquad (109)$$

The induced dipole moment in turn polarizes the surrounding media and introduces a change in the polarization, ΔP, of the form

$$\Delta P = N\alpha \langle E \rangle \qquad (110)$$

where $<E>$ is the average electric field throughout the mixture whose effective dielectric constant, ε_m , is given by

$$(\varepsilon_m - \varepsilon_h) E = \Delta P \qquad (111)$$

Polder and Van Santen then proceed to calculate $<E>$ by deriving the polarization of the neighborhood of the ellipsoid and arrive at the expression

$$\langle E_a \rangle = \frac{\varepsilon_h {}_a E}{\varepsilon_h + A_a (\varepsilon_i - \varepsilon_h)} \qquad (112)$$

137

where ε_{ha} is the permittivity of the host dielectric surrounding the ellipsoid and, in general, is not equal to ε_h. This allows the effective dielectric constant of the medium to be calculated. When averaged over all possible orientations one obtains

$$\varepsilon_m = \varepsilon_h + \frac{p}{3}(\varepsilon_i - \varepsilon_h)\,\varepsilon_{h\,a}\left[\sum_{j=a,b,c}\frac{1}{\varepsilon_{h\,a} + A_j(\varepsilon_i - \varepsilon_{h\,a})}\right] \quad (113)$$

where p is related to the number of ellipsoids per unit volume in a straightforward manner. As yet the quantity ε_{ha} has not been specified and is most likely a function of p. Often it is taken to be equal to either ε_h or ε_m.

For a needle shaped, disc shaped, and spherical ellipsoid, the depolarization factors tend, respectively, to 1/2 , 1/2 , 0 ; 0 , 0 , 1 ; and 1/3 , 1/3 , 1/3 . In the case of the sphere with ε_{ha} taken to be ε_h one recovers Wagner's equation for suspension of spherical particles

$$\frac{\varepsilon_m - \varepsilon_h}{3\varepsilon_h} = p\left(\frac{\varepsilon_i - \varepsilon_h}{2\varepsilon_h + \varepsilon_i}\right) \quad (114)$$

which is pervasive in the literature dealing with heterogeneous dielectrics.

Polder and Van Santen's result (valid for p <<1) serves as a basis for a host of mixing models valid in different regimes. There is some justification for replacing the denominator in the left side of the above equation with $\varepsilon_m + 2\varepsilon_h$ to give, for spheres,

138

$$\frac{\varepsilon_m - \varepsilon_h}{\varepsilon_m + 2\varepsilon_h} = p\left(\frac{\varepsilon_i - \varepsilon_h}{2\varepsilon_h + \varepsilon_i}\right) \qquad (115)$$

which is known as the Rayleigh mixture formula (Polder and Van Santen, 1946). For large volume fractions of the ellipsoids, it is appropriate to approximate ε_{ha} as being equal to ε_h which gives for spheres

$$\frac{\varepsilon_m - \varepsilon_h}{3\varepsilon_m} = p\left(\frac{\varepsilon_i - \varepsilon_h}{2\varepsilon_m + \varepsilon_i}\right) \qquad (116)$$

which is known as the Bottcher mixture formula (Hastead, 1973). One approach to calculating the effective dielectric is to convert the Rayleigh mixture formula into the following differential equation.

$$\frac{d\varepsilon_m}{\varepsilon_m} = \left(\frac{dp}{1 - p}\right)\left(\frac{\varepsilon_i - \varepsilon_m}{2\varepsilon_m + \varepsilon_i}\right) \qquad (117)$$

This equation is then integrated between the limits ε_h and ε_m which amounts to assuming that at infinite dilution, ε_m is equal to ε_h. For a differential addition of ellipsoidal particles a differential change in ε_m is calculated using the above equation. This procedure is repeated until one reaches the occupied volume fraction, p. The result is Bruggeman's mixture formula (Hastead, 1973).

$$1 - p = \left(\frac{\varepsilon_i - \varepsilon_m}{\varepsilon_i - \varepsilon_h}\right)\left(\frac{\varepsilon_h}{\varepsilon_m}\right)^{1/3} \qquad (118)$$

For symmetrical composite dielectrics, an objection to the above result can be made which stems from the fact that it is not symmetrical with respect to the volume fraction occupied by the host and the spherical particles. The above procedure can be modified to yield the symmetrical result

$$\varepsilon_m = \left[\varepsilon_h^{1/3} + p\left(\varepsilon_i^{1/3} - \varepsilon_h^{1/3}\right)\right]^3 \qquad (119)$$

which is known as Looyenga's equation (Debye, 1929 ; Hastead, 1973).

Considerable experimental data exist for spherical particles suspended in a host dielectric. Agreement between theory and experiment can be quite good for values of p as high as .5. One can make the generalization that the Looyenga, Bruggeman, and Looyenga equations agree with experiment much better than the Wagner and Rayleigh equations for large p (Hastead, 1973).

As a simple test to see if these simple mixing models could explain the frequency behavior of the dielectric constants of soil, a model based on the Looyenga equation (eq. 119) was constructed. In the model the dielectric constant of soil particles was taken to be purely real and equal to 7. The real dielectric constant of water was set equal to 80. The imaginary dielectric constant of water was given the value of 1000 (which is the loss due to approximately .005M

NaCl) at 1 MHz and the same frequency dependence as the .001M NaCl solution in the conductivity section. The water inclusions were assumed to occupy a volumetric fraction of .31. The results for this model are shown in figure #53.
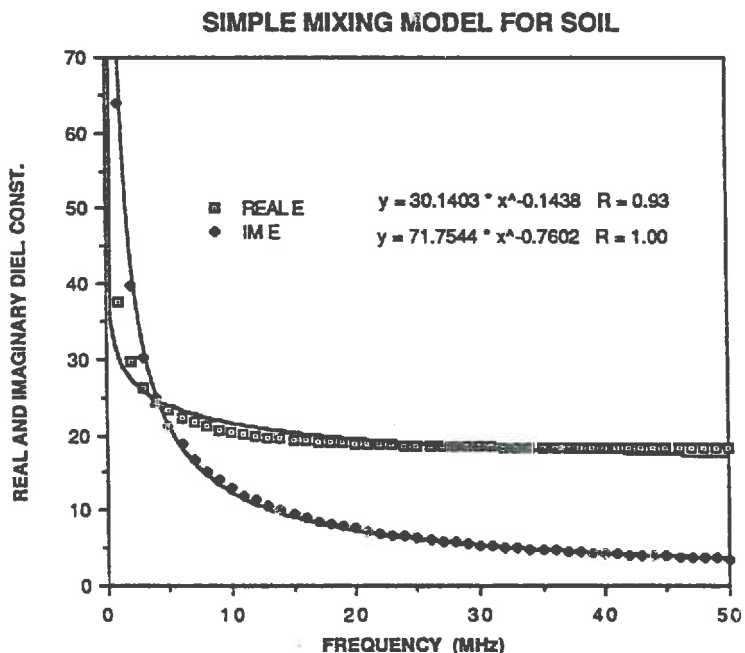

FIG. 53 SIMPLE LOOYENGA MODEL FOR A LOSSY SOIL

The results are quite striking in that the Looyenga model predicts a very significant dispersion in the real dielectric constant. Both the real and imaginary dielectric constants follow simple power law

dependences on the frequency with remarkably similar exponents as encountered in the Tempe cell data section.

However, there is need for great caution in applying this simple model. By using the Looyenga mixing equation with complex dielectric constants, the dispersion in the real dielectric constant is a Maxwell-Wagner effect. In the section on the Maxwell-Wagner effect, the Wagner mixing equation (eq. 114) was used to derive dispersion equations showing that the Maxwell-Wagner effect is relatively insignificant. I believe the disparity arises because in the Wagner equation the effective dielectric constant of the media surrounding the spherical inclusions, ε_{ha} , is taken to be that of the dielectric constant of the media surrounding the spherical inclusions. This is a good approximation as long as the volumetric fraction of the inclusions is small and the contrast in dielectric constants is not to high. However, in a soil with water inclusions occupying a volumetric water content near .3 with complex dielectric constants of magnitude 1000, this approximation breaks down. The derivation of the Looyenga equation is such that this effect should be of less importance, however there is some question as to the validity of the Looyenga equation in this extreme regime.

In conclusion, it appears that the Looyenga mixing equation can very satisfactorily reproduce many of the features of the dielectric response of moist soils. Modifications of this simple model to include non-spherical ellipsoids may allow the observed dielectric properties of soils to be modeled more satisfactorily. There is some question as to the applicability of the Looyenga eq. for very high dielectric contrast mixtures.

LOCAL ENVIRONMENT DEGREE OF FREEDOM MODEL

One possible model of a heterogeneous dielectric considers the local environment a charge would experience in the media. Ansoult (Ansoult, et. al., 1984) considers a model of this type for moist soils. Following Ansoult's presentation, consider a charge located at a microscopic point in the soil where one can find all of the soils components - air, soil, and water. Each of these components is characterized by a dielectric constant. The fraction of each component present at the point characterize the vicinity of the point. The vicinity of the point is also specified by a number of zones, u, each of which is assigned a soil component. The number of zones inside an environment is known as the number of degrees of freedom of the charge.

One then simulates the charge environment by assuming random assignment of a dielectric constant to a zone. This dielectric constant is determined by the probabilities of finding air, soil, and water in the vicinity of the particle. These probabilities are directly related to the soil porosity, ϕ, and volumetric water content, θ . The environment of the charge is simulated by u capacitors connected to a common pole that contains the electric charge. Furthermore, the separation between the capacitor plates has the same value regardless of the component present. The number of capacitors having dielectric constants corresponding to air, soil and water is given by a polynomial law distribution. In response to an electric field, the electric charge moves from one local environment to

another and traces out a "streamline". The effective dielectric constant is obtained by averaging over all possible streamlines. Thus, as Ansoult details, for each volumetric water content an effective dielectric constant can be calculated using a statistical approach.

Besides the values chosen to represent the dielectric constant of air, soil, and water and the soil porosity, the only variable parameter of the model is the number of degrees of freedom, u. When u=1, a series results is obtained while u=∞ produces a parallel result. The agreement between Ansoult's degree of freedom model and experimental transmission line data (Topp, et. al., 1980) is quite good for values of u between 6 and 8.

One limitation to this approach is that there are very significant differences in the dielectric behavior of soils as one progresses from sands through silts to clays. These classes of soils will, in general, require different values for the number of degrees of freedom present in order to successfully model their dielectric behavior. Why these soils should have different degrees of freedom is a question that can not be easily answered, nor is their a good explanation or theoretical basis for soils apparently possessing roughly seven degrees of freedom. In addition, the dielectric behavior of some soil samples encountered in this thesis can not be satisfactorily explained using this model. Nevertheless, this approach is of interest in studying the transition from series to parallel mixing and helps to place the generalized series-parallel mixing equation (eq. 103) on a more sound footing.

Percolation methods are a powerful theoretical technique for dealing with disordered and stochastic geometry situations. Percolation techniques have been used to model a wide range of physical systems including the flow of liquid in a porous medium, conductor-insulator composite materials, mobility in semiconductors, resistor networks, as well as the dielectric properties of heterogeneous media (Zallen, 1983). Percolation concepts have proved useful in explaining the viscosity and light-scattering properties of water-oil microemulsions (Hilfiker and Eicke, 1987) and the dielectric properties of water-isooctane microemulsions (Eicke, et. al., 1986), as well as other more complicated microemulsions (Clarkson and Smedley, 1988).

According to Zallen, percolation theory "deals with the effects of varying, in a random system, the richness of interconnections present." One of the hallmarks of percolation theory is the "percolation transition". At the percolation transition, long-range connectivity suddenly appears.

As a simple example of percolation behavior (adapted from Zallen, 1983), consider a square grid as illustrated in figure #54.
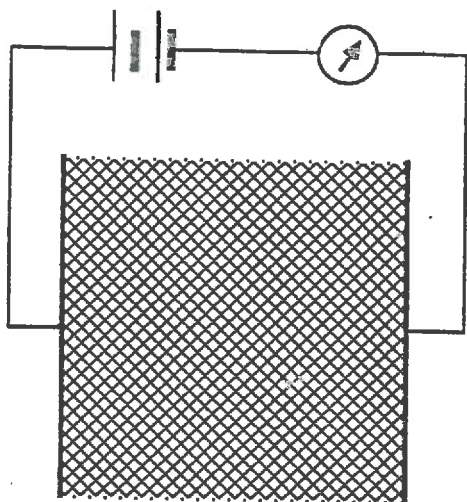
FIG. 54 GRID SYSTEM USED TO VISUALIZE PERCOLATION CONCEPTS
(ADAPTED FROM ZALLEN, 1983)

Initially, with none of the grid lines cut, some fixed current flows in response to the applied potential. The grid lines are then randomly snipped between junction points. As the fraction of snipped grid lines increases the current begins to fall. For an infinite grid, percolation theory predicts a mathematically sharp transition point. When the fraction of cut grid lines equals one-half, the current falls to zero. Looking at the situation from the other direction, when the fraction of the number of possible connections reaches one-half, long-range connectivity appears and every part of the grid is connected together.

For only a few simple geometries, can one calculate a transition point at which this long-range connectivity is established. For more

146

complicated systems, Monte-Carlo numerical techniques are used to estimate threshold points.

Percolation models have the potential to explain many of the features of the dielectric behavior of soils. Typically, when small amounts of water are added to dry soils, the dielectric constant initially rises relatively slowly. As the water content of the soil increases, the rate at which the dielectric constant rises with additional water increases. Percolation theory might be able to explain this behavior for the following reasons. At low water contents (i.e. below the percolation transition point) long-range connectivity of the dispersed water droplets is not present. Thus, in any direction in the sample, one can not travel any distance large compared to a soil particle size without encountering many air/soil particle/water interfaces. It is not unreasonable to expect that in this regime series mixing is appropriate and the dielectric constant rises slowly. As the water content of the soil increases above the percolation transition point, long-range connectivity is present. It then becomes possible to travel in any direction along connected water capillaries which allows the lower dielectric constant soil particles and air to be electrically bypassed. It is not unreasonable to expect that parallel mixing then becomes reasonable in this regime, and the dielectric constant increases at a more rapid rate. In order to test the above explanation, the following computer experiment was undertaken.

The computer model assumes that the soil is composed of a random mixture (in this model, the extension to three dimension gives identical results) of soil, air, and water droplets assumed to be

147

squares of uniform size. Initially, the computer sets up a random grid of soil and air squares such that porosity is some fixed specified value. A uniform electric field is assumed to exist across the grid, and the effective dielectric constant of the grid is calculated. One of the air grid points is then chosen at random and replaced with water. The dielectric constant of the new configuration is then calculated. This process is repeated until all of the air grid points have been replaced with water. The situation existing during the course of a simulation is shown below in figure #55.

SOIL MODEL

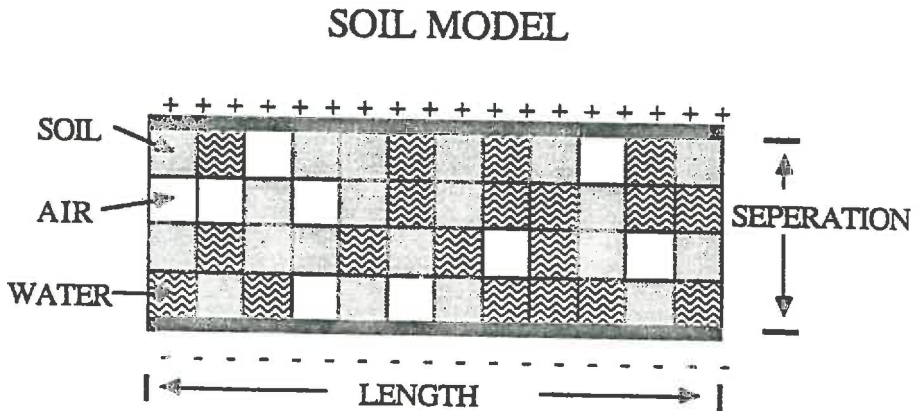FIG. 55 SCHEMATIC SHOWING A TYPICAL PERCOLATION MODEL
CONFIGURATION FOR A MOIST SOIL

The effective dielectric constant of the model is calculated in the following manner. First, the electric field is assumed to point only in the direction perpendicular to the plates. By making this approximation, the effective dielectric constant is underestimated, but insuperable mathematical difficulties are avoided. This allows

148

the effective dielectric constant of each column to be calculated using simple series mixing, i.e.

$$\varepsilon_{\text{eff.}} = \frac{1}{\dfrac{N_s/S}{\varepsilon_s} + \dfrac{N_w/S}{\varepsilon_w} + \dfrac{N_a/S}{\varepsilon_a}} \qquad (120)$$

where S = the separation of the capacitor in grid units, N_a, N_w, N_s are the number of air water and soil grid particles in the column, and ε_a, ε_w, ε_s are the dielectric constants of air (1), water (78), and soil (a parameter that can be varied). The computed effective dielectric constant for each water content is the average value of the effective column dielectric constants which amounts to parallel mixing of the columns and series mixing within each column. Increasing the length of the capacitor, in grid points, serves to damp out fluctuations in this inherently statistical model. Doubling the length of the capacitor tends to smooth out the calculated dielectric response as a function of water content but gives essential the same dependence on water content, all things else being equal.

A large number of runs were made with this model varying porosity, the dielectric constant of the soil particles, and the width of the capacitor. A typical run is shown in figure #56.

RESULTS OF A PERCOLATION MODEL FOR SOILS

Porosity = .5
Dielectric Constant of Soil = 8
Seperation of Cap. = 4 grid units
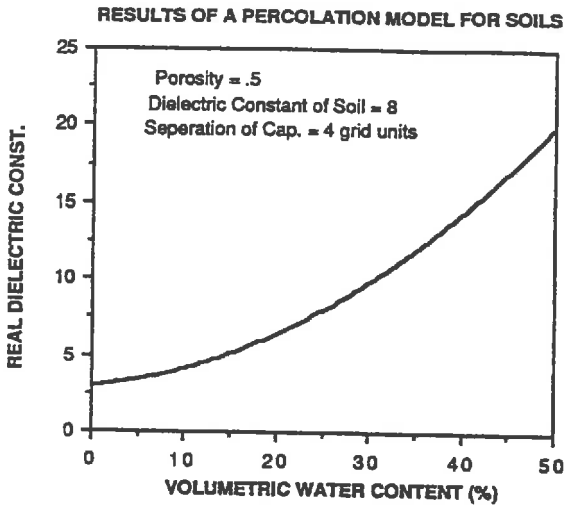
FIG. 56 TYPICAL DIELECTRIC BEHAVIOR PRODUCED BY A
PERCOLATION MODEL FOR MOIST SOIL

The dielectric response of the model run illustrated above is close to the behavior of some soils.

A number of generalizations regarding this modeling approach can be made. First, in order to reproduce the behavior of real soils, the width of the capacitor must be of the order of four grid cells. With a capacitor separation of 1 grid cell a parallel mixing result is obtained while an infinite separation leads to a series result. Second, the dielectric constant assumed for the soil particles must be around 8 which is reasonable considering the dielectric constants of common materials composing soils. Finally, the porosity of the soil should lie in the range of .4 to .6 which is also typical of naturally occurring soils.

150

However, a number of objections can be made to this modelling approach. The procedure used to calculate the dielectric constant gives only an approximate dielectric constant. In addition, there is no clear link, besides the porosity and the dielectric constant of the soil material, to parameters of the soil such as particle size. Also, the model does not scale properly. Doubling all the dimensions of the capacitor leads to a different result due to the critical dependence of the model on the capacitor separation.

SIMPLE PORE FILLING MODEL

A simple model of moist soils is as follows. Water droplets are assumed to be dispersed in a regular array in a background dielectric of soil and air considered to be characterized by a single dielectric constant. As additional water is added, the droplets (assumed to rectangular in shape) increase in size. The grid is infinite in size. This situation is shown in figure #57.
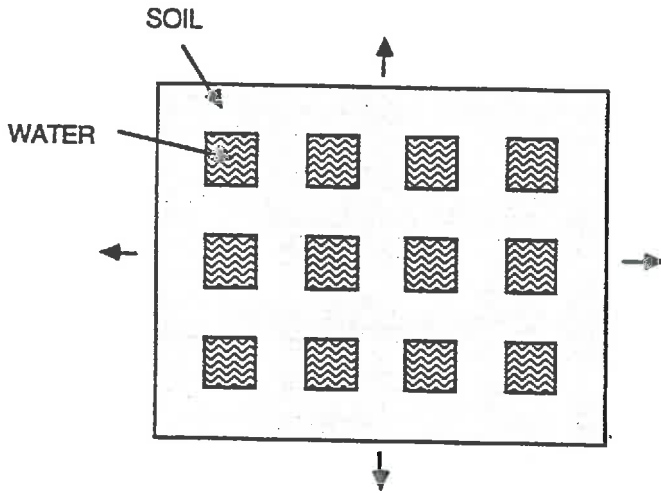
FIG. 57 CONFIGURATION OF SOIL AND WATER USED IN THE
COMPUTER SIMULATION

Even for this rather simple configuration, an expression for the
effective dielectric constant can not be obtained. The effective
dielectric constant of this configuration was evaluated numerically.
Due to the symmetry present in the configuration shown above, the
effective dielectric constant of the system can be calculated using the
simpler unit cell illustrated in figure #58.
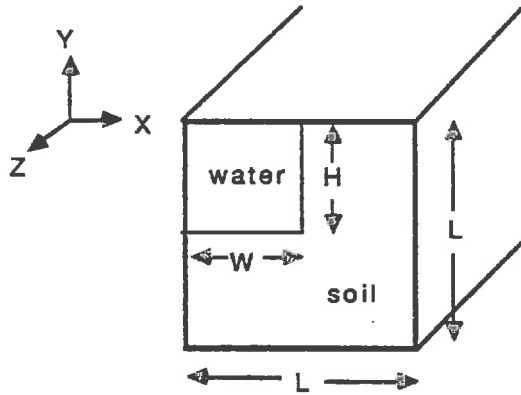
FIG. 58 PARAMETERS OF THE UNIT CELL USED IN THE COMPUTER
MODEL

The large scale structure is obtained by reflecting through both the
y-z plane and the x-z plane, and then repeating this procedure. As
this is a two-dimensional model, infinite extent is assumed in the z-
direction.

When the dielectric constants of the soil and water media are
specified, the problem becomes that of solving Laplace's equation
subject to appropriate boundary conditions. From symmetry
considerations, the normal field across the sidewalls is zero while the
top and bottom walls are equipotential surfaces. Additionally, the
tangential electric field and normal electric displacement are
constrained to be continuous across the soil-water interface. With
these boundary conditions, the problem is well specified.

In order to calculate the effective dielectric constant of the unit
cell, the following scheme was employed. At each point of a 200 x
200 grid, an electrical potential was specified. By taking spatial

153

derivatives of grid points electric fields can be calculated and the appropriate boundary conditions can be maintained. By stepping through the grid and replacing the potential value at each point with the average value of the four nearest neighbors, Laplace's equation is momentarily satisfied at each point. This procedure is repeated until a near steady state value of the total energy, U_e, of the system found by integrating the potential energy density of the system. The relationship between these quantities is shown below

$$U_e = \frac{1}{2} CV^2 = \int_{vol.} \varepsilon E^2 d v \qquad (121)$$

where C is the effective capacitance of the system, E is the electric field and V is the voltage difference between the top and bottom walls. The effective capacitance of the system is directly related to the effective dielectric constant.

This numerical routine is very computationally intensive. In order to reduce the required run time for the code, the standard numerical technique of over-relaxation was used. This markedly reduces the required computation time. However, for each soil-water configuration approximately two hours on a Micro-Vax computer is required to produce an effective dielectric constant.

In order to test the validity of the numerical routine, a large number of test runs with soil-water configurations adjusted to give simple series or parallel configurations were run. Typically the

agreement between the theoretical dielectric constant and the value produced by the model was better than .5 %.

In order to characterize the dielectric response produced by a given water inclusion shape, the effective dielectric constant of approximately ten different soil-water configurations was modeled. The water inclusion shapes that produced dielectric response curves closest to those of real soils were long in the direction of the applied field. A typical water inclusion shape modeled was one initially .5L in length and .1L in width (to give a "volumetric water content" of .05). The effective dielectric constant of this configuration was then numerically calculated. The length and width of the inclusion were then proportionally increased and the new effective dielectric constant was calculated. This procedure was then repeated until the length was equal to 1L. This process is shown schematically in figure.#59.
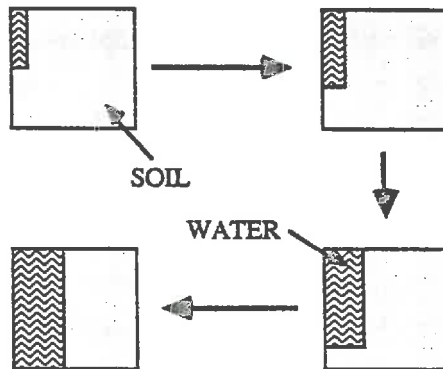
FIG. 59 THE SCHEME USED TO SIMULATE INCREASING SOIL
MOISTURE IN THE COMPUTER MODEL

The results for two typical modeling runs are shown in figure #60. In model A, the initial inclusion was .6L in length and .08L in width. In model B the initial inclusion was .36L in length and .14L in width. Both models assumed a dielectric constant of 80 for water and 4 for the soil.
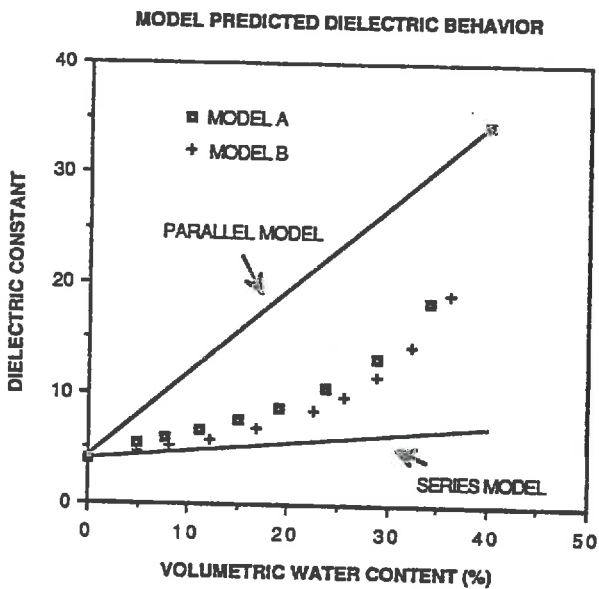
FIG. 60 THE DIELECTRIC BEHAVIOR PRODUCED BY THE COMPUTER MODEL FOR TWO TYPICAL RUNS

The models are clearly able to simulate the roughly parabolic dependence of the dielectric constant on water content in soils. However, there are a number of limitations to this modelling scheme. The model is two-dimensional which does not represent a soil very

well. In addition, for all water inclusion width to length ratios other than unity, there is a very strong asymmetry in the effective dielectric constant. If the potential difference is applied across the sidewalls instead of across the top and bottom walls, a different effective dielectric constant will be obtained. Due to periodic nature of this model, the dielectric constant scales properly. The dielectric constant is independent of sample size as long as a sufficiently large number of unit cells is included so that the assumption of periodicity of the electric fields is valid.

This model is similar to the randomly oriented ellipsoidal inclusion models discussed earlier. The difference between the ellipsoidal models and the simple pore model is that the water inclusion are considered to be regularly placed and of a non-random orientation. One strength of this simple pore model is that no approximations are made considering the effects of the polarization fields. When the volume fraction of inclusions is approximately one-half, the ellipsoidal models are of questionable validity, but this is a moisture regime of significant interest in soils.

This model is of significance in that it helps to deduce the importance of water inclusion geometry on the dielectric response of moist soils. It provides a clear and intuitive model for the characteristic dielectric response of moist soils.

FRACTAL PORE FILLING MODEL

In recent years, fractal concepts have seen increasing use in the description and understanding of disordered media. Fractal ideas

have been employed in the study of heterogeneous dielectrics such as water-in-oil emulsions (Hilfiker and Eicke, 1987; Eicke and Geiger, 1986). Fractal models have been proposed to explain the dielectric behavior of bound water in sandstones (Gusev, et. al., 1987). In Gusev's paper, a random fractal model (i.e. a structure heterogeneity composed of a random distribution of fractal scales) is used to understand the dielectric behavior of sandstones containing water absorbed from humid atmospheres. Fractals have been used to explain the widely used empirical relationship known as Archie's law (Katz and Thompson, 1985; Brouers and Ramsamugh, 1988). Archie's law (Archie, 1952) predicts for brine saturated rocks the simple relationship

$$\sigma = \sigma_w \phi^m \qquad (122)$$

where σ is the measured conductivity of the sample, σ_w is the conductivity of the brine solution, ϕ is the porosity of the sample, m is an experimentally determined parameter with a typical value of about 2. In Katz and Ramsamugh's work, the electron scanning microscope determined fractal dimensions of sandstones (with a range 2.57-2.87) is related to the exponent m in Archie's law. In Brouers and Ramsamugh's work, Archie's law is also correlated with fractal dimensionality and the frequency behavior of the real and imaginary dielectric constants in the high frequency regime is given by a simple power law dependence on the frequency.

The above mentioned attempts to use fractal concepts to understand the dielectric response of porous media have considered only two regimes of moisture content- saturated and bound water. In moist soils, the moisture regime between these two extremes is of great interest. However an extensive review of the literature fails to produce any work dealing with this intermediate regime of porous media. The following idealized model of moist soils is proposed in order to lend insight into the possible fractal behavior of these porous media.

Let us now make the following assumptions in a fractal model of the dielectric response of moist soils: 1) Water enters into a soil in a uniform fractal manner, i.e. fractal clusters form and due to surface tension, adsorption onto soil particle surfaces, etc. the water molecules are distributed evenly between clusters and all the clusters are of the same size. 2) The individual clusters grow in pore spaces which are assumed to be all of equal size, l, and of a characteristic size equal to the average particle size. 3) Until the individual clusters attain a size equal to the pore space (i.e. until the percolation threshold is reached), there is no long range water "connectivity" in the sample and the dielectric constant of the sample rises in a manner consistent with series mixing (discussed in the Percolation Models section). 4) When the individual clusters attain a size equal to the pore size, long-range connectivity occurs and additional water enters in a non-fractal manner and in a parallel manner (discussed in the Percolation Models section) so that the dielectric constant rises rapidly in a manner consistent with parallel mixing. 5) The soil sample is neither a gravel where surface tension

159

forces are not strong enough to allow the pore space to be spanned, nor is the sample such a fine clay that all of the water is bound due to surface adsorption and absorption effects to the soil particle even at high water contents. The implications of these assumptions will now be explored.

One interesting property of fractal clusters is that they have an unusual dependence on the number of particles in the cluster as a function of the characteristic size of the cluster (Meakin, P., 1986 ; Niemeyer, et. al., 1984). We now assume soil pores are fractal over the size range r_1 to r_2 but become homogeneous (3 dimensional) for lengths greater than r_2 and that r_2 is at least as large as a single pore but small compared to the soil sample in question. Then the number of water molecules in a cluster in this fractal pore space is given by

$$n_w = c_1 \left(\frac{r}{r_1} \right)^D \qquad (123)$$

where n_w is the number of water molecules in the cluster, c_1 is some constant on the order of unity, r is the characteristic size of the cluster (its diameter), and D is the fractal dimension of the cluster. The fractal dimension must be less than or equal to the dimensionality of the space that the cluster occupies which in this case is three. The total volume of water in the cluster, V_{wc} , is then simply

$$V_{wc} = C \left(\frac{r}{r_1} \right)^D \qquad (124)$$

where C is some new constant. If we have a total of n_c clusters, all of diameter r, then the total volume of water contained in the sample is

$$V_{tw} = n_c C \left(\frac{r}{r_1}\right)^D \qquad (125)$$

The volumetric water content of a sample, θ_w , in the shape of a cube with sides L is then given by

$$\theta_w = \frac{n_c C \left(\frac{r}{r_1}\right)^D}{L^3} \qquad (126)$$

Assume now that there exists some critical water content, θ_c , where all n_c water clusters are of size 1 equal to a pore space which is taken to be the average soil particle size, then we have the following relationship

$$\theta_c = \frac{n_c C \left(\frac{1}{r_1}\right)^D}{L^3} \qquad (127)$$

We then use the following expression to substitute for the number of water clusters, n_c , i.e.

161

$$\phi L^3 = \frac{4\pi}{3} n_c l^3 \qquad (128)$$

where ϕ is the porosity of the soil. This criteria is simply that the volume occupied by the fractal clusters is equal to the total pore volume at the critical water content. Using the above result to eliminate n_c from eq. 127 gives

$$\theta_c = \phi C' l^{D-3} \qquad (129)$$

where C' is some new constant. This critical water content occurs when the fractal clusters have filled all the pore spaces. The critical water content serves to divide the dielectric response of soils into two regimes. Below the critical water content, the water is "isolated" and there is no long-range connectivity. Above the critical water content, the water in the sample becomes connected and the dielectric constant begins to rise rapidly with increasing water content. The physical mechanism of this rapid increase in the dielectric constant is that the long-range connectivity of the water allows the low dielectric soil and air components to be electrically bypassed. The connectivity also means that dissolved ions now have long range mobility throughout the sample. If this is the mechanism causing dielectric loss, one would expect the imaginary dielectric constant to rise sharply as the critical water content is approached.

There are a number of interesting features in this model. First the model predicts that soils should be isotropic dielectrics. The physical size of the sample, L, does not enter into the equation for

the critical water content and thus the dielectric constant of the sample is independent of the sample size as long as L >> l, which is in accordance with experiment. If we assume a non-fractal model, then the fractal dimension is 3 and eq. 129 predicts that the critical water content should depend only on the soil porosity which is near one-half for almost all naturally occurring soils. Thus a non-fractal model would predict very little variation in the dielectric response between soils. In addition, the critical water content would occur at the saturation point of the soil and thus one would expect the dielectric constant to rise very slowly until just before saturation. The experimental data (particularly in sands) do not support this. The significant difference in the dielectric behavior of soils with wetting also refutes a non-fractal model.

In order to test this model, some criterion is needed to determine the critical water content from the experimental data. The criterion that was chosen was that the critical water content occurs where the loss tangent of the soil drops precipitously. This is chosen with the idea that this represents the point at which a loss mechanism dependent on long range connectivity begins to be eliminated. As was mentioned in the Dielectric Loss Mechanisms section, the loss mechanism in question appears to be ionic conductivity and it is reasonable to assume that ionic conductivity will not be present unless there is long range water connectivity. Although this assumption is not rigorously justified, it is a reasonable one. In the two following graphs (figures #61 and #62) of two soils with very greatly differing particle sizes some of the aspects of this model are illustrated.
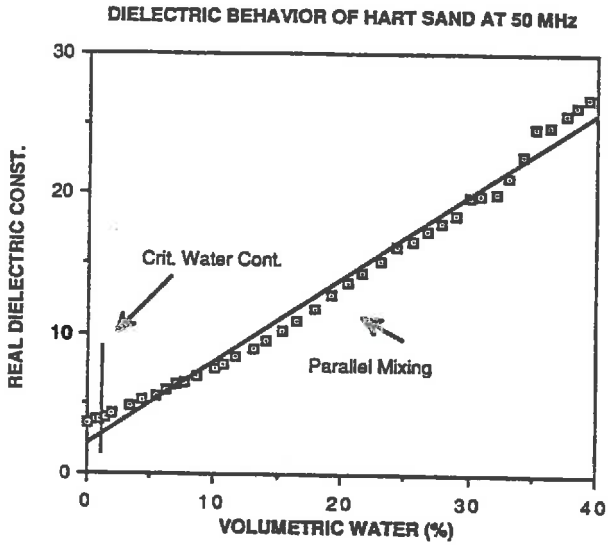
163

FIG. 61 FRACTAL MODEL INTERPRETATION OF THE OBSERVED
DIELECTRIC BEHAVIOR FOR HART SAND

164

DIELECTRIC BEHAVIOR OF FT. EDWARDS CLAY AT 50 MHz
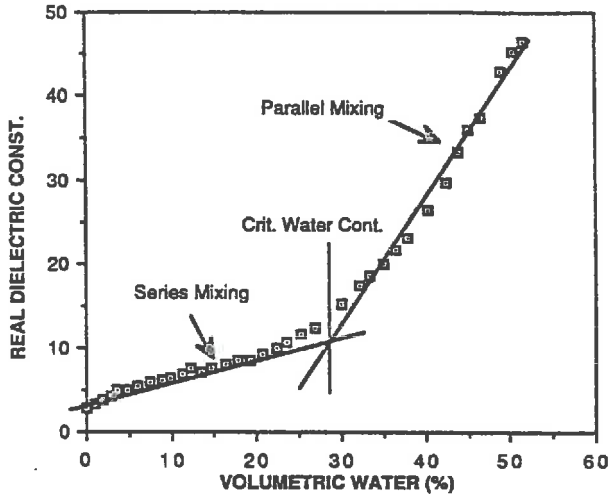
FIG. 62 FRACTAL MODEL INTERPRETATION OF THE OBSERVED
DIELECTRIC BEHAVIOR FOR FT. EDWARDS CLAY

In the first graph the dielectric behavior of Hart sand is shown. For
Hart sand, the experimentally determined critical water content is so
low that basically all of the water enters into the sample above the
critical water content. One then expects the dielectric constant to rise
rapidly with increasing water content which is observed. A linear fit
to the Hart sand gives a slope of .59. If the water in the soil was
behaving in a purely "parallel manner" the slope would be expected
to be .78. The steep slope lends support to the idea that there is
long-range connectivity present in Hart sand at low water contents.

165

On the other hand, in Fort Edwards clay, the critical water content occurs at an intermediate moisture level and the fractal model predicts that there should be roughly two regimes in the dielectric behavior. This is exactly what is observed. In the first regime, the dielectric constant rises at a relatively slow rate, albeit not as slow as a pure series mixing model would predict. In the second regime, the dielectric constant rises very quickly at a rate that exceeds the prediction from a pure parallel mixing model.

As a further test of this model, eq 129 predicts that a plot of $\log(\theta_c/\phi)$ vs. $\log(l)$ should be a straight line with a slope equal to D-3. This plot is shown in figure #63.

SCALED CRITICAL WATER CONTENT VS. PORE SIZE

$y = 0.9818 * x^{-0.6051}$ $R = 0.92$
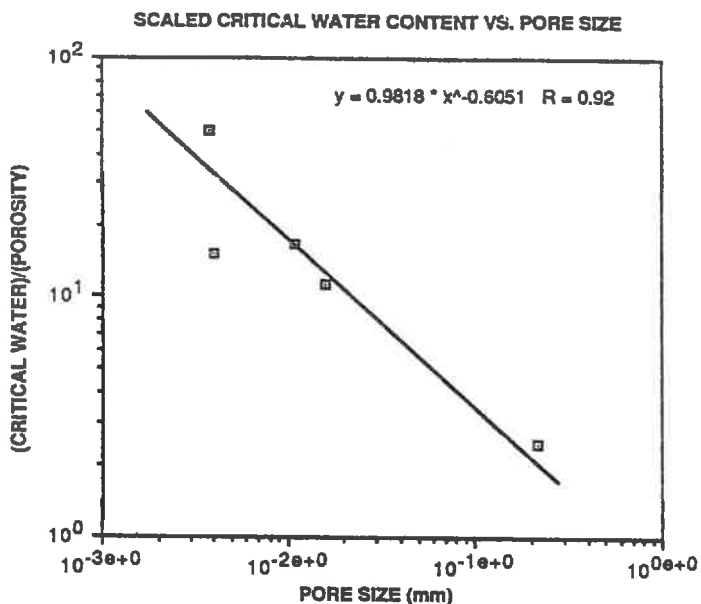
FIG. 63 PLOT USED TO DEDUCE THE FRACTAL DIMENSION OF MOIST
SOILS IN THE SIMPLE FRACTAL MODEL

The pore size was taken to be equal to the median particle size.
Particle size distributions for these soils were obtained from CRREL
as well as the density of the soil particles which allowed the porosity
to be calculated from the bulk density to which the samples were
packed in the Tempe cell.

As the model predicts, a linear fit (although with considerable
scatter) is obtained. The slope produces a fractal dimension of 2.4.
The typical fractal dimensions encountered in aggregate clustering
are about 2.5. A word of caution is appropriate in that if the energy

167

loss mechanism in soils is a relaxation mechanism due to adsorbed water then this could simulate a fractal dimension of 2 because the surface area of a sample per unit volume is inversely proportional to the particle size. However the relatively small variation in the observed loss tangents between soils compared to the wide range in soil particle size does not support this contention.

This proposed fractal model is highly idealized and simplistic. However, the similar dielectric behavior of soils with huge ranges in particle size and shape of particles argues against a complicated model which considers many different soil parameters. This models weakest point is probably the assumption that pore spaces have a characteristic size equal to the median particle size. If information concerning the pore size distribution in soils was available, it is possible that this model could be significantly improved. I feel this model deserves further scrutiny.

CONCLUSION

An extensive data set for the dielectric behavior of moist soils was produced. Both the RF coax and resonant cavity measurements give similar real dielectric constant dependence on water content as that reported in the literature (Cihilar and Ulaby, 1974; Topp, et al., 1980). The low frequency RF coax data is somewhat anomalous in that the real dielectric constant is rather high at the wet end and that the dielectric constant drops steeply with moisture content at the dry end.

A number of generalizations regarding the RF data can be made and they are that: 1) The loss tangent is relatively independent of soil moisture over a wide range but shows considerable variation between soils. 2) The real dielectric constant shows considerable frequency dependence particularly in soils with high loss tangents and at high water contents. 3) The dispersion in the real dielectric constant is highest for soils with large loss tangents. 4) There is considerable temperature dependence in the dielectric properties, particularly in the imaginary dielectric constant. 5) As the moisture content of the soil falls, a marked transition is encountered where the loss tangent and the real dielectric constant fall precipitously.

In regard to the resonant cavity data at higher frequencies the following generalizations can be made: 1) At equivalent moisture levels, the real dielectric constants are significantly lower than the RF values. 2) The variation in both the real and imaginary dielectric

169

constants between soil types is much smaller than at RF frequencies. 3) For Ottawa sand, the temperature dependence of the imaginary dielectric constant has a completely different behavior from that encountered in the RF data. 4) In Ottawa sand, the imaginary dielectric constant can be successfully modeled as resulting from free water dipole relaxation. 5) For the other soils investigated, another loss mechanism must be operating (most likely either relaxation of surface adsorbed water or ionic conductivity).

The most interesting feature in this data set is the extensive information gained about dielectric loss in soils and the strong correlation between the real and imaginary dielectric properties. At the higher frequencies encountered in the resonant cavity experiment, it appears likely that the dielectric loss may be due simply to the free water in the sample. At lower frequencies, such as those used in the RF coax measurements, dielectric loss due to Debye Relaxation of water is several orders of magnitude too small to account for the observed dielectric loss.

At RF frequencies, the data very strongly supports an ionic conductivity loss mechanism. Dissolved trace salts in the soil could introduce a conductivity giving rise to dielectric loss. This mechanism is supported by a number of observations. First, the imaginary dielectric constant falls rapidly with increasing frequency typical of conductivity effects. In addition, the observed increase in dielectric loss with temperature is in very good agreement with that measured in saline solutions. The presence of high conductivity in pore water filtered from a soil sample is also highly indicative that conductivity effects are of importance. Also, the steep drop in the

170

imaginary dielectric constant which is observed at low moisture levels is consistent with an ionic conductivity mechanism. The ability of the soil to support the movement of ions depends on the presence of unbound water. It is possible, though I consider it highly unlikely, that a low frequency relaxation mechanism might exist with a wide spread of relaxation times. This relaxation mechanism with dielectric dispersion characterized by eqs. 33 and 34 could mimic the observed data fairly well.

A fractal based model of the dielectric properties of soils has been attempted. The model shows considerable promise as a theoretical concept which explains the rather universal behavior of the real dielectric constant as a function of water content. In addition, the model may be able to account for the the marked rise in the loss tangent at a transition moisture content and subsequent leveling off. A larger data base and a more detailed knowledge of the size and distribution of pores in soils is needed to further test this model.

A simple Looyenga mixing model is able to account for the marked correlation between the real and imaginary dielectric constants in soils at RF frequencies. In addition, the model is able to account for the dispersion in the real dielectric constant by assuming relatively moderate salinities are present in the soil. The simple power law dependence of the imaginary dielectric constant can also be explained quite simply by this model. However, the applicability of the Looyenga mixing equation is subject to some doubt.

A considerable step forward has been made in the understanding of the dielectric behavior of soils at RF and microwave

frequencies. However, additional work is required in order to more satisfactorily model the dielectric response of soils and further test the proposed conductivity loss mechanism.

REFERENCES

Auty, R. P. and R. H. Cole, 1952. Dielectric Properties of Ice and Solid D_2O Journal of Chemical Physics 20:1309.

Ansoult, M., L. W. DeBacker, and M. Declercq, 1984. Statistical Relationship Between Apparent Dielectric Constant and Water Content in Porous Media. Journal of the Soil Science Society of America, 48:47-50.

Archie, G. E. ,1952. Bulletin of the American Association of Petroleum Geologists, 36:278.

Bard, A. J., 1980. Electrochemical Methods. John Wiley & Sons, Inc., New York.

Batlivala, P. and F. T. Ulaby, 1977. Estimation of Soil Moisture with Radar Remote Sensing. Proceedings of the 11th Intl. Symposium, Remote Sensing of the Environment and Environmental Res. Inst. of Michigan, pp. 1557-1566.

Belcher, D. J., T. R. Cuykendall, and H. S. Sack, 1950. The Measurement of Soil Moisture and Density by Neutron and Gamma-Ray Scattering, CAA Tech. Dev. and Eval. Center, Tech Dev. Rep. No. 127, pp. 1-20.

Belcher, D. J., T. R. Cuykendall, and H. S. Sack, 1950. Nuclear Meters for Measuring Soil Density and Moisture in Thin Surface Layers, CAA Tech. Dev. and Eval. Center, Tech Dev. Rep. No. 161, pp. 1-8.

Blanchard, B. J., A. J. Blanchard, S. Theis, W. D. Rosenthal, and C. L. Jones, 1981. Seasat SAR Response from Water Resources Parameter. U.S. Dept. of Commerce/NOAA Contract 78-4332, Final Report 3891.

Bouyoucos, G. J. and R. L. Cook, 1965. Humidity Sensor Permanent Electric Hygrometer for Continuous Measurement of the Relative Humidity of the Air (1). RILEM/CIB Symposium on Moisture Problems in Building, Vol. II, Sec. 6, "In-Situ Measurement of Moisture," Helsinki.

Brouers, F. and A. Ramsamugh, 1988. Percolation and Anomalous Conduction on Fractals in Fluid-Saturated Porous Media. Journal of Physic C: Solid State Physics, 21:1839-1847.

Burke, W. J., T. Schmugge, and J. F. Paris, 1979. Comparison of 2.8 and 21 cm Microwave Radiometer Observations Over Soils With Emission Model Calculations. Journal of Geophysical Research, 84:287-294.

173

Cihilar, J. and P. Ulaby, 1974. Dielectric Properties of Soils as a Function of Moisture Content. NASA CRES Technical Report 177-47.

Clarkson, M. T., 1988. Electrical Conductivity and Permittivity Measurements Near the Percolation Transition in a Microemulsion. II. Interpretation. Physical Review A, Vol. 37 No. 6 pp. 2079-2090.

Cole, K. S. and R. H. Cole, 1941. Dispersion and Absorption in Dielectrics. Journal of Chemical Physics, 9:341.

Collins, R. E., 1966. Foundations for Microwave Engineering. McGraw Hill, New York.

Condit, H. R.,1965. The Spectral Reflectance of American Soils. Photogrammetric Engineering, 955-966.

Davis, J. L., and A. P. Annan, 1977. Electromagnetic Detection of Soil Moisture: Progress Report I. Canadian Journal of Remote Sensing 3:76-86.

Debye, P., 1929. Polar Molecules. Dover Publications Inc., United States.

Dryden, J. S., and R. J. Meakins, 1957. Proceedings of the Physical Society of London, 70:427.

Eagleman, J. and W. Lin, 1976. Remote Sensing of Soil Moisture by a 21 cm Passive Radiometer. Journal of Geophysical Research, 81:3660.

Eicke, H. , S. Geiger, F. A. Sauer, and H. Thomas, 1986. Dielectric Study of Fractal Clusters Formed by Aqueous Nanodroplets in Apolar Media. Berichte Bunsenges Physical Chemistry, 90:872-876.

Falkenhagen, H. , 1934. Electrolytes, Oxford University Press, London.

Ferguson, H. and W. Gardner, 1962. Water Content Measurement in Soil Columns by Gamma Ray Absorption. Soil Sci. Soc. Am. Proc., 26:11-18.

Fröhlich, H., 1949 Theory of Dielectrics. Oxford University Press, London.

Geiger, F. E., and D. Williams, 1972. Dielectric Constants of Soils at Microwave Frequencies. NASA Report TMS-65987.

Gurr, C. G., 1962. Use of Gamma Rays in Measuring Water Content and Permeability in Unsaturated Columns of Soil. Soil Sci., 94:224-229.

Gusev, Y., R. R. Nigmatullin, and N. N. Soutougin, 1987. The Random Fractal Model and Dielectric Response of Bonded Water in the Sandstone. 9th International Conference of Conduction and Breakdown in Dielectric Liquids, Salford, U.K. pp. 175-177.

Hamon, B. V., 1953. Maxwell-Wagner Loss and Absorption Currents in Dielectrics. Australian Journal of Physics, 6:305-315.

Hartshorn, L., and W. H. Ward, 1935. Journal of the institute of Electrical Engineers, 77:723.

Hashin, Z. and S. Shtrikman, 1962. A Variational Approach to the Theory of the Effective Magnetic Permeability of Multiphase Materials. Journal of Applied Physics, 33:3125-3131.

Hastead, J. B., 1973. Aqueous Dielectrics. Chapman and Hall, London.

Hastead, J. B., 1961. The Dielectric Properties of Water. Progress in Dielectrics, 3:101-152.

Heim, P. J., 1984. Dielectric Properties of Moist Soil. Thesis at Dartmouth College, Hanover, N.H. 03755.

Hilfiker, R. and H. Eicke, 1987. Self-Consistency of the Percolation Model as applied to a Macrofluid-like Water-in-Oil Microemulsion. Journal of the Chemical Society, Faraday Transactions 1, 83:1621-1629.

Hillel, D., 1980. Fundamentals of Soil Physics. Academic Press, New York.

Hipp, J. E., 1974. Soil Electromagnetic Parameters as a Function of Frequency, Soil Density and Soil Moisture. Proceedings of I.E.E.E. 62(1):98-103.

Hoekstra, P., and A. Delaney, 1974. Dielectric Properties of Soils at UHF and Microwave Frequencies. Journal of Geophysical Research, 79:1699-1708.

Hoekstra, P., and W. T. Doyle, 1971. Dielectric Relaxation of Surface Adsorbed Water. Journal of Colloid and Interface Science, 36:513-521.

Hoekstra, P., and H. W. O'Brien, 1969. The Dielectric Properties of Clay Suspensions in the Frequency Range From 50 Hz to 20 KHz. Research Report 266, US. Army Cold Region Research and Engineering Laboratory, Hanover N.H. pp. 1-16.

Idso, S. B., T. J. Schmugge, R. D. Jackson, and R. J. Reginato, 1975. The Utility of Surface Temperature Measurements for the Remote Sensing of Soil Water Status. J. Geophysical Research, 80:3044-3049.

Jackson, J. D., 1975. Classical Electrodynamics. John Wiley & Sons, New York.

Katz, A. J., and A. H. Thompson, 1985. Fractal Sandstone Pores: Implications for Conductivity and Pore Formation. Physical Review Letters, 54:1325-1328.

Kharadly, M. M. Z., and W. Jackson, 1953. Proceedings of the Institution of Electrical Engineers, 100:199.

175

Malmberg, C. G. and A. A. Maryott, 1956. J. Res. National Bureau of Standards, 56:1.

Maxwell, J. C., 1873. A Treatise on Electricity and Magnetism. Oxford University Press. Article 314.

Meakin, P. , 1983. Diffusion-Controlled Cluster Formation in 2-6-Dimensional Space. Physical Review, A 27:1495

Meakins, R. J., 1961. Mechanisms of Dielectric Absorption in Solids. Progress in Dielectrics, 3:151-202.

Milton, G. W., 1981. Bounds on the Complex Permittivity of a Two-Component Composite Material. Journal of Applied Physics, 52:5286-5295.

Muir, J., 1953. Dielectric Loss in Water Films Adsorbed By Some Silicate Clay Minerals. Journal of Faraday Transactions, 2:249-254.

Newton, R. W., 1977. Microwave Remote Sensing and Its Application to Soil Moisture Detection, Technical Report RSC-81, Remote Sensing Center Texas A&M University, College Station Texas, 500 pp.

Niemeyer, L. , L. Pietronero, and H. J. Wiesmann, 1984. Physics Review Letters, 52:1033.

O'Konski, C. T., 1960. Electrical Properties of Macromolecules. V. Theory of Ionic Polarization in Polyelectrolytes. Journal of Chemical Physics, 64:605.

O'Konski, C. T., 1955. Effect of Interfacial Conductivity on Dielectric Properties. Journal of Chemical Physics, 23:1559.

Phene, C., G. J. Hoffman, and S. L. Rawlins, 1971. Measuring Soil Matric Potential In-Situ by Sensing Heat Dissipation Within a Porous Body: I. Theory and Sensor Construction. Soil Sci. Soc. Amer. Proc., 35:27-33.

Polder, D. and J. H. Van Santen, 1946. The Effective Permeability of Mixtures of Solids. Physica, Vol. 12, No. 5 pp. 257-271.

Reginato, R. J., S. B. Idso, J. F. Vedder, R. D. Jackson, M. B. Blanchard, and R. Gottleman, 1976. Soil Water Content and Evaporation Determined by Thermal Parameters Obtained from Ground-Based and Remote Measurements. J. Geophys. Res., 81:1617-1620.

Reginato, J. R., and C. H. M. Van Bevel, 1962. Pressure Cell for Soil Cores. Soil Science of America Proceedings, 26:1-3.

Richards, L. A. and W. Gardner, 1936. Tensiometers for Measuring the Capillary Tension of Soil Water. J. Amer. Soc. of Agronomy, 28:352-358.

Sabins, F. F.,1987. Remote Sensing: Principles and Interpretation. 2nd edition, W. H. Freeman and Company, New York, 449 pp.

Schanda, E., R. Hofer, D. Wyssen, A. Musy, D. Meylan, C. Morzier, and W. Good, 1978. Soil Moisture Determination and Snow Classification with Microwave Radiometry. Proc. 12th Intl. Symp. on Remote Sensing of the Environment, Manilla, Philippine Islands.

Schmugge, T. J., Jackson, T. J. and McKim, H. L., 1979. Survey of In-Situ and Remote Sensing Methods For Soil Moisture Determination. American Water Resources Association Satellite Hydrology Symposium.

Schmugge, T. J., B. Blanchard, A. Anderson, and J. Wang, 1978. Soil Moisture Sensing with Aircraft Observations of the Diurnal Range of Surface Temperature. Water Resources Bull. 14:317-323.

Schwan, H. P., G. Schwarz, J. Maczuk, and H. Pauly, 1962. The Low-Frequency Dielectric Dispersion of Colloidal Particles in Electrolyte Solution. Journal of Physical Chemistry 66:2626-2635.

Schwarz, G., 1962. A Theory of the Low-Frequency Dielectric Dispersion of Colloidal Particles in Electrolyte Solution. Journal of Chemical Physics 66:2636-2642.

Scott, J. H., R. D. Carroll, and D. R. J. Cunningham, 1967. Dielectric Constant and Electrical Conductivity of Moist Rock from Laboratory Measurements. Journal of Geophysical Research, 72:5101-5110.

Selig, E. T., and S. Mansukhani, 1975. Relationship of Soil Moisture to the Dielectric Property. Journal of Geotechnical Engineering Division, American Society of Civil Engineers, 101(GT8):755-769.

Shahidi, M., J. B. Hastead, and A. K. Jonscher, 1975. Electrical Properties of Dry and Humid Sand. Nature 258:595-597.

Smith-Rose, R. L., 1933. The Electrical Properties of Soils for Alternating Currents at Radio Frequencies. Proceedings of the Royal Society of London, 140:39-56.

Smyth, J. W., 1955. Electric Dipole Moments, Butterworth's Scientific Publications, London pp. 12-13.

Topp, G., Davis, J., and P. Annan 1980. Electromagnetic Determination of Soil Water Content: Measurements in Coaxial Transmission Lines. Water Resources Research Vol. 16, No. 3 pp 574-582.

Ulaby, F. T., P. T. Batlivala, and J. E. Bane, 1980. Crop Identification with L-band radar: Photogrammetric Engineering and Remote Sensing, V. 46:101-105.

Wagner, K. W., 1914. Arch. Elektrotech., 2:378.

Weast, R. C., 1978. Handbook of Chemistry and Physics, CRC Press Inc. Cleveland.

Zallen, R., 1983. The Physics of Amorphous Solids, John Wiley & Sons, New York.